

**UC Berkeley**  
**SEMM Reports Series**

**Title**

A Double Doubly Curved Quadrilateral Element for Thin Elastic Shells of Revolution

**Permalink**

<https://escholarship.org/uc/item/9616672q>

**Author**

Fonder, Ghislain

**Publication Date**

1972

UC SESM 72-1

STRUCTURES AND MATERIALS RESEARCH  
DEPARTMENT OF CIVIL ENGINEERING

**A DOUBLY CURVED  
QUADRILATERAL ELEMENT FOR  
THIN ELASTIC SHELLS  
OF REVOLUTION**

by

GHISLAIN A. FONDER

This Research was partially supported by an  
ESRO/NASA International Fellowship

JANUARY 1972

STRUCTURAL ENGINEERING LABORATORY  
UNIVERSITY OF CALIFORNIA  
BERKELEY CALIFORNIA

To Professor R. L. Taylor with my sincere thanks for  
his guidance during my research

Ghislain Fonder

Structures and Materials Research  
Department of Civil Engineering

Report No. UC SESM 72-1

A DOUBLY CURVED QUADRILATERAL ELEMENT  
FOR THIN ELASTIC SHELLS OF REVOLUTION

by

Ghislain A. Fonder  
Graduate Student, University of California, Berkeley  
Chargé de Recherches F.N.R.S., University of Liège, Belgium  
(Researcher with the Belgian National Fund for Scientific Research)

Structural Engineering Laboratory  
University of California  
Berkeley, California

January 1972

ABSTRACT

A new finite element for the linear analysis of thin elastic shells of revolution by the displacement method is derived, tested and discussed. It offers an alternative to the curved elements of revolution, with displacements represented by polynomials and Fourier series in the meridional and circumferential directions respectively, which are ordinarily used to solve nonsymmetrical deflections of this type of shell. The principal lines of curvature, which coincide with parallel and meridian lines in axisymmetric shells, are used to delimit the new element and as a basis for the curvilinear coordinates used throughout the derivation.

Because later extension of the element to the large deflection range is foreseen, special care is taken in the selection of strain-displacement relationships. Sanders' expressions are chosen and discussed with regard to linearization, effects of small and large rigid-body motions.

Bilinear and bicubic interpolation functions approximate the surface and transverse displacements, respectively. Because they are expressed in terms of curvilinear coordinates, these functions provide compatible displacements but do not include rigid-body motions.

A general procedure to describe rigid modes, to find if they are already represented in the stiffness matrix, and add them if they are not, is presented and applied to the new shell element. Unfortunately, the addition of rigid modes can render the displacements incompatible.

Several examples are solved by means of a specialized computer program: rectangular and circular plates, rings, cylindrical and spherical shells, hyperboloids of revolution. They permit drawing conclusions about the efficiency of the element and the relative importance of rigid modes and displacement incompatibilities.

ACKNOWLEDGEMENTS

I feel greatly indebted toward Professor Charles Massonnet, University of Liege, Belgium, whose insight was an important factor in my decision to study in the United States.

In Berkeley, I was very fortunate to work under Professor R. W. Clough's supervision: his continuous encouragement, support and confidence in the final success were priceless to me. Valuable help was also offered by the other members of my thesis committee, Professors R. L. Taylor, B. Parlett, E. P. Popov, and, at various times by Professors E. L. Wilson, G. H. Powell and R. De Vogelaere; to all of them I wish to express my deepest gratitude.

I also express my appreciation to Mrs. Debbie Aoki for her fast and accurate typing of my manuscript, to the University of California Computer Center and Chancellor Patent Fund for the computer time they made available for this research.

Financial support during the course of my studies was provided by the CRB, Harry H. Hilp, Charles Atwood Kofoid Eugenics, and ESRO/NASA fellowships. I sincerely thank the Belgo-American Educational Foundation, the University of California and the European Space Research Organization who awarded me these fellowships.

Last but not least, tribute should be paid to that unsung heroine of graduate studies: the student's wife. To Nicole, who spent countless evenings and weekends alone, somehow managed three energetic children and provided cheerful moral support, I gratefully dedicate this work.



TABLE OF CONTENTS

	<u>Page</u>
ABSTRACT . . . . .	ii
ACKNOWLEDGEMENTS . . . . .	iv
TABLE OF CONTENTS . . . . .	v
NOMENCLATURE . . . . .	ix
1. INTRODUCTION . . . . .	1
1.1 Objective and Scope . . . . .	1
1.2 Presentation of the Problem . . . . .	2
1.2.1 Review of Shell Theory . . . . .	2
1.2.2 The Problem of Shell Instability . . . . .	5
1.2.3 Numerical Solutions for Shells . . . . .	7
1.3 The Finite Element Method . . . . .	10
1.4 Specialized Finite Elements for Shells of Revolution . . . . .	12
1.5 Finite Elements for General Shells . . . . .	17
1.5.1 Flat Plate Elements . . . . .	18
1.5.2 Curved Elements Based on Shell Theory . . . . .	19
1.5.3 Curved Elements with Relaxed Shell Theory . . . . .	21
1.6 Selection of a New Element . . . . .	23
1.7 Summary of the New Element Development . . . . .	25
2. STRAIN-DISPLACEMENT RELATIONSHIPS . . . . .	27
2.1 Geometrical Preliminaries . . . . .	27
2.1.1 Some Results from the Geometry of Euclidean Space . . . . .	27
2.1.2 Some Results from the Geometry of a Surface . . . . .	28



	<u>Page</u>
2.2 Nonlinear Strains . . . . .	30
2.2.1 Exact Derivation . . . . .	30
2.2.2 Small Strain Approximations . . . . .	35
2.2.3 Linearized Curvature Changes . . . . .	37
2.2.4 Physical Components of Strains . . . . .	38
2.3 Application to Shells of Revolution . . . . .	40
2.3.1 General Shell of Revolution . . . . .	40
2.3.2 Particular Cases of Shell of Revolution . . . . .	44
2.4 Effect of Rigid Motions . . . . .	47
2.4.1 Small Motions in Linear Theory . . . . .	47
2.4.2 Large Motions in Nonlinear Theory . . . . .	49
2.5 Discussion of Nonlinear Strains . . . . .	54
3. APPLICATION OF THE FINITE ELEMENT METHOD TO SHELLS OF REVOLUTION . . . . .	59
3.1 Preliminary Remarks on Notations . . . . .	59
3.2 Representation of the Element Geometry . . . . .	59
3.2.1 General Meridian Curve . . . . .	59
3.2.2 Particular Cases of Meridian Curve . . . . .	62
3.3 Displacement Fields . . . . .	63
3.4 Derivation of Element Stiffness . . . . .	69
3.4.1 Strains . . . . .	69
3.4.2 Strain Energy . . . . .	69
3.4.3 Virtual Work Principle . . . . .	71
3.4.4 Numerical Integration . . . . .	72

	<u>Page</u>
3.4.5 Interpretation of Stiffness Terms . . . . .	74
3.5 Generalized Nodal Forces . . . . .	77
3.6 Structure Stiffness . . . . .	80
4. REPRESENTATION OF RIGID BODY MODES . . . . .	81
4.1 General . . . . .	81
4.2 Exact Small Rigid Motions for the Quadrilateral Element . . . . .	82
4.2.1 Relationships Between Bases . . . . .	82
4.2.2 Translations . . . . .	84
4.2.3 Small Rigid Rotations . . . . .	85
4.2.4 Summary . . . . .	87
4.3 Representation of the Rigid Modes by the Displacement Functions . . . . .	87
4.3.1 Almost Flat Elements . . . . .	88
4.3.2 Degenerate Shells . . . . .	90
4.4 Eigenvalues and Rigid-Body Modes . . . . .	92
4.5 Determination of Represented Rigid Modes . . . . .	96
4.5.1 Addition of Rigid-Body Modes . . . . .	96
4.5.2 Static Condensation of Rigid Modes . . . . .	98
4.5.3 Determination of the Rigid Modes Included in the Displacement Functions . . . . .	100
4.5.4 Example of Cylindrical Shell . . . . .	102
4.6 Rigid Modes to be Added for Different Types of Shells of Revolution . . . . .	108
4.7 Computation of Shell Forces . . . . .	111

	<u>Page</u>
5. NUMERICAL EXAMPLES . . . . .	115
5.1 General . . . . .	115
5.2 Computer Program . . . . .	115
5.2.1 Description . . . . .	115
5.2.2 Additional Comments . . . . .	119
5.3 Rectangular Plate Examples . . . . .	121
5.3.1 Rectangular Plate Under Uniform Load . . . . .	121
5.3.2 Twisted Square Plate . . . . .	124
5.4 Circular Plate Examples . . . . .	124
5.4.1 Curved Slab . . . . .	124
5.4.2 Circular Plate with Concentrated Force . . . . .	128
5.5 Cylindrical Shells . . . . .	130
5.5.1 Circular Ring Under Diametral Load . . . . .	130
5.5.2 Pinched Cylinder . . . . .	137
5.5.3 Cylindrical Shell Roof . . . . .	139
5.6 Spherical Shells . . . . .	142
5.6.1 Sphere Under Internal Pressure . . . . .	142
5.6.2 Sphere Under Point Load . . . . .	145
5.7 Hyperboloids of Revolution . . . . .	149
5.7.1 Hyperboloid Under Dead Load . . . . .	149
5.7.2 Hyperboloid Under Wind Load . . . . .	152
5.8 Discussion of Incompatibilities . . . . .	152
6. SUMMARY AND CONCLUSIONS . . . . .	157
BIBLIOGRAPHY . . . . .	162

NOMENCLATURE

A list of all important symbols in the text is compiled here; most often, the place where they first appear is also indicated. Very few of them have two meanings; these are clearly defined and should not confuse the reader.

The diagonal summation convention is used in Chapter 2 with Latin indices ranging from 1 to 3 and Greek indices from 1 to 2. In all other chapters, the matricial notation is used and subscripts refer either to the element corners  $i, j, k, \ell$  or to some descriptive characteristic of the element they affect.

$[ ] , [ ]^T$	matrix and matrix transposed
$\{ \} = \langle \rangle^T$	column vector
$\langle \rangle = \{ \}^T$	row vector
$( ) , {}_I ( ) , ( ) _I$	partial and covariant derivative with respect to variable $X^I$ (2.8)
$( )  _A$	surface covariant derivative with respect to $X^A$ (2.20)
$( )' = \frac{\partial}{\partial s} , ( )^\circ = \frac{\partial}{r\partial\theta}$	partial derivatives with respect to the element surface coordinates (Table 3.1)
$A$	element area
$\underline{A}_A$ and $\underline{a}_\alpha$	surface base vectors in the undeformed and deformed configuration (2.13)
$A_{AB}$ and $a_{\alpha\beta}$	surface metric tensor in the undeformed and deformed configuration (2.15)
$A$ and $a$	determinant of the above two metric tensors
$B_{AB}$ and $b_{\alpha\beta}$	second fundamental form in the undeformed and deformed configuration (2.18)
$[B]$	matrix of interpolation functions for strains (3.30)

$[D]$	elasticity matrix (3.33)
$E$	Young's modulus
$E_{IJ}$	Almansi strain tensor (2.30)
$\overset{\circ}{E}_{AB}$	middle surface components of $E_{IJ}$ (2.44)
$E\langle AB \rangle$	physical components of $\overset{\circ}{E}_{AB}$ (2.84) to (2.86)
$\{E\}$	vector of physical components of the linearized surface strains and changes of curvature (3.31)
$f_1, \dots, f_6$	displacement interpolation functions (3.20)
$f'_1, \dots, f''_6$	first and second derivatives of the above functions
$f_u, f_v, f_w$ and $F_u, F_v, F_w$	distributed and concentrated external loads in the direction of $u, v, w$ displacements
$\{F\}$	vector of the generalized nodal forces equivalent to the external loading (3.52)
$\tilde{G}_I$ and $\underline{g}_i$	base vectors in the undeformed and deformed state (2.3), (2.33)
$G_{IJ}$ and $g_{ij}$	metric tensor in the undeformed and deformed state (2.3), (2.29)
$G$ and $g$	determinant of the above two metric tensors
$h$	shell thickness
$\hat{i}_1, \hat{i}_2, \hat{i}_3$	normalized orthogonal base vectors
$K_{AB}$	tensor of surface curvature changes (2.44)
$[K]$	element stiffness matrix (3.39)
$[K_D], [K_T]$	element stiffness matrix when it is necessary to specify that deformation displacements (4.40) or total displacements (4.45) are involved

$[K_{DD}]$ , $[K_{DR}]$ , $[K_{RD}]$ , $[K_{RR}]$	submatrices in the augmented stiffness matrix (4.41)
$l$	element meridian length
$M\langle 11 \rangle, \dots, M\langle 21 \rangle$	physical components of shell bending moments (4.61)
$N\langle 11 \rangle, \dots, N\langle 21 \rangle$	physical components of shell membrane forces (4.61)
$\underline{n} \equiv \underline{a}_3$ and $\underline{\tilde{n}} \equiv \underline{\tilde{a}}_3$	unit vector normal to the middle surface before and after deformation (2.11) and (2.36)
$p$	uniform pressure force (Table 3.2)
$\underline{p}$ and $\underline{\tilde{p}}$	position vector of the point $P$ in the shell middle surface before and after deformation (2.35), (2.36)
$P_1, P_2, P_3$	components of the position vector $\underline{p}$ with respect to the local Cartesian basis at the element center $O$ (4.10)
$\underline{Q}$ and $\underline{\tilde{Q}}$	position vector of a point $Q$ before and after deformation (2.27)
$r$	parallel radius, first component of the cylindrical coordinates $(r, \theta, z)$ used to define points on the shell middle surface (2.91)
$r_0$	parallel radius at the element center $O$
$R$	radius of a circular meridian arc or spherical shell
$R_1, R_2$	curvature radii of a surface along the coordinate lines (2.25)
$S_1, S_2, S_3$	rigid translations along the general Cartesian basis (Section 2.9.2)
$\{S\}$	vector of the generalized nodal forces (Table 3.1)
$\{S_T\}, \{S_D\}, \{S_R\}$	same as above when it is necessary to specify that total, deformation or rigid displacements are involved (4.35)

$s$	meridian curvilinear coordinate
$t = rd\theta$	parallel curvilinear coordinate in case of large radius (2.107)
$T$	torsion of a surface (2.26)
$[T_P]$	transformation matrix between local Cartesian bases at the element center 0 and the middle surface point P (4.4)
$T_{11}, \dots, T_{33}$	components of the above matrix (4.5)
$[T_R]$	transformation matrix between $\{U_R\}$ and $\{V_R\}$ (4.20)
$U$	strain energy (3.32)
$\underline{U}$	displacement vector of a point P in the shell middle surface (2.38)
$U^A$	surface components of the above vector (2.38)
$u = U\langle 1 \rangle$	first physical component of the displacement vector $\underline{U}$ (2.74)
$u_0$	rigid translation at element center 0 (4.6)
$\{U_R\}$	vector of the small rigid motions at the element center 0 (4.19)
$\underline{v}$	displacement vector
$v = U\langle 2 \rangle$	second physical component of the displacement vector $\underline{U}$ (2.74)
$v_0$	rigid translation at the element center 0 (4.6)
$\{V\}$	vector of nodal degrees of freedom (Table 3.1)
$\{V_T\}, \{V_D\}, \{V_R\}$	same as above when it is necessary to specify that total, deformation or rigid displacements are meant (4.32)
$W$	normal component of the displacement vector $\underline{U}$ (2.38)

$w = W$	third physical component of the displacement vector $\underline{U}$ (2.74)
$w_o$	rigid translation at the element center 0 (4.6)
$\{W_n\}$	eigenvector corresponding to the eigenvalue $\lambda_n$ (Section 4.4)
$X^I$ and $x^i$	curvilinear coordinates in the undeformed and deformed state (Fig. 2.1)
$Z^I$ and $z^i$	general Cartesian coordinates in the undeformed and deformed state (Fig. 2.1)
$Z_1, Z_2, Z_3$ and $z_1, z_2, z_3$	local Cartesian coordinates referred to the element basis at 0 before and after rigid motions (4.12)
$Z = X^3$ and $z = x^3$	curvilinear coordinate normal to the shell middle surface before and after deformation (2.11), (2.36)
$z$	third component of the cylindrical coordinates $(r, \theta, z)$ used to define points in the shell middle surface (2.91)
$z_0$	same as above at element center 0
$\alpha$	element parallel opening (3.19)
$\alpha_A^3, \alpha_3^3$	intermediate quantities defined in (2.57) to (2.59)
$\beta_1, \beta_2, \beta_3$	rigid rotations (Sections 2.4.2 and 4.2.3)
$\Gamma_{IJK}^I, \Gamma_{IJ}^K$	Christoffel symbols of first and second kind (2.6)
$\delta_J^I$	Kronecker delta
$\epsilon_A^\Gamma, \epsilon_A^3$	intermediate quantities defined in (2.49), (2.50)
$\epsilon\langle 11 \rangle, \dots, \epsilon\langle 32 \rangle$	physical components of the linear strains (2.78) to (2.83)
$\eta\langle 11 \rangle, \dots, \eta\langle 12 \rangle$	physical components of the nonlinear part of the Lagrangian strains (2.84) to (2.86)



$\eta$	dimensionless element curvilinear coordinate in the parallel direction (3.18)
$\theta$	second component of the cylindrical coordinates $(r, \theta, z)$ used to define points in the shell middle surface (2.91)
$\theta_0$	same as above at the element center 0
$\kappa\langle 11 \rangle, \dots, \kappa\langle 21 \rangle$	physical components of the linearized curvature changes (2.88) to (2.90)
$\lambda_n$	nth eigenvalue of the element stiffness matrix (Section 4.4)
$\nu$	Poisson's ratio
$\xi$	dimensionless element curvilinear coordinate in the meridian direction (3.13)
$\varphi$	meridian slope measured from the vertical (Fig. 2.2)
$[\Phi]$	matrix of interpolation function for displacements $u, v, w$ (3.29)
$[\Phi_R], [\Phi_D]$	same as above when it is necessary to specify that deformation or rigid displacements are involved (4.17), (4.47)
$\underline{\Psi}$	vector measuring the rotation of the middle surface normal (2.37)
$\Psi^A, \Psi$	components of $\underline{\Psi}$ (2.39)
$\omega_{AB}$	intermediate quantity defined in (2.69)
$\omega = \omega\langle 12 \rangle$	physical component defined in (2.75)

1. INTRODUCTION

1.1 Objective and Scope

The purpose of the present thesis is to formulate and test a new finite element for thin shells of revolution, capable of solving axisymmetric and asymmetric problems. Only linear applications will be considered here but a possible extension to geometrically nonlinear problems was considered from the start and played an important role in the selection and development of the element.

This introductory chapter will review the background material and explain the decision-making process which finally led to the method chosen to solve the problem at hand: how, by successive elimination, it was decided to select a numerical approach, the finite element method, and finally, a doubly curved, quadrilateral element.

Section 1.2 will justify the problem discussed in the thesis: Why are shells of revolution used, what are the difficulties encountered in analyzing them, why should one study large deflections of shells, why is a numerical approach desirable? Past attempts at a numerical solution will be briefly reviewed.

Then, the attention will focus on one method: the application to shells of finite elements. After a general presentation of the technique, the conical frusta and curved segments specialized for shells of revolution will be critically examined. Next, one will proceed to the general elements for shells: the assemblage of flat plates, the elements based on classical shell

theory, those derived from a three-dimensional solid and including shear deformations. Each category will be discussed in the light of the special problem one has in mind.

Finally, on the basis of the accumulated knowledge, a new finite element will be chosen and the steps to be taken for its development summarized.

## 1.2 Presentation of the Problem

### 1.2.1 Review of Shell Theory

The structural advantages of thin shells have long been acknowledged: the combination of membrane and bending stiffness lead to an almost ideal utilization of the material and to light, elegant structures which have found numerous applications. The construction industry uses them in domes, cylindrical or hyper roofs and hyperboloid cooling towers; other industrial applications include submarine hulls, pressure vessels, pipe-lines, storage tanks, refinery equipment and the like. But it is in the aerospace industry, where weight is of such paramount importance, that the most dramatic and sophisticated uses of thin shells are currently being made.

Because it is a very challenging problem, stress analysis in shells has received considerable attention and has been the subject of innumerable papers in the last fifty years [89]\*.

---

\*The number between brackets refers to the alphabetically ordered bibliography.

From the beginning, it was understood that to make a solution possible, the otherwise three-dimensional shell problem had to be reduced to one characterized by two-dimensional field equations. The first complete linear theory, based to some extent on Kirchhoff's earlier work on plates [64], was given by Love [73]. Most authors have derived their equations on the basis of the so-called Love-Kirchhoff assumptions:

Love-Kirchhoff  
ASSUMPTIONS

- a) points which lie on a normal to the undeformed middle surface also lie on a normal to the deformed middle surface;
- b) the effect of the normal stress acting on surfaces parallel to the middle surface may be neglected in the stress-strain relations;
- c) the displacements in the direction of the normal to the middle surface are approximately equal for all points on the same normal.

But, to quote Naghdi (1963) [85]: "Since the appearance of Love's work, so far as the foundations of the theory are concerned, despite extensions, generalizations, re-examinations and re-derivations of the equations of the linear theory, there are still unsettled questions!" Namely, what constitutes a first approximation (comparable to the one used in the theory of bending of plates)? In the light of the contradictory assumptions b and c, what are satisfactory constitutive equations?

Koiter [66] pointed out that complete rigor in an analysis based on approximative basic assumptions is, of course, meaningless. He then proceeded to derive a set of equations, for both

the linear and nonlinear theory of shells in as simple a form as is consistent with the basic assumptions. His equations coincide with those independently derived by Sanders [106, 107].

They do not present any of the inconveniences affecting some other theories:

- a) the equilibrium equation of a shell element about the normal to the middle surface is identically satisfied;
- b) Betti's reciprocity principle is satisfied;
- c) the equations are invariant under rigid body displacements;
- d) they remain invariant under a transformation of the middle surface coordinates.

Sanders-Koiter equations, and sometimes the less consistent Novozhilov's equations [93] are widely accepted as the best linear and nonlinear equations for practical use.

More refined theories were developed. For instance, Naghdi and Nordgren [87] presented an exact, complete and fully general nonlinear theory of elastic shells founded under the Kirchhoff hypothesis; but an application of Koiter's criterion for consistency can show that the additional terms are practically unimportant. In recent works, Naghdi [86] and Krätzig [67, 68] abandon Kirchhoff hypothesis and represent the deformed normal by a power series of the curvilinear coordinates; their formulation includes ordinary shell theory and Reissner's theory with shear deformation [103] as a particular case; although of considerable academic interest, these works present the same defect as most refined theories: they are much too complicated for

practical solutions either in analytical form or through numerical computations.

### 1.2.2 The Problem of Shell Instability

A linear stress analysis is not sufficient for most of the shells used in the aerospace industry. Here the quest for minimum-weight optimum structural designs inherently tends to undercut the validity of the assumptions leading to linear formulations of the structural analysis problem. In order to predict structural behavior, it frequently has become necessary to base equilibrium equations on deformed geometry, to employ more exact deformation-displacement relations and to consider the nonlinear behavior of materials.

Material nonlinearities and general shell geometries will not be considered in the present work; but, even when the interest is restricted to linear elastic materials and to shells of revolution, a number of interesting problems remain to be solved.

Many papers have been published about the stability problem of shell structures. The objective of these studies has been to find the buckling load i.e. the load for which

- a) a perfect system admits a non trivial equilibrium configurations (equilibrium method),
- b) the deflections of an imperfect system increase beyond any prescribed limit (imperfection method),
- c) the potential energy of the perfect system ceases to be positive definite (energy method),

d) the most general free motion of the system ceases to be bounded  
(kinetic method)

Because of the mathematical complexity of the problem, the analytical treatments of shell stability have been mostly restricted to the particular cases of cylindrical, conical and shallow spherical shells.

The first investigators assumed a homogeneous solution or membrane-type solutions for the prebuckling equilibrium. To their great disappointment, the buckling loads determined experimentally were only a fraction of their computed results [88].

Koiter [65], by studying the neighborhood of the bifurcation point and the postbuckling behavior showed that the buckling load really represents a peak of the load-deflection curve that could be obtained only under the most ideal test conditions. The real models are always imperfect, the real boundary conditions imperfectly simulate the assumed ones, and asymmetrical deformations do occur in symmetrical shells symmetrically loaded. When the possibilities were considered analytically, the theoretical results for both the cylinder [52], [3] and the shallow spherical cap [53], [124] were reduced to the level of the experimental values, or even lower.

Even though their importance was suspected for some time, the initial imperfections and deformations prior to buckling were too difficult to be taken into account. Since modern computing techniques make it feasible, most recent papers stress the need for plotting the whole load deflection curve, preferably including the

postbuckling range, rather than being satisfied with the buckling load. A few papers have been published already describing the complete nonlinear behavior of some shells but much remains to be done in this field.

### \* 1.2.3 Numerical Solutions for Shells

Until the fifties, analytical results were available only for linear shell structures: closed forms or series solutions for particular types of shells (membranes, cylinder, sphere, cone, shallow shells) subjected to special loadings. Collections of such results can be found in books by Timoshenko [117, 118], Flugge [32], Girkmann [41], for instance. A few buckling loads had also been found but they were known to be unreliable.

With the advent of high speed computer, numerical methods took over. A few of the more important developments will be mentioned here.

The invariant imbedding method reformulates the boundary value problem into an initial value problem. It was applied by Junghanss [57] and Kalnins, Lestingi [58] respectively to linear and nonlinear elastic shells of revolution. The inconveniences of this method are said to be:

- a) the risk of numerical instability,
- b) a family of problems is to be solved instead of a single problem.

The nonlinear differential equations obtained in the equilibrium approach to the stability problem have been solved using the perturbation technique [60], the power series [124],



trigonometric series expansions [111] and parametric differentiation [99]. These methods determine the buckling loads and mode shapes only and tend to be abandoned in favor of techniques covering the whole nonlinear range.

The finite differences method has been highly successful in finding linear and nonlinear solutions of some complex shell forms. A few significant contributions are reviewed here below.

The small axisymmetric deflection problem of shells of revolution was solved by Radkowski et al. [100]. Budianski, Radkowski [12] and Albasiny, Martin [2] solved the asymmetric case by using Fourier series in the circumferential direction and finite differences along the meridian.

\* Archer [5] and Bushnell [14] treated large axisymmetrical deflections; both of them use Reissner nonlinear shallow shell equations [102]; Bushnell also shows that initially imperfect spherical shells can yield locally at pressures well below the theoretical elastic collapse.

Family, Archer [29] and Kao, Perrone [59] solved the large asymmetrical deformation problem by applying parallel and meridian finite differences to the Marguerre equations of shallow shells [75]. This choice of the strain expressions essentially restricts their investigation to shallow spherical caps.

Ball [8] solved the large asymmetrical deformations by means of Fourier series and finite differences in parallel and meridian directions, respectively; Sanders' nonlinear strain-displacement, and linearized curvature-displacement relationships are used.

One inconvenience is that the nonlinear strain terms introduce a coupling of the Fourier series terms; some are taken care of by using trigonometric identities which lead to series whose coefficients are series themselves; others are transferred to the right hand side of the system of equations and treated as pseudo-loads. Another inconvenience is that Sanders' equations, especially after dropping the nonlinear curvature terms, are valid for "moderately large rotations" only; this implicitly imposes limitations on their range of applicability although this must be considered much less severe than the restrictions on Archer's and Perrone's solutions. Indeed, Ball's paper only shows examples of shallow caps; on the other hand he also includes studies of dynamic effects.

Up to the present time, finite differences have not been applied to large asymmetric deformations of deep shells or shells with variable curvature like the junction of a cylinder and a toroidal segment. Finite difference methods are difficult to use for some boundary conditions. They also lead to trouble if variations of the shell geometry or material properties (a discontinuity like a porthole for instance) cannot be easily represented analytically or by curve fitting.

On the other hand, the finite element method can take care of these problems and, since it was selected for use in the present work, its application to the shell problems will now be more closely examined.

### 1.3 The Finite Element Method

The initial development of the finite element method in the field of structural mechanics can be traced back to a paper by Turner et al. [121]; the term "Finite Element" itself was coined by Clough in 1960 [19]. Since then, the method has progressed with giant strides. A survey of its present versatility can be found in the monographs by Zienkiewicz [129, 130] and the contributions of Argyris [6, 7].

Concurrently with the development of new elements, papers by Fraeys de Veubeke [33], Melosh [77], Arantes de Oliveira [4], Felippa, Clough [31] provided the mathematical background for the method. They showed that it is a specialized form of the well-known Rayleigh-Ritz procedure for constructing approximate solutions to a governing variational principle; in elasticity, this variational principle is equivalent to the minimization of the total energy, strain energy plus load potential, of the system. This mathematical formulation permits a general approach to the questions of convergence, error bounds or estimates, element expansion requirements, etc.

Theoretically, equilibrium models or displacement models can be developed by assuming stress fields or displacement fields over the finite elements [34]. But in shell theory, the second approach has been used primarily and the following requirements for the displacement functions have gradually taken shape as a result of theoretical work and practical experience by a number of researchers.

- a. The continuity of displacement and slope must be enforced at the inter-element boundaries. This is due to the fact that the equilibrium equations of thin shells with the Kirchhoff hypothesis, written in terms of displacements, are a set of fourth order differential equations; the related minimum potential energy functional requires second order derivatives in the unknown displacements to be evaluated; in the finite element method this means that the element displacement assumption must lead to continuous displacement fields which have continuous first derivatives.
- b. The rigid body motion of an element must be represented in the displacement functions. This condition will be discussed at length later in the thesis.
- c. All "pertinent" constant strain modes must be included [37]. As the grid is refined, the strain state within an element approaches a constant value; if a constant value of strain lacks representation in the subject formulation however, convergence to the correct result cannot be achieved. A typical example, borrowed from the plate theory, is the square plate simply supported at three corners and loaded at the fourth; satisfactory convergence cannot be achieved unless the finite element contains a constant twisting mode [9].
- d. Greene et al. [48] claim that the meridian, parallel and perpendicular displacements  $u$ ,  $v$  and  $w$  should be represented with equal accuracy, which, in general, means by polynomials of equal degree. This requirement is indispensable to maintain continuity if  $u$ ,  $v$ ,  $w$  are displacements in some global

coordinate system but may be relaxed if they are curvilinear displacements expressed as functions of convected coordinates.

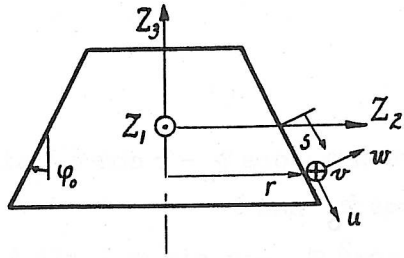
This condition may also have arisen in the need to better approximate the rigid body modes; although desirable indeed, it should not be considered as an absolute requirement.

All these conditions presuppose that the continuum itself, i.e. the shell and its boundary conditions, are correctly represented. A number of successful shell elements have been developed, however, in which one or several of these requirements were not met. They are now going to be reviewed.

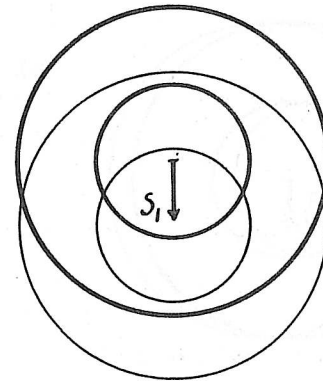
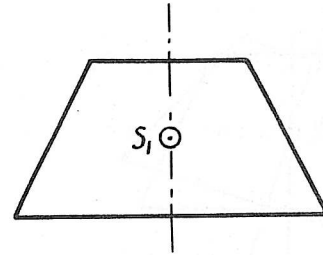
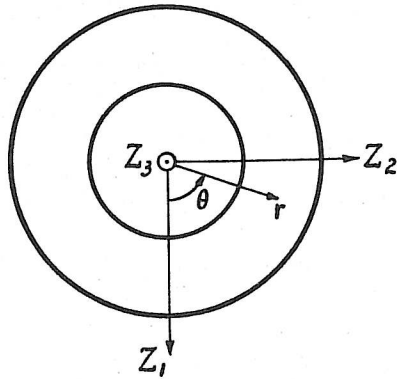
#### 1.4 Specialized Finite Elements for Shells of Revolution

The first efforts were directed towards axisymmetrically loaded shells of revolution. After pioneering attempts by Meyer, Harmon [80] and Popov et al. [74], a conical frustrum element was set up [44], [98], [27], in which  $u$  and  $v$  were represented by linear functions and  $w$  by a cubic function of the meridian coordinate  $s$ ; asymmetric deformations were represented by Fourier series expansions of  $u$ ,  $v$ ,  $w$  in the parallel coordinate  $\theta$ . In this element, all rigid body modes are correctly represented (Fig. 1.1). Its disadvantages are that many elements are needed where the shell is strongly curved, residual meridional moments may exist even with consistent loading and inaccuracies can be expected in the regions of high stress gradients [56].

This was corrected by the introduction of a curved element for axisymmetric [56] and asymmetric problems [117]. The disadvantage of this element, however, is that, unless explicitly



a) Definition of Coordinates

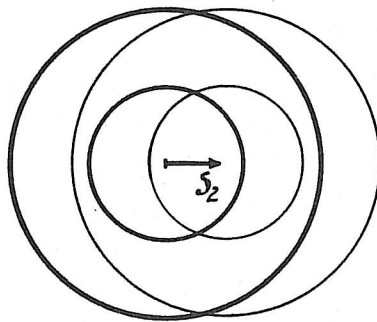
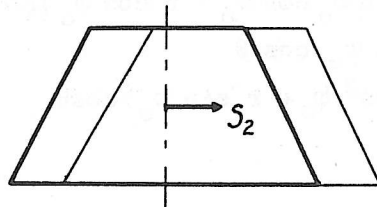


$$u = S_1 \sin \varphi_0 \cos \theta$$

$$v = -S_1 \sin \theta$$

$$w = S_1 \cos \varphi_0 \cos \theta$$

b) Horizontal Translation  $S_1$

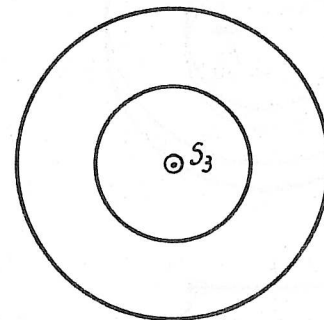
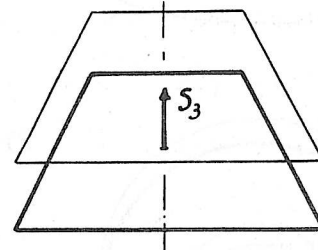


$$u = S_2 \sin \varphi_0 \sin \theta$$

$$v = S_2 \cos \theta$$

$$w = S_2 \cos \varphi_0 \sin \theta$$

c) Horizontal Translation  $S_2$

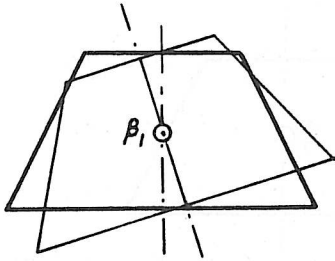


$$u = -S_3 \cos \varphi_0$$

$$v = 0$$

$$w = S_3 \sin \varphi_0$$

d) Vertical Translation  $S_3$

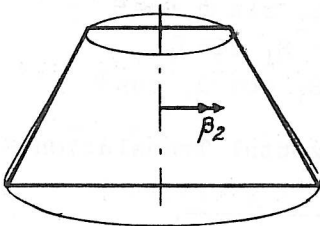
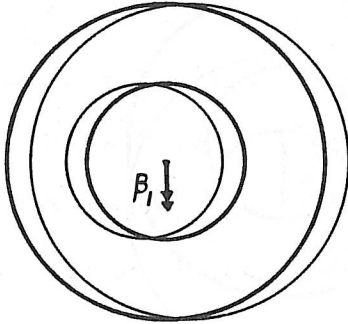


$$u = \beta_1 (s \sin \varphi_0 \cos \varphi_0 - r \cos \varphi_0) \sin \theta$$

$$v = \beta_1 s \cos \varphi_0 \cos \theta$$

$$w = \beta_1 (s \cos^2 \varphi_0 + r \sin \varphi_0) \sin \theta$$

e) Tilting  $\beta_1$

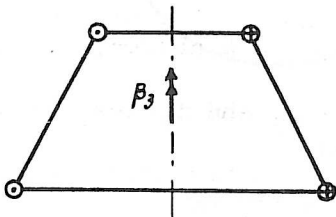
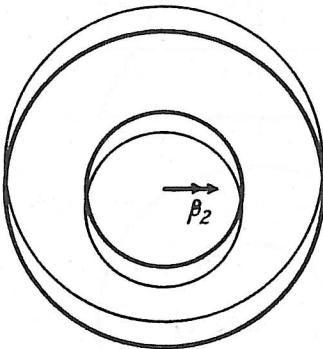


$$u = \beta_2 (s \sin \varphi_0 \cos \varphi_0 - r \cos \varphi_0) \cos \theta$$

$$v = \beta_2 s \cos \varphi_0 \cos \theta$$

$$w = \beta_2 (s \cos^2 \varphi_0 + r \sin \varphi_0) \cos \theta$$

f) Tilting  $\beta_2$



$$u = 0$$

$$v = \beta_3 r$$

$$w = 0$$

g) Rotation  $\beta_3$  About Revolution Axis

Fig. 1.1. Rigid Body Motions of a Conical Frustum.

introduced as in [56], [40], the rigid-body motions cease to be present except in the limit when the curved segments are so small as to be almost conical. This may require again many elements for deep shells and is even more disturbing in nonlinear theory when large rigid motions may be involved.

Yaghmai [12] and Sharifi [110] avoided the difficulty in the large axisymmetric deformations of elasto-plastic and sandwich shells by using a curved element but displacements measured along its chord; they also found that a cubic rather than a linear polynomial for  $u$  was desirable.

Stricklin [49] first showed that for a slope change of  $2^\circ$  or less the axial rigid motion could be considered as included in the curved element with linear  $u$  and cubic  $w$ . Later [76], he also acknowledged that cubic  $u$  and  $v$  were preferable to reasonably approximate the asymmetric rigid motions. His discussion is based on a comparison of the eigenvalues of the element stiffness matrix; they are representative of the energy associated with straining eigenmodes and should be zero for rigid modes. Nevertheless, he used trigonometric series along  $\theta$ , cubic  $w$  and linear  $u$ ,  $v$  along  $s$  in a series of papers dealing with large asymmetric deflections of shells of revolution [113, 114, 115, 116].

Several criticisms may be made of Stricklin's approach.

- a) Novozhilov's nonlinear strain-displacements and linear curvature-displacements were used; but some terms were dropped with the effect that some rigid body modes produce strains even if



these displacements are perfectly represented.

- b) Fourier expansions are effective in linear cases because trigonometric relationships make the coupling of the different terms in the series disappear when the stiffness matrix is formed by integration over the element area. In the nonlinear case, triple and quadruple products of trigonometric functions have to be integrated; the coupling does not disappear. Stricklin himself [114] confesses that "the numerical integration over the element involves many terms and requires 20,000 computer storage locations for the program statements alone," and that was at a time when he considered only third order trigonometric terms! Later he realized that fourth order terms were required especially in the vicinity of the buckling load and included them at the expense of further programming complexity [50].
- c) The rigid motions of the element of revolution are roughly those of a parallel circle of the shell. In some applications it is conceivable that important rotations occur within the element itself, for instance a twisting along the parallel direction (Fig. 1.2). In such a case, the use of a linearized curvature-displacements relationship becomes questionable.

Navaratna [92] also used the same kind of element in a non-linear analysis. But he chose the stability approach i.e. restricted himself to the study of buckling loads and modes and linearized the prebuckling state which allowed him to consider only third order trigonometric terms. Even so, a close

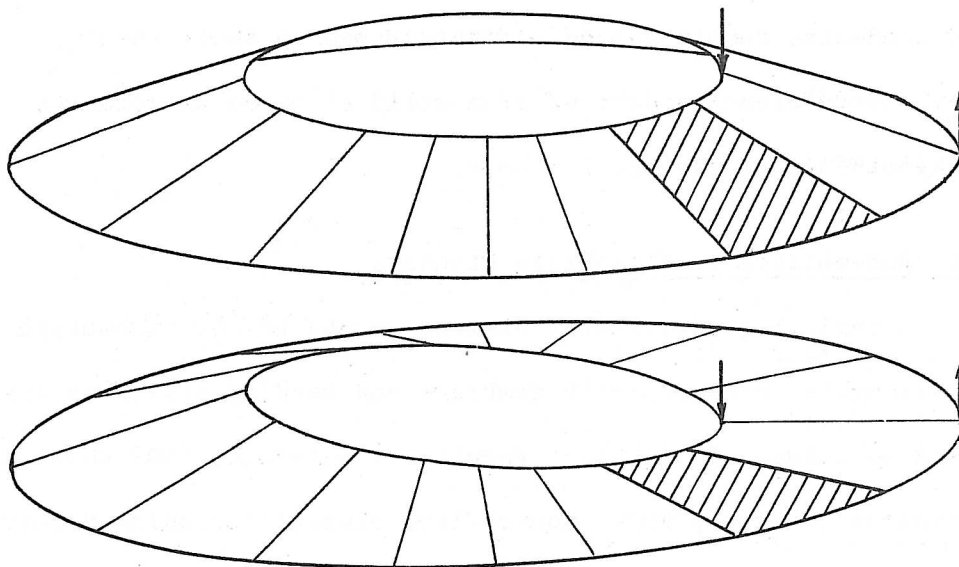


Fig. 1.2. Rigid Motion and Deformation Applied to a Conical Frustum or to a Quadrilateral Element.

examination of his work [91] reveals again the complex coding problems generated by the coupling of the Fourier terms.

### 1.5 Finite Elements for General Shells

Since the element of revolution leads to undesirable characteristics under large asymmetric deflections, the alternatives will now be considered. An extensive critical survey of general shell elements existing in 1969 was given by Gallagher [37] while a more limited review accompanied by numerical examples was given by Clough, Johnson in 1970 [20]. The most significant contribution since then were presented at the Third Conference on Matrix Methods in Structural Mechanics, 1971 [24], [38], [131].

The general shell elements used in the displacement method can be divided into three broad categories: assemblages of flat

plate elements, doubly curved elements based on shell theory, doubly curved elements derived from solid elements or relaxing some hypotheses of the shell theory.

#### 1.5.1 Assemblages of Flat Plate Elements

A typical quadrilateral element formed by the assemblage of four triangular elements with membrane and bending stiffness was devised by Johnson [20],[55]. Results of reference [20] show that it compares favorably with a more refined element including doubly curved triangles [112], [25]. In a version modified by Felippa it was even successfully applied to nonlinear dynamic problems [18].

The shortcomings of the flat plate models are:

- a) The behavior represented by the differential equation is not approached in the limit of refinement by the flat plate representation. Fulton et al. [35] indicate that this effect is of small magnitude.
- b) The discontinuities of slope between adjacent elements may introduce residual bending moments as already mentioned for the conical frustum.
- \* c) The rigid body modes are easily represented but lack of interelement compatibility of displacements may be expected.
- d) The effects of curvature in the form of the coupling of membrane and flexural behavior is lost in the interiors of the individual elements.

The last defect might prove crucial in a stability analysis. Anyway, it seems pointless to base a general refined nonlinear shell

analysis on an element which poorly approximates the geometry in the first place.

### 1.5.2 Curved Elements Based on Shell Theory

Gallagher's discussion of doubly curved shell elements [37] will not be repeated. Only a few characteristics and their importance in nonlinear shell analysis will be singled out.

Several rectangular [23], parallelogram [97], quadrilateral [24] or triangular [122], [112], [11] elements are based on shallow shell theory, either Marguerre's [75], Novozhilov's [94] or Reissner's [104]. Consequently, some aspects of the difference between the shell surface and its projection are neglected in the strain-displacement relationships. Even within the framework of the finite element theory, Argyris [7] strongly advises against using this kind of element to analyze deep shells; but Cooper, Lindberg [24] have recently devised a suitable transformation between the shallow shell degrees of freedom and those for the deep shell. The extension of these elements into the realm of large displacements has not been tested yet.

Doubly curved elements for deep shells seldom have midside or internal nodes; they generally differ from each other in the number of Degrees of Freedom\* at corner nodes which, after multiplication by the number of corners, is directly related to the order of the interpolation polynomials. Doubly curved triangles range from 36 DOF elements with incomplete quartic polynomial for  $w$  and complete cubic for  $u, v$  [24] to 63 DOF elements with

---

\*Later abbreviated as DOF.

complete quartic for  $u, v, w$  [7]. Doubly curved quadrilaterals may possess from 20 DOF with incomplete quartic for  $w$  and bilinear for  $u, v$  [23] to 48 DOF with bicubic polynomials for  $u, v, w$  [10]. Generally speaking, more DOF mean improved or perfect displacement compatibility and representation of rigid modes; but Argyris' SHEBA element [7], for instance, requires more than 2000 computer storage locations for one half element stiffness; the number of equations and corresponding bandwidth for a refined grid would be prohibitive for most of the available computer facilities, especially in a nonlinear analysis!

Except for specialized geometries like the cylinder, these curved elements only approximate the true shell, matching the coordinates, slopes and sometimes the curvature at the nodal points. This seems to be of little concern to the analysts, probably because there is already such an improvement over the idealization by an assemblage of flat plates.

Most of the doubly curved elements include the rigid-body motions only in an implicit manner, i.e. they are present in the limit when the grid is so refined that the finite element is almost flat. At the price of a loss of compatibility, the rigid motions have been explicitly introduced by Cantin [16, 17] in a 24 DOF rectangular element for cylindrical shell. This made the element superior to a similar one having twice as many DOF [10].

~~When the isoparametric concept is used, the element geometry and the displacement field are approximated by the same type of~~

interpolation functions and the rigid body modes are automatically included. This approach is useful when the middle surface described in a shell coordinate system ceases to be the most convenient system of reference; this happens in the third category of shell elements described hereafter but has been little used in the frame of classical shell theory.

To the author's knowledge, few of these doubly curved elements based on shell theory have been applied to geometrically nonlinear problems. Schmit, Bogner, Fox [108] studied finite deflections of curved panels. Gallagher studied the elastic stability of cylinders and shallow shells [40] using his first element, lacking compatibility and rigid modes, and the postbuckling behavior of a curved plate [38] using an extension of Bogner, Fox, Schmit element. Finally, Dupuis et al. [28] studied a shallow spherical cap under point load using a triangular element.

### 1.5.3 Curved Elements with Relaxed Shell Theory

Recently many authors have proposed to relax some of the Kirchhoff-Love hypothesis.

Wempner, Oden and Kross [126] derived a linear theory for the deformation of thin shells, including transverse shear deformation, in terms of the middle surface displacements and the rotations of normals to the middle surface. The advantage of this formulation is that the equilibrium equations of thin shells with transverse shear strains are a set of second order differential equations; the related minimum potential energy functional

requires only first derivatives in the unknown displacements to be evaluated; in the finite element method, this means that the element displacement assumptions need only provide continuous displacement fields (instead of continuous displacement and slopes as required with classical shell theory).

On the basis of this theory, Key [61, 62] has developed a successful 36 DOF quadrilateral element for shells of revolution, while Dhatt [25] concentrated on curved triangles with 27 DOF after static condensation.

A broader approach was taken by Ahmad, Irons, Zienkiewicz [1] in which a shell element with shear deformation is obtained by degenerating a three-dimensional solid element. Reference [1] and [96] show remarkably good results for shells of revolution with symmetric or asymmetric loading and general moderately thick to thin shells.

With the development of these degenerate three dimensional elements, it seems that one has come full circle: the Kirchhoff-Love hypotheses, which were originally introduced because one was unable to solve the three-dimensional problem, are dropped because this problem is now becoming tractable. Does this mean that the classical shell theory will disappear? Probably not because its foundation is a solid one for thin shells, where a three-dimensional approach may fail, and reasons of economy will always give the edge to a two-dimensional element over a three-dimensional one whenever equal accuracy is expected.

The nonlinear theory corresponding to this third category of shell elements is still in development. An element for large deformations of membranes [51] and another for large axisymmetric displacements of shells of revolution [70] are being tested in Berkeley, while Zienkiewicz and Nayak just published their first nonlinear results [130]. Much more can be expected along these lines in the future.

#### 1.6 Selection of a New Element

The experience gained by critically reviewing past attempts can now be used to select a new element well adapted to the present problem: a linear solution of shells of revolution nonsymmetrically loaded, susceptible of later extension in the field of large displacements.

The elements of revolution must use Fourier series in the asymmetric case; attempts to replace these by other functions, in particular by Hermite polynomials covering parts of the circumference were unsuccessful. If large deformations are expected, higher order strain must be used; these are known to introduce coupling of Fourier terms and almost insurmountable programming difficulties.

To solve geometrically nonlinear problems with finite elements, a special technique has been used frequently in frame problems [54]. It consists in dividing the element displacements into a rigid part and a deformation part. When the elements are small enough, this insures that the deformation displacements are small; less refined strain expressions can be used; most of the




geometric effects will be taken into account when the displaced element is reincorporated into the global structure. This technique was extended to plates by Murray [81, 82] and proposed, but not effectively used, for shells by Wempner [125]. Because so much deformation can occur within one element (see Fig. 1.2), it could not be applied with elements of revolution.

Therefore, elements of revolution are eliminated and the search is restricted to triangular or quadrilateral elements.

Assemblages of flat plates are inconsistent with the level of refinement expected from a nonlinear solution; they are not considered.

The elements including shear deformations are not considered either although this decision is much harder to justify. The primary goal of solving thin shells is one reason; the lack of a nonlinear theory for these elements straddling the fence between shell and three-dimensional theory was certainly another at the time of the choice. By contrast, with classical shells, the trouble would rather be a plethora of theories!

Among the doubly curved elements, the best having a reasonable number of DOF seem to be Cowper's triangle with 36 DOF [24] and Bogner et al. quadrilateral [108] with 48 DOF generalized by Gallagher [38]. Both of them give compatible displacements but do not include explicit rigid body modes.

 Nonlinear shell theories are less complex when the curvilinear coordinates coincide with principal lines of curvatures. These are easiest to find in shells of revolution: they are the

meridian lines and parallel circles. For these reasons, the quadrilateral element with edges cut along parallels and meridian lines is preferred.

If the element is to be used in a nonlinear problem, where the structural system is going to be solved again and again, it is very important to limit the number of DOF, and 48 is a pretty high number of DOF for one element.

In the case of a cylindrical shell element, Cantin [17] simplified Bogner's element by using bilinear instead of bicubic polynomials for u and v, which reduced the DOF to 24. But he also added, and condensed out, explicit rigid body modes. Since his element was successful, the same approach will be attempted here.

#### 1.7 Summary of the New Element Development

In Chapter 2, Sanders' strain-displacement relationships in convected coordinates will be established and specialized to shells of revolution. Effects of small and large rigid-body displacements will be considered in Sanders' expressions and a few other shell theories of frequent use.

In Chapter 3, the stiffness matrix of the selected doubly curved quadrilateral element for shells of revolution will be established. The number of Gaussian points necessary for numerical integration will be experimentally determined.

The element gives compatible displacements but lacks rigid body modes; if the rigid modes are introduced, it ceases to give compatible displacements. The relative importance of

compatibility and rigid modes is still a subject of controversy and it is impossible to decide a priori which one of the two alternatives hereabove is best. This question will be settled in Chapters 4 and 5.

A general procedure to find which rigid modes should be added and how to add them will be presented in Chapter 4 and demonstrated on a circular plate, cylindrical, conical, spherical and toroidal shells.

Different examples with predominant membrane or bending states, with symmetric or asymmetric deflections, with or without rigid modes, will finally be solved in Chapter 5 to evaluate the general behavior of the element and assess the effect of rigid modes.

## 2. STRAIN-DISPLACEMENT RELATIONSHIPS

### 2.1 Geometrical Preliminary

#### 2.1.1 Some Results from the Geometry of Euclidean Space

Let  $Z^I$  ( $I=1,2,3$ ) refer to a fixed right-handed orthogonal Cartesian system in a Euclidean three-dimensional space and let  $X^I$  denote an arbitrary curvilinear coordinate system defined by the transformation

$$Z^I = Z^I(X^J). \quad (2.1)$$

Denoting by  $\underline{Q}$  the position vector of a generic point with coordinates  $X^I$ , the square of a line element is given by

$$\underline{dQ} \cdot \underline{dQ} = G_{IJ} dX^I dX^J \quad (2.2)$$

where

$$\underline{G}_I = \underline{Q}_{,I} \quad , \quad G_{IJ} = \underline{G}_I \cdot \underline{G}_J \quad (2.3)$$

represent the covariant base vectors and the metric tensor respectively, and the comma indicates partial differentiation.

The reciprocal, contravariant base vectors  $\underline{G}^I$  and the conjugate tensor  $G^{IJ}$  are defined by

$$\underline{G}^I = G^{IJ} \underline{G}_J \quad , \quad G^{IJ} = G^{JI} = \underline{G}^I \cdot \underline{G}^J = \frac{\underline{g}^{JI}}{G} \quad (2.4)$$

where  $\underline{g}^{JI}$  are the cofactors of  $G_{IJ}$  in the expansion of the determinant  $G = |G_{IJ}|$ .

The Christoffel symbols of the first and second kinds, defined by

$$\Gamma_{IJK} = G_{LK} \Gamma_{IJ}^L = \frac{1}{2} (G_{IK,J} + G_{JK,I} - G_{IJ,K}) \quad , \quad (2.5)$$

may, in view of (2.3), also be expressed as

$$\Gamma_{IJK} = \underline{G}_K \cdot \underline{G}_{I,J} \quad , \quad \Gamma_{JK}^I = \underline{G}^I \cdot \underline{G}_{J,K} \quad (2.6)$$

and hence

$$\underline{G}_{I,J} = \Gamma_{IJ}^K \underline{G}_K . \quad (2.7)$$

The covariant differentiation will be designated by a stroke ( $|$ ).

As an example, the covariant derivative of a mixed tensor of second rank  $T_J^I$  is defined by

$$T_{J|K}^I = T_{J,K}^I + \Gamma_{LK}^J T_J^I - \Gamma_{JK}^L T_L^I . \quad (2.8)$$

### 2.1.2 Some Results from the Geometry of a Surface

Let  $X^I$  be identified with a set of normal coordinates in a Euclidean three-dimensional space (Fig. 2.1, page 31) so that the position vector  $\underline{Q}$  now assumes the form

$$\underline{Q} = \underline{P}(X^1, X^2) + X^3 \underline{A}_3(X^1, X^2) \equiv \underline{P}(X^1, X^2) + Z \underline{N}(X^1, X^2) \quad (2.9)$$

subject to the restriction

$$\underline{Q}_{,A} \cdot \underline{A}_3 \equiv \underline{Q}_{,A} \cdot \underline{N} = 0 \quad , \quad \underline{A}_3 \cdot \underline{A}_3 \equiv \underline{N} \cdot \underline{N} = 1 . \quad (2.10)$$

In what follows, Greek capital indices A, B,  $\Gamma$  will have the range 1, 2, while Latin indices will continue to assume the range 1, 2, 3. Thus, for the space of normal coordinates defined by (2.9) and (2.10), the base vectors and the components of the metric tensor are

$$\underline{G}_A = \underline{Q}_{,A} = \underline{P}_{,A} + X^3 \underline{A}_{3,A} \equiv \underline{P}_{,A} + Z \underline{N}_{,A} \quad , \quad \underline{G}_3 = \underline{A}_3 \equiv \underline{N} \quad , \quad (2.11)$$

$$\underline{G}_{AB} = \underline{G}_A \cdot \underline{G}_B \quad , \quad \underline{G}_{A3} = 0 \quad , \quad \underline{G}_{33} = 1 \quad . \quad (2.12)$$

The equation  $X^3 \equiv Z = 0$  defines a surface whose position vector is  $\underline{P}$ . If one introduces the notation

$$\underline{A}_A = \underline{P}_{,A} = \underline{G}_A(X^B, 0) \quad , \quad (2.13)$$

one has, from (2.10),

$$\underline{A}_A \cdot \underline{A}_3 \equiv \underline{A}_A \cdot \underline{N} = 0 \quad , \quad \underline{A}_{3,A} \cdot \underline{A}_3 = \underline{N}_{,A} \cdot \underline{N} = 0 \quad (2.14)$$

the first of which reveals that  $\underline{A}_3$  is perpendicular to the surface

$X^3 = Z = 0$  at every point:  $\underline{A}_3$  is the unit normal to the surface defined by  $\underline{P}$  (hence the notation  $\underline{N}$  used in parallel with  $\underline{A}_3$ ). The  $X^1$  and  $X^2$  coordinate curves form a system of curvilinear coordinates on this surface whose metric and conjugate tensors are given by

$$A_{AB} = A_{BA} = \underline{A}_A \cdot \underline{A}_B, \quad (2.15)$$

$$A^{AB} = \underline{A}^A \cdot \underline{A}^B = \frac{A^{BA}}{A}. \quad (2.16)$$

The square of a line element on the surface  $X^3 \equiv Z = 0$ , called the first fundamental form of the surface, is given by

$$d\underline{P} \cdot d\underline{P} = A_{AB} dX^A dX^B. \quad (2.17)$$

The second fundamental form is defined by the scalar product

$$d\underline{P} \cdot d\underline{N} = -B_{AB} dX^A dX^B \quad (2.18)$$

where, by (2.13) and (2.14),

$$B_{AB} = B_{BA} = -\underline{A}_A \cdot \underline{N}_{,B} = \underline{N} \cdot \underline{A}_{,B}. \quad (2.19)$$

The covariant derivative with respect to the surface metric will be designated by double strokes ( $\parallel$ ); when applied to a surface tensor such as  $T_B^A$ , it reads

$$T_B^A \parallel_{\Gamma} = T_{B,\Gamma}^A + \Gamma_{\Gamma\Lambda}^A T_B^\Lambda - \Gamma_{B\Gamma}^\Lambda T_\Lambda^A \quad (2.20)$$

with the surface Christoffel symbols given by

$$\Gamma_{B\Gamma}^A = \underline{A}^A \cdot \underline{A}_{B,\Gamma}, \quad \Gamma_{AB\Gamma} = \underline{A}_A \cdot \underline{A}_{B,\Gamma}. \quad (2.21)$$

The second fundamental form also satisfies the formulas of Gauss, Weingarten and Codazzi

$$\underline{A}_A \parallel_B = \underline{A}_{A,B} - \Gamma_{AB}^\Lambda \underline{A}_\Lambda = B_{AB} \underline{A}_3, \quad (2.22)$$

$$\underline{N} \parallel_A = \underline{N}_{,A} = -B_A^B \underline{A}_B, \quad (2.23)$$

$$B_{AB} \parallel_\Gamma = B_{A\Gamma} \parallel_B. \quad (2.24)$$

When the surface coordinates are orthogonal, the curvatures and surface torsion along the coordinate lines are equal to the physical components of the second fundamental form

$$B'_1 = \frac{B_{11}}{A_{11}} = -\frac{1}{R_1} \quad , \quad B'_2 = \frac{B_{22}}{A_{22}} = -\frac{1}{R_2} \quad , \quad (2.25)$$

$$\sqrt{\frac{A_{11}}{A_{22}}} B'_2 = \sqrt{\frac{A_{22}}{A_{11}}} B'_1 = -\frac{1}{T} \quad . \quad (2.26)$$

## 2.2 Nonlinear Strains

### 2.2.1 Exact Derivation

Let  $\underline{Q}$  be the position vector of an arbitrary point  $Q$  in the undeformed shell space (Fig. 2.1). Under the influence of external loads, the shell occupies a new configuration defined by a displacement field  $\underline{v}$ . The position of  $Q$  in the deformed state is labelled  $q$ ; it is described by the position vector

$$\underline{q} = \underline{Q} + \underline{v} \quad . \quad (2.27)$$

The squares of the length of differential elements at  $Q$  and  $q$  are given by

$$dS^2 = G_{IJ} dX^I dX^J \quad I, J = 1, 2, 3 \quad (2.28)$$

$$ds^2 = g_{ij} dx^i dx^j \quad i, j = 1, 2, 3 \quad (2.29)$$

where  $G_{IJ}$  and  $g_{ij}$  are the metric of the undeformed and deformed space, respectively.

When the Lagrangian point of view is adopted, the deformation is described by the Almansi strain tensor  $E_{IJ}$ ,

$$ds^2 - dS^2 = 2 E_{IJ} dX^I dX^J \quad , \quad (2.30)$$

from which it follows that

$$2 E_{IJ} = g_{ij} \frac{\partial x^i}{\partial X^I} \frac{\partial x^j}{\partial X^J} - G_{IJ} \quad . \quad (2.31)$$

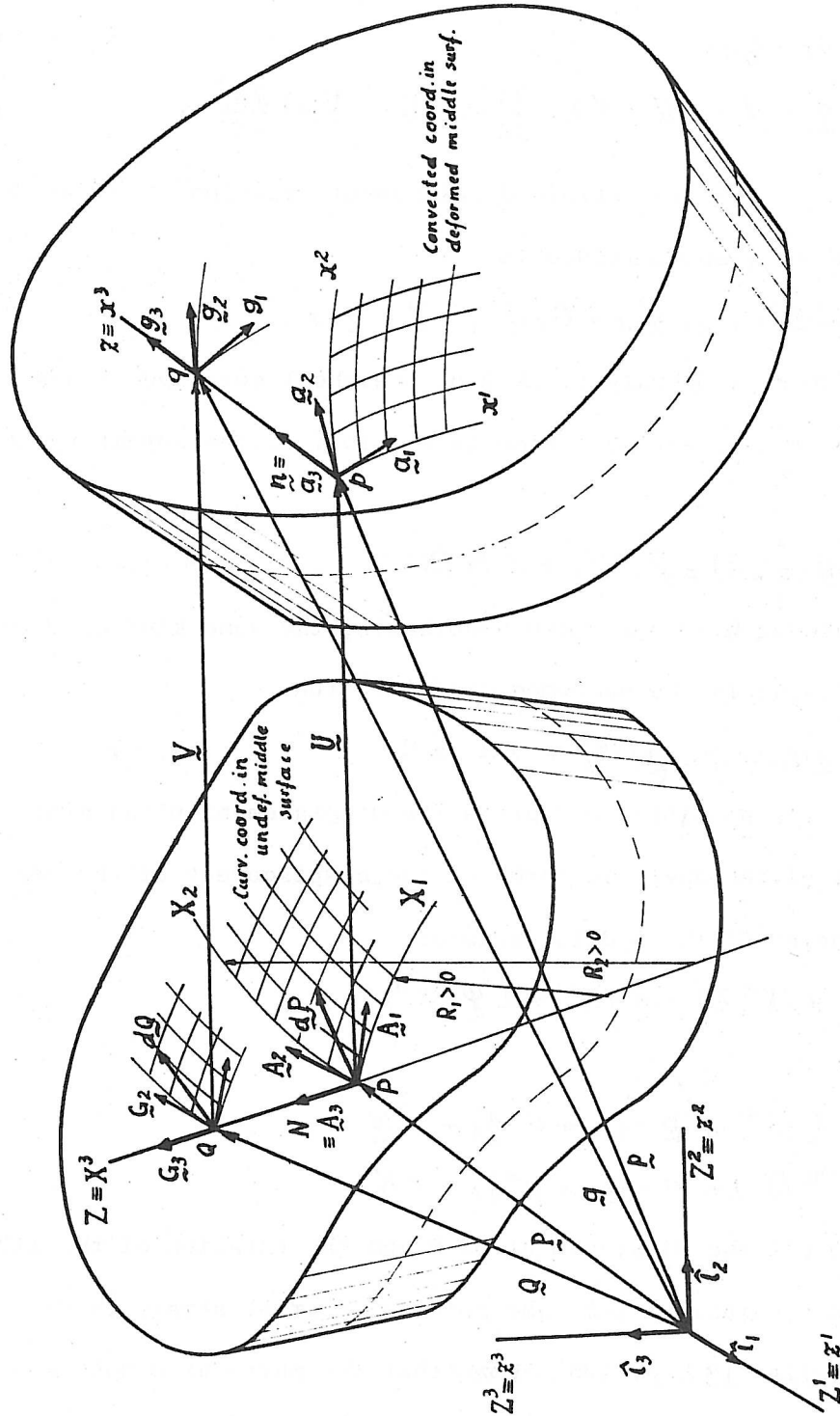


Fig. 2.1. Undeformed and Deformed Shell Space.



Using the definition of base vectors,

$$\underline{G}_I = \underline{Q}_{,I} \quad (2.32)$$

$$\underline{g}_i = \underline{q}_{,i} = (\underline{Q} + \underline{V})_{,I} \frac{\partial X^I}{\partial x^i} = (\underline{G}_I + \underline{V}_{,I}) \frac{\partial X^I}{\partial x^i}, \quad (2.33)$$

in Eq. (2.31), the strain-displacement relations for the three-dimensional space reduce to

$$2 E_{IJ} = \underline{G}_I \cdot \underline{V}_{,J} + \underline{G}_J \cdot \underline{V}_{,I} + \underline{V}_{,I} \cdot \underline{V}_{,J}. \quad (2.34)$$

To an arbitrary point Q of the shell corresponds a point P on the middle surface which is the foot of the normal to it through Q:

$$\underline{Q}(X^A, Z) = \underline{P}(X^A) + Z \underline{N}(X^A) \quad A = 1, 2. \quad (2.35)$$

Because of Kirchhoff-Love hypothesis, the same kind of relation holds true in the deformed configuration:

$$\underline{q}(x^\alpha, z) = \underline{p}(x^\alpha) + z \underline{n}(x^\alpha) \quad \alpha = 1, 2 \quad (2.36)$$

and it is possible to express the displacement of an arbitrary point of the shell in terms of the displacement of the corresponding point of the middle surface:

$$\underline{V}(X^A, Z) = \underline{U}(X^A) + Z \underline{\Psi}(X^A) \quad (2.37)$$

where

$$\underline{U}(X^A) = \underline{p} - \underline{P} = U^A \underline{A}_A + W \underline{N} \quad (2.38)$$

$$\underline{\Psi}(X^A) = \underline{n} - \underline{N} = \psi^A \underline{A}_A + \varphi \underline{N} \quad (2.39)$$

represent the displacement of P and the rotation of the middle surface normal at the same point. In small strain theory, Novozhilov [93, p. 195] shows that the physical components of  $\underline{\Psi}$  can be related to the direction cosines of that fiber of the shell in the strained state which, in the unstrained state, was normal to the middle surface.

Substituting (2.35) into (2.32), the expressions for the base vectors reduce to

$$\underline{G}_A = (\delta_A^B - Z B_A^B) \underline{A}_B \quad (2.40)$$

$$\underline{G}_3 = \underline{N} \quad (2.41)$$

where  $B_{AB}$  is the metric of the second fundamental form of the undeformed shell space

Using results established in the theory of surfaces, the derivatives of the displacement vectors are found to be

$$\begin{aligned} \underline{V}_{,A} = & \left\{ (U^B \parallel_A - W B_A^B) + Z (\psi^B \parallel_A - \psi B_A^B) \right\} \underline{A}_B \\ & + \left\{ (W_{,A} + B_{\Gamma A} U^\Gamma) + Z (\psi_{,A} + B_{\Gamma A} \psi^\Gamma) \right\} \underline{N} \end{aligned} \quad (2.42)$$

$$\underline{V}_{,3} = \psi^A \underline{A}_A + \psi N \quad (2.43)$$

Substituting from Eqs. (2.40) to (2.43) into (2.34) and rearranging, the strain-displacement relations for the shell reduce to

$$2E_{AB} = 2\hat{E}_{AB} + 2Z K_{AB} + \text{terms in } Z^2 \quad (2.44)$$

$$2E_{3A} = [\psi_A + \psi_B \epsilon_A^B + (1+\psi)\epsilon_A^3] + Z [A^{B\Gamma} \psi_B \psi_\Gamma \parallel_A + (1+\psi)\psi_{,A}] \quad (2.45)$$

$$2E_{33} = (1+\psi)^2 + A^{AB} \psi_A \psi_B - 1 \quad (2.46)$$

where

$$2\hat{E}_{AB} = U_A \parallel_B + U_B \parallel_A - 2B_{AB} W + A_{\Gamma\Delta} \epsilon_A^\Gamma \epsilon_B^\Delta + \epsilon_A^3 \epsilon_B^3 \quad (2.47)$$

$$\begin{aligned} 2K_{AB} = & (\psi_A \parallel_B + \psi_B \parallel_A) - 2B_{AB} \psi - B_{\Gamma A} \epsilon_B^\Gamma - B_{\Gamma B} \epsilon_A^\Gamma \\ & + \epsilon_A^3 (\psi_{,B} + B_B^\Gamma \psi_\Gamma) + \epsilon_B^3 (\psi_{,A} + B_A^\Gamma \psi_\Gamma) \\ & + \epsilon_A^\Gamma (\psi_\Gamma \parallel_B - B_{\Gamma B} \psi) + \epsilon_B^\Gamma (\psi_\Gamma \parallel_A - B_{\Gamma A} \psi) \end{aligned} \quad (2.48)$$

$$\epsilon_A^\Gamma = U^\Gamma \parallel_A - B_A^\Gamma W \quad (2.49)$$

$$\epsilon_A^3 = B_{\Gamma A} U^\Gamma + W_{,A} \quad (2.50)$$

The first two quantities represent the middle surface or membrane strains and the middle surface changes of curvature or bending

strains, respectively. In convected coordinates, they can be interpreted as the changes of the first and second fundamental forms of the surface between the deformed and undeformed state:

$$2 \dot{E}_{AB} = a_{\alpha\beta} \frac{\partial x^\alpha}{\partial X^A} \frac{\partial x^\beta}{\partial X^B} - A_{AB} \quad (2.51)$$

$$-2K_{AB} = b_{\alpha\beta} \frac{\partial x^\alpha}{\partial X^A} \frac{\partial x^\beta}{\partial X^B} - B_{AB} \quad (2.52)$$

The mathematical statement of the Kirchhoff-Love hypothesis is now used to find the components of  $\underline{\Psi}$  in terms of the components of  $\underline{U}$ . The conservation of the normal in direction and length gives

$$E_{31} = E_{32} = E_{33} = 0 \quad (2.53)$$

i.e., with results (2.45) and (2.46),

$$(\delta_A^B + \varepsilon_A^B) \Psi_B + (1 + \Psi) \varepsilon_A^3 = 0 \quad (2.54)$$

$$(1 + \Psi)^2 + A^{AB} \Psi_A \Psi_B - 1 = 0 \quad (2.55)$$

Equation (2.54) can be solved for  $\Psi_A$  in terms of  $(1 + \Psi)$ :

$$\Psi_A = \frac{\alpha_A^3}{\alpha_3^3} (1 + \Psi) \quad (2.56)$$

where

$$\alpha_1^3 = \varepsilon_1^2 \varepsilon_2^3 - \varepsilon_1^3 (1 + \varepsilon_2^2) \quad (2.57)$$

$$\alpha_2^3 = \varepsilon_2^1 \varepsilon_1^3 - \varepsilon_2^3 (1 + \varepsilon_1^1) \quad (2.58)$$

$$\alpha_3^3 = (1 + \varepsilon_1^1)(1 + \varepsilon_2^2) - \varepsilon_2^1 \varepsilon_1^2 \quad (2.59)$$

Substituting into (2.55) and rearranging, one gets

$$1 + \Psi = \frac{\alpha_3^3}{\sqrt{(\alpha_3^3)^2 + A^{AB} \alpha_A^3 \alpha_B^3}} \quad (2.60)$$

Notice that in (2.47) the first three terms are linear in the displacements, all the others are quadratic. Although further simplifications are theoretically possible, the finite membrane strains can be used in their present form. On the other hand, an exact computation of bending strains would require the evaluation of  $\epsilon_B^A$  and  $\epsilon_A^3$  by (2.49) and (2.50),  $\alpha$ 's by (2.57) to (2.59),  $\psi$  and  $\psi_A$  by (2.60) and (2.56); finally, all these intermediate quantities should be introduced in (2.48); it is almost unfeasible and simplifications are desirable.

### 2.2.2 Small Strain Approximations

Small strains lead to two approximations.

The first one is to neglect the change in volume. It can be shown (see, for instance, [93], page 191) that the denominator in (2.60) is equal to the ratio of surface metric determinants after and before deformation. Hence,

$$\sqrt{(\alpha_3^3)^2 + A^{AB} \alpha_A^3 \alpha_B^3} \simeq \sqrt{A} \simeq 1 \quad (2.61)$$

$$1 + \Psi \simeq \alpha_3^3 \quad (2.62)$$

$$\Psi_A \simeq \alpha_A^3 \quad (2.63)$$

The second approximation is to neglect the strains with respect to the metric, i.e.

$$G_{IJ} + 2 E_{IJ} \simeq G_{IJ} \quad (2.64)$$

This leads to a series of approximate relationships between  $\epsilon_B^A$ ,  $\epsilon_A^3$ ,  $\psi_A$ ,  $\psi$ ; they are given by Mushtari [83, page 19] and, with indicial notations, by Sanders [107, page 29].

Simplifications are also obtained if orthogonal curvilinear coordinates are chosen, not necessarily along the lines of principal curvature.

These approximations and simplifications do not affect the membrane strains. But, after steps not reproduced here, the bending strains become

$$2K_{AB} = B_{\Gamma A} \varepsilon_B^{\Gamma} - B_{\Gamma B} \varepsilon_A^{\Gamma} + \varepsilon_{A,B}^3 (1 + \psi) - \varepsilon_A^{\Gamma} \parallel_B \Psi_{\Gamma} . \quad (2.65)$$

To show off the real complexity hidden behind the indicial notations, consider a conical frustum with slope  $\varphi$ , parallel radius  $r$ , curvilinear coordinates  $s$  along the meridian and  $\theta$  along the parallel; the curvature change along the  $\theta$  coordinate line is:

$$\begin{aligned} 2K_{22} = & -r \cos \varphi \frac{\partial U'}{\partial s} \\ & + \left( \frac{\partial^2 W}{\partial \theta^2} - \frac{\partial U^2}{\partial \theta} \right) \left\{ \left( 1 + \frac{\partial U'}{\partial s} \right) \left[ 1 + \frac{1}{r} (U' \sin \varphi + W \cos \varphi) + \frac{\partial U^2}{\partial \theta} \right] \right. \\ & \quad \left. - \left( \frac{\partial U^2}{\partial s} + \frac{1}{r} U^2 \sin \varphi \right) \left( \frac{\partial U'}{\partial \theta} - U^2 r \sin \varphi \right) \right\} \\ & + \left[ \frac{\partial^2 U'}{\partial \theta^2} - \sin \varphi (r + U' \sin \varphi + W \cos \varphi) \right] \left\{ \left( \frac{\partial U^2}{\partial s} + \frac{1}{r} U^2 \sin \varphi \right) \left( \frac{\partial W}{\partial \theta} - U^2 r \cos \varphi \right) \right. \\ & \quad \left. - \left[ 1 + \frac{1}{r} (U' \sin \varphi + W \cos \varphi) + \frac{\partial W}{\partial \theta} \right] \frac{\partial W}{\partial s} \right\} \\ & + \left[ \frac{\partial^2 U^2}{\partial \theta^2} + \frac{\sin \varphi}{r} \left( \frac{\partial U'}{\partial \theta} - U^2 r \sin \varphi \right) + \left( \frac{\sin \varphi}{r} \frac{\partial U'}{\partial \theta} + \frac{\cos \varphi}{r} \frac{\partial W}{\partial \theta} \right) \right] \\ & \quad \left\{ \left( \frac{\partial U'}{\partial \theta} - U^2 r \sin \varphi \right) \frac{\partial W}{\partial s} - \left( 1 + \frac{\partial U'}{\partial s} \right) \left( \frac{\partial W}{\partial s} - U^2 r \cos \varphi \right) \right\} . \quad (2.66) \end{aligned}$$

And a conical frustum must be considered as a simple type of shell! Nevertheless, this is the kind of formula that should theoretically be used if a conical element of revolution is expected to undergo an important twisting as shown on Fig. 1.2.

### 2.2.3 Linearized Curvature Changes

If one retains linear terms only, the membrane strains

(2.47) becomes

$$2\overset{\circ}{E}_{AB} = U_A \parallel_B + U_B \parallel_A - 2B_{AB}W. \quad (2.67)$$

If one uses the small strain results (2.62) and (2.63) and drops all nonlinear terms in (2.57), (2.58) and (2.48), the bending strains reduce to

$$2K_{AB} = -(\varepsilon_A^3 \parallel_B + \varepsilon_B^3 \parallel_A) - 2B_{AB}A^{\Gamma\Delta}\varepsilon_{\Delta\Gamma} - B_A^\Gamma \varepsilon_{\Gamma B} - B_B^\Gamma \varepsilon_{\Gamma A}. \quad (2.68)$$

Let

$$2\omega_{AB} = U_B \parallel_A - U_A \parallel_B. \quad (2.69)$$

One can rewrite  $\varepsilon_{AB}$  in terms of  $\omega_{AB}$  and the linearized  $\overset{\circ}{E}_{AB}$ :

$$\varepsilon_{AB} = \frac{1}{2}(U_A \parallel_B + U_B \parallel_A - 2B_{AB}W) + \frac{1}{2}(U_A \parallel_B - U_B \parallel_A) = \overset{\circ}{E}_{AB} + \omega_{BA}. \quad (2.70)$$

Then,

$$\boxed{-2K_{AB} = \varepsilon_A^3 \parallel_B + \varepsilon_B^3 \parallel_A + B_A^\Gamma \omega_{B\Gamma} + B_B^\Gamma \omega_{A\Gamma}} \quad (2.71)$$

$$-B_{AB}A^{\Gamma\Delta}\overset{\circ}{E}_{\Delta\Gamma} - B_A^\Gamma \overset{\circ}{E}_{\Gamma B} - B_B^\Gamma \overset{\circ}{E}_{\Gamma A}.$$

Koiter-Sanders' linearized changes of curvature are identical to the first line of the present result; both authors consider as negligible the additional terms of the second line. Koiter, who is only interested in a consistent linear theory, systematically drops the terms of order "strain over curvature radius." Sanders neglects  $A^{\Gamma\Delta} \overset{\circ}{E}_{\Delta\Gamma}$  with respect to unity when the "small strain" hypothesis is introduced; he neglects  $\overset{\circ}{E}_{AB}$  with respect to  $\omega_{BA}$  in (2.70) in his "small strains, moderately large rotations" theory.

### 2.2.4 Physical Components of Strains

For practical computations, covariant and contravariant tensor components should be replaced by their physical equivalent. In oblique coordinates, there is no consensus about what are the physical components. But, if an orthogonal basis is chosen, the physical components of a vector or tensor are respectively defined as

$$V_{\langle I \rangle} = V^I \sqrt{G_{II}} = V_I \sqrt{G^{II}} = \frac{V_I}{\sqrt{G_{II}}} \quad , \text{ (no sum) } \quad (2.72)$$

$$T_{\langle IJ \rangle} = T^{IJ} \sqrt{G_{II} G_{JJ}} = T_J^I \sqrt{\frac{G_{II}}{G_{JJ}}} = \frac{T_{IJ}}{\sqrt{G_{II} G_{JJ}}} \quad . \text{ (no sum) } \quad (2.73)$$

Special notations are introduced for the displacements and the rotation about the normal

$$u = U_{\langle 1 \rangle} \quad , \quad v = U_{\langle 2 \rangle} \quad , \quad w = W \quad , \quad (2.74)$$

$$\omega = \Omega_{\langle 12 \rangle} \quad . \quad (2.75)$$

For the physical components of the curvature tensor, one has previously written

$$B_{\langle 11 \rangle} = B_1' = -\frac{1}{R_1} \quad , \quad B_{\langle 22 \rangle} = B_2^2 = -\frac{1}{R_2} \quad , \quad (2.25)$$

$$B_{\langle 12 \rangle} = \sqrt{\frac{A_{11}}{A_{22}}} B_2' = \sqrt{\frac{A_{22}}{A_{11}}} B_1^2 = -\frac{1}{T} \quad , \quad (2.26)$$

where  $R_1$ ,  $R_2$  and  $T$  are the principal radii of curvature and torsion of the middle surface along the orthogonal coordinate lines.

With an orthogonal basis,

$$A_{12} = A_{21} = A^{12} = A^{21} = 0$$

$$A = A_{11} A_{22}$$

$$A'' = \frac{1}{A_{11}} \quad , \quad A^{22} = \frac{1}{A_{22}} \quad (2.76)$$

and the only nonzero Christoffel symbols reduce to

$$\begin{aligned}\Gamma_{11}^1 &= \frac{1}{\sqrt{A_{11}}} \frac{\partial \sqrt{A_{11}}}{\partial X^1}, & \Gamma_{22}^2 &= \frac{1}{\sqrt{A_{22}}} \frac{\partial \sqrt{A_{22}}}{\partial X^2}, \\ \Gamma_{12}^1 &= \frac{1}{\sqrt{A_{11}}} \frac{\partial \sqrt{A_{11}}}{\partial X^2}, & \Gamma_{21}^1 &= \frac{1}{\sqrt{A_{22}}} \frac{\partial \sqrt{A_{22}}}{\partial X^1}, \\ \Gamma_{11}^2 &= -\frac{\sqrt{A_{11}}}{A_{22}} \frac{\partial \sqrt{A_{11}}}{\partial X^2}, & \Gamma_{22}^1 &= -\frac{\sqrt{A_{22}}}{A_{11}} \frac{\partial \sqrt{A_{22}}}{\partial X^1}.\end{aligned}\quad (2.77)$$

When results and new notations (2.74) to (2.77) are brought into (2.49), (2.50) and (2.47), one finds for the nonlinear strains

$$\epsilon_{\langle 11 \rangle} = \frac{1}{\sqrt{A_{11}}} \frac{\partial u}{\partial X^1} + \frac{v}{\sqrt{A}} \frac{\partial \sqrt{A_{11}}}{\partial X^2} - \frac{w}{R_1} \quad (2.78)$$

$$\epsilon_{\langle 21 \rangle} = \frac{1}{\sqrt{A_{11}}} \frac{\partial v}{\partial X^1} - \frac{u}{\sqrt{A}} \frac{\partial \sqrt{A_{11}}}{\partial X^2} - \frac{w}{T} \quad (2.79)$$

$$\epsilon_{\langle 31 \rangle} = -\frac{1}{\sqrt{A_{11}}} \frac{\partial w}{\partial X^1} + \frac{u}{R_1} + \frac{v}{T} \quad (2.80)$$

$$\epsilon_{\langle 12 \rangle} = \frac{1}{\sqrt{A_{22}}} \frac{\partial u}{\partial X^2} - \frac{v}{\sqrt{A}} \frac{\partial \sqrt{A_{22}}}{\partial X^1} - \frac{w}{T} \quad (2.81)$$

$$\epsilon_{\langle 22 \rangle} = \frac{1}{\sqrt{A_{22}}} \frac{\partial v}{\partial X^2} + \frac{u}{\sqrt{A}} \frac{\partial \sqrt{A_{22}}}{\partial X^1} - \frac{w}{R_2} \quad (2.82)$$

$$\epsilon_{\langle 32 \rangle} = -\frac{1}{\sqrt{A_{22}}} \frac{\partial w}{\partial X^2} + \frac{v}{R_2} + \frac{u}{T} \quad (2.83)$$

$$\begin{aligned}2E_{\langle 11 \rangle} &= 2\epsilon_{\langle 11 \rangle} + 2\eta_{\langle 11 \rangle} \\ &= 2\epsilon_{\langle 11 \rangle} + \epsilon_{\langle 11 \rangle} \epsilon_{\langle 11 \rangle} + \epsilon_{\langle 21 \rangle} \epsilon_{\langle 21 \rangle} + \epsilon_{\langle 31 \rangle} \epsilon_{\langle 31 \rangle}\end{aligned}\quad (2.84)$$

$$\begin{aligned}2E_{\langle 22 \rangle} &= 2\epsilon_{\langle 22 \rangle} + 2\eta_{\langle 22 \rangle} \\ &= 2\epsilon_{\langle 22 \rangle} + \epsilon_{\langle 12 \rangle} \epsilon_{\langle 12 \rangle} + \epsilon_{\langle 22 \rangle} \epsilon_{\langle 22 \rangle} + \epsilon_{\langle 32 \rangle} \epsilon_{\langle 32 \rangle}\end{aligned}\quad (2.85)$$

$$\begin{aligned}E_{\langle 12 \rangle} + E_{\langle 21 \rangle} &= \epsilon_{\langle 12 \rangle} + \epsilon_{\langle 21 \rangle} + \eta_{\langle 12 \rangle} + \eta_{\langle 21 \rangle} \\ &= \epsilon_{\langle 12 \rangle} + \epsilon_{\langle 21 \rangle} + \epsilon_{\langle 11 \rangle} \epsilon_{\langle 21 \rangle} + \epsilon_{\langle 21 \rangle} \epsilon_{\langle 22 \rangle} + \epsilon_{\langle 31 \rangle} \epsilon_{\langle 32 \rangle}.\end{aligned}\quad (2.86)$$



The linearized changes of curvature become

$$\frac{2\omega}{\sqrt{A}} = \frac{1}{\sqrt{A_{11}}} \frac{\partial v}{\partial X^1} + \frac{v}{\sqrt{A}} \frac{\partial \sqrt{A_{22}}}{\partial X^1} - \frac{1}{\sqrt{A_{22}}} \frac{\partial u}{\partial X^2} - \frac{u}{\sqrt{A}} \frac{\partial \sqrt{A_{11}}}{\partial X^2} \quad (2.87)$$

$$-2\mathcal{K}_{\langle 11 \rangle} = \frac{1}{\sqrt{A_{11}}} \frac{\partial \varepsilon_{\langle 31 \rangle}}{\partial X^1} - \frac{\varepsilon_{\langle 32 \rangle}}{\sqrt{A}} \frac{\partial \sqrt{A_{11}}}{\partial X^2} - \frac{1}{T} \frac{\omega}{\sqrt{A}} \quad (2.88)$$

$$-2\mathcal{K}_{\langle 22 \rangle} = \frac{1}{\sqrt{A_{22}}} \frac{\partial \varepsilon_{\langle 32 \rangle}}{\partial X^2} - \frac{\varepsilon_{\langle 31 \rangle}}{\sqrt{A}} \frac{\partial \sqrt{A_{22}}}{\partial X^1} + \frac{1}{T} \frac{\omega}{\sqrt{A}}$$

$$-\mathcal{K}_{\langle 12 \rangle} - \mathcal{K}_{\langle 21 \rangle} = \frac{1}{\sqrt{A_{11}}} \frac{\partial \varepsilon_{\langle 32 \rangle}}{\partial X^1} + \frac{\varepsilon_{\langle 31 \rangle}}{\sqrt{A}} \frac{\partial \sqrt{A_{11}}}{\partial X^2} \quad (2.89)$$

$$+ \frac{1}{\sqrt{A_{22}}} \frac{\partial \varepsilon_{\langle 31 \rangle}}{\partial X^2} + \frac{\varepsilon_{\langle 32 \rangle}}{\sqrt{A}} \frac{\partial \sqrt{A_{22}}}{\partial X^1} + \left( \frac{1}{R_1} - \frac{1}{R_2} \right) \frac{\omega}{\sqrt{A}} \quad (2.90)$$

## 2.3 Application to Shells of Revolution

### 2.3.1 General Shell of Revolution

With the systems of Cartesian  $(Z^1, Z^2, Z^3)$ , cylindrical  $(r, \theta, z)$  and curvilinear coordinates  $(X^1, X^2, Z)$  defined in Fig.

2.2, one has, before deformation:

$$\begin{aligned} \underline{P} &= Z^1 \hat{i}_1 + Z^2 \hat{i}_2 + Z^3 \hat{i}_3 = (r_0 + \int_0^P \sin \varphi ds) \sin \theta \hat{i}_1 \\ &\quad + (r_0 + \int_0^P \sin \varphi ds) \cos \theta \hat{i}_2 \\ &\quad + (z_0 + \int_0^P \cos \varphi ds) \hat{i}_3 \end{aligned} \quad (2.91)$$

$$\underline{A}_1 = \frac{\partial \underline{P}}{\partial X^1} = \sin \varphi \sin \theta \hat{i}_1 + \sin \varphi \cos \theta \hat{i}_2 + \cos \varphi \hat{i}_3$$

$$\underline{A}_2 = \frac{\partial \underline{P}}{\partial X^2} = r \cos \theta \hat{i}_1 - r \sin \theta \hat{i}_2 \quad (2.92)$$

$$\underline{A}_3 = \frac{\underline{A}_1 \times \underline{A}_2}{|\underline{A}_1 \times \underline{A}_2|} = \cos \varphi \sin \theta \hat{i}_1 + \cos \varphi \cos \theta \hat{i}_2 - \sin \varphi \hat{i}_3$$

$$A_{11} = 1, \quad A_{22} = r^2, \quad A_{12} = A_{21} = 0, \quad A = r^2 \quad (2.93)$$

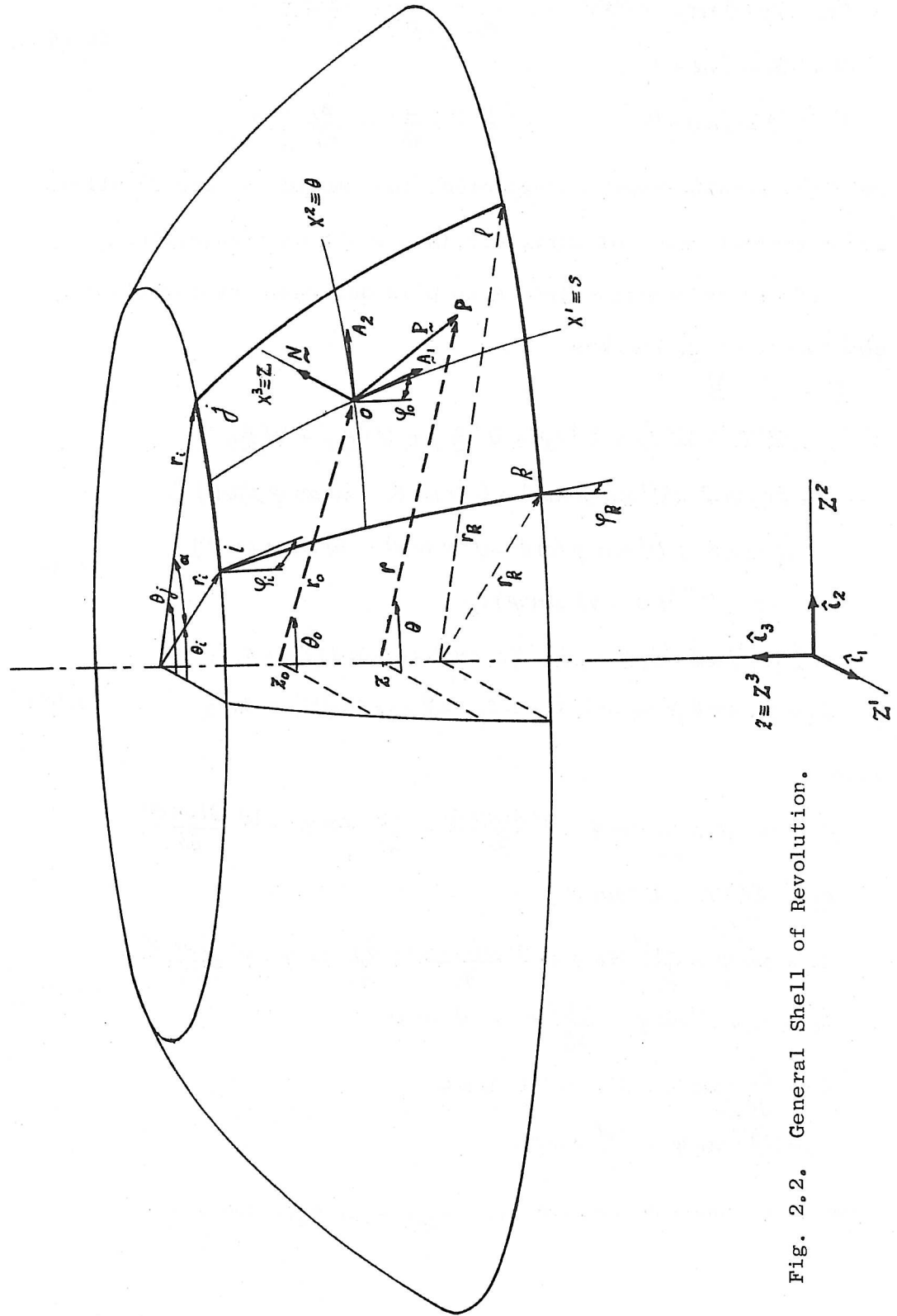


Fig. 2.2. General Shell of Revolution.

$$\begin{aligned}
B_{11} &= \underline{A}_3 \cdot \underline{A}_{1,1} = \partial\varphi / \partial s, & \frac{1}{R_1} &= -\frac{B_{11}}{A_{11}} = -\frac{\partial\varphi}{\partial s}, \\
B_{22} &= \underline{A}_3 \cdot \underline{A}_{2,2} = -r \cos\varphi, & \frac{1}{R_2} &= -\frac{B_{22}}{A_{22}} = \frac{\cos\varphi}{r}, \\
B_{12} &= \underline{A}_3 \cdot \underline{A}_{1,2} = 0, \\
B_{21} &= \underline{A}_3 \cdot \underline{A}_{2,1} = 0, & \frac{1}{T} &= -\frac{B_{12}}{\sqrt{A}} = -\frac{B_{21}}{\sqrt{A}} = 0.
\end{aligned} \tag{2.94}$$

The last result shows, as expected, that meridians and parallels are principal lines of curvature in a shell of revolution.

If the deformation from P to p is described by curvilinear components of  $\underline{U}$ , one has

$$\begin{aligned}
\underline{p} &= \underline{P} + \underline{U} \\
&= Z^1 \hat{i}_1 + Z^2 \hat{i}_2 + Z^3 \hat{i}_3 + U^1 \underline{A}_1 + U^2 \underline{A}_2 + W \underline{A}_3 \\
&= (r \sin\theta + U^1 \sin\varphi \sin\theta + U^2 r \cos\theta + W \cos\varphi \sin\theta) \hat{i}_1 \\
&\quad + (r \cos\theta + U^1 \sin\varphi \cos\theta - U^2 r \sin\theta + W \cos\varphi \cos\theta) \hat{i}_2 \\
&\quad + (z + U^1 \cos\varphi - W \sin\varphi) \hat{i}_3
\end{aligned} \tag{2.95}$$

$$\begin{aligned}
\underline{a}_1 &= (c_1 \sin\theta + c_2 \cos\theta) \hat{i}_1 + (c_1 \cos\theta - c_2 \sin\theta) \hat{i}_2 + c_3 \hat{i}_3 \\
\underline{a}_2 &= (c_4 \cos\theta + c_5 \sin\theta) \hat{i}_1 + (-c_4 \sin\theta + c_5 \cos\theta) \hat{i}_2 + c_6 \hat{i}_3
\end{aligned} \tag{2.96}$$

with

$$\begin{aligned}
c_1 &= \sin\varphi + \frac{\partial U^1}{\partial s} \sin\varphi + U^1 \frac{\partial(\sin\varphi)}{\partial s} + \frac{\partial W}{\partial s} \cos\varphi + W \frac{\partial(\cos\varphi)}{\partial s} \\
c_2 &= \frac{\partial U^2}{\partial s} r + U^2 \sin\varphi \\
c_3 &= \cos\varphi + \frac{\partial U^1}{\partial s} \cos\varphi + U^1 \frac{\partial(\cos\varphi)}{\partial s} - \frac{\partial W}{\partial s} \sin\varphi - W \frac{\partial(\sin\varphi)}{\partial s} \\
c_4 &= r + U^1 \sin\varphi + \frac{\partial U^2}{\partial \theta} r + W \cos\varphi \\
c_5 &= \frac{\partial U^1}{\partial \theta} \sin\varphi - U^2 r + \frac{\partial W}{\partial \theta} \cos\varphi \\
c_6 &= \frac{\partial U^1}{\partial \theta} \cos\varphi - \frac{\partial W}{\partial \theta} \sin\varphi.
\end{aligned} \tag{2.97}$$

From this, one can compute  $a_{11}$ ,  $a_{22}$ ,  $a_{12}$ ,  $a_{21}$ , and

$$2E_{11} = a_{11} - A_{11}$$

$$2E_{22} = a_{22} - A_{22}$$

$$E_{12} + E_{21} = (a_{12} - A_{12}) + (a_{21} - A_{21}) .$$

After switching to physical components, one gets

$$E_{\langle 11 \rangle} = \left( \frac{\partial u}{\partial s} - w \frac{\partial \varphi}{\partial s} \right) \quad (2.98)$$

$$+ \frac{1}{2} \left[ \left( \frac{\partial u}{\partial s} - w \frac{\partial \varphi}{\partial s} \right)^2 + \left( \frac{\partial v}{\partial s} \right)^2 + \left( \frac{\partial w}{\partial s} - u \frac{\partial \varphi}{\partial s} \right)^2 \right]$$

$$E_{\langle 22 \rangle} = \left( \frac{\partial v}{r \partial \theta} + \frac{u \sin \varphi + w \cos \varphi}{r} \right) \quad (2.99)$$

$$+ \frac{1}{2} \left[ \left( \frac{\partial u}{r \partial \theta} - \frac{\sin \varphi}{r} v \right)^2 + \left( \frac{\partial v}{r \partial \theta} + \frac{u \sin \varphi + w \cos \varphi}{r} \right)^2 + \left( \frac{\partial w}{r \partial \theta} - \frac{\cos \varphi}{r} v \right)^2 \right]$$

$$\frac{1}{2} (E_{\langle 12 \rangle} + E_{\langle 21 \rangle}) = \frac{1}{2} \left( \frac{\partial v}{\partial s} + \frac{\partial u}{r \partial \theta} - \frac{\sin \varphi}{r} v \right)$$

$$+ \frac{1}{2} \left[ \left( \frac{\partial u}{\partial s} - w \frac{\partial \varphi}{\partial s} \right) \left( \frac{\partial u}{r \partial \theta} - \frac{\sin \varphi}{r} v \right) + \left( \frac{\partial v}{\partial s} \right) \left( \frac{\partial v}{r \partial \theta} + \frac{u \sin \varphi + w \cos \varphi}{r} \right) \right] \quad (2.100)$$

$$+ \left( \frac{\partial w}{\partial s} - u \frac{\partial \varphi}{\partial s} \right) \left( \frac{\partial w}{r \partial \theta} - \frac{\cos \varphi}{r} v \right) \Bigg\} .$$

Although these results could have been obtained by a direct application of (2.78) to (2.86), it was estimated useful to demonstrate once the metric approach.

To find the linearized curvature change, (2.80), (2.83) and (2.87) to (2.90) are used

$$E_{\langle 31 \rangle} = -\frac{\partial w}{\partial s} + u \frac{\partial \varphi}{\partial s} \quad (2.101)$$

$$E_{\langle 32 \rangle} = -\frac{\partial w}{r \partial \theta} + \frac{\cos \varphi}{r} v \quad (2.102)$$

$$\frac{2\omega}{\sqrt{A}} = \frac{\partial v}{\partial s} + \frac{\sin \varphi}{r} v - \frac{\partial u}{r \partial \theta} \quad (2.103)$$

$$-\mathcal{R}_{\langle 11 \rangle} = \frac{\partial^2 w}{\partial s^2} + \frac{\partial u}{\partial s} \frac{\partial \varphi}{\partial s} + u \frac{\partial^2 \varphi}{\partial s^2} \quad (2.104)$$

$$-\mathcal{R}_{\langle 22 \rangle} = \frac{\partial^2 w}{r^2 \partial \theta^2} - \frac{\cos \varphi}{r} \frac{\partial v}{r \partial \theta} + \frac{\sin \varphi}{r} \frac{\partial w}{\partial s} + \frac{\sin \varphi}{r} u \frac{\partial \varphi}{\partial s} \quad (2.105)$$

$$\begin{aligned}
 -\frac{1}{2}(\mathcal{K}_{\langle 12 \rangle} + \mathcal{K}_{\langle 21 \rangle}) &= \frac{\partial^2 w}{r \partial \theta \partial s} - \frac{\sin \varphi}{r} \frac{\partial w}{r \partial \theta} \\
 + \left( \frac{3}{4} \frac{\cos \varphi}{r} + \frac{1}{4} \frac{\partial \varphi}{\partial s} \right) \left( \frac{\sin \varphi}{r} v - \frac{\partial v}{\partial s} \right) &+ \left( \frac{1}{4} \frac{\cos \varphi}{r} + \frac{3}{4} \frac{\partial \varphi}{\partial s} \right) \frac{\partial u}{r \partial \theta}. \quad (2.106)
 \end{aligned}$$

### 2.3.2 Particular Cases of Shell of Revolution

Strains for different degenerate cases of shells of revolution are given in Table 2.1 in the next two pages. A few results deserve special attention.

- a) The linear strains in a cylindrical shell are identical to Sanders' results [106]. Note, however, that the last curvature change differs from Timoshenko's and Flugge's cylindrical shell equations by terms  $\frac{1}{4r} \frac{\partial u}{r \partial \theta}$  and  $\frac{1}{4r} \frac{\partial v}{\partial s}$  which are of order "strain over radius."
- b) The circular plate gives the strains of plane elasticity and curvature changes of plate theory expressed in polar coordinates.
- c) The same results, in Cartesian coordinates, are obtained for the cylinder, cone or plate with "large radius", by which it is meant that

$$\lim_{\substack{r \rightarrow \infty \\ d\theta \rightarrow 0}} r d\theta = dt. \quad (2.107)$$

- d) The symmetric case with "large radius" eventually permits to solve beam problems for which strains and curvature changes reduce to

TABLE 2.1. LINEAR STRAINS IN DEGENERATE SHELLS OF REVOLUTION

STRAINS	GENERAL SHELL OF REVOLUTION	CONICAL SHELL	CYLINDRICAL SHELL
$\epsilon_{\langle 11 \rangle}$	$\frac{\partial u}{\partial s} - w \frac{\partial \varphi}{\partial s}$	$\frac{\partial u}{\partial s}$	$\frac{\partial u}{\partial s}$
$\epsilon_{\langle 22 \rangle}$	$\frac{\sin \varphi}{r} u + \frac{\partial v}{r \partial \theta} + \frac{\cos \varphi}{r} w$	$\frac{\sin \varphi}{r} u + \frac{\partial v}{r \partial \theta} + \frac{\cos \varphi}{r} w$	$\frac{\partial v}{r \partial \theta} + \frac{w}{r}$
$\epsilon_{\langle 12 \rangle}$	$\frac{\partial u}{r \partial \theta} - \frac{\sin \varphi}{r} v$	$\frac{\partial u}{r \partial \theta} - \frac{\sin \varphi}{r} v$	$\frac{\partial u}{r \partial \theta}$
$\epsilon_{\langle 21 \rangle}$	$\frac{\partial v}{\partial s}$	$\frac{\partial v}{\partial s}$	$\frac{\partial v}{\partial s}$
$\epsilon_{\langle 31 \rangle}$	$\frac{\partial \varphi}{\partial s} u + \frac{\partial w}{\partial s}$	$\frac{\partial w}{\partial s}$	$\frac{\partial w}{\partial s}$
$\epsilon_{\langle 32 \rangle}$	$-\frac{\cos \varphi}{r} v + \frac{\partial w}{r \partial \theta}$	$-\frac{\cos \varphi}{r} v + \frac{\partial w}{r \partial \theta}$	$-\frac{v}{r} + \frac{\partial w}{r \partial \theta}$
$-\mathcal{R}_{\langle 11 \rangle}$	$\frac{\partial \varphi}{\partial s} \frac{\partial u}{\partial s} + \frac{\partial^2 \varphi}{\partial s^2} u + \frac{\partial^2 w}{\partial s^2}$	$\frac{\partial^2 w}{\partial s^2}$	$\frac{\partial^2 w}{\partial s^2}$
$-\mathcal{R}_{\langle 22 \rangle}$	$\frac{\sin \varphi}{r} \frac{\partial \varphi}{\partial s} u - \frac{\cos \varphi}{r} \frac{\partial v}{\partial \theta} + \frac{\partial^2 w}{r \partial \theta} + \frac{\sin \varphi}{r} \frac{\partial w}{\partial s}$	$\frac{\partial^2 w}{r \partial \theta} - \frac{\cos \varphi}{r} \frac{\partial v}{\partial \theta} + \frac{\sin \varphi}{r} \frac{\partial w}{\partial s}$	$\frac{\partial^2 w}{r \partial \theta} - \frac{1}{r} \frac{\partial v}{\partial \theta}$
$-\frac{1}{2}(\mathcal{R}_{\langle 12 \rangle} + \mathcal{R}_{\langle 21 \rangle})$	$\left( \frac{1}{4} \frac{\cos \varphi}{r} + \frac{3}{4} \frac{\partial \varphi}{\partial s} \right) \frac{\partial u}{r \partial \theta} + \left( \frac{3}{4} \frac{\cos \varphi}{r} + \frac{1}{4} \frac{\partial \varphi}{\partial s} \right) \left( \frac{\sin \varphi}{r} v - \frac{\partial v}{\partial s} \right) + \left( \frac{\partial^2 w}{r \partial \theta} - \frac{\sin \varphi}{r} \frac{\partial w}{\partial s} \right)$	$\left( \frac{1}{4} \frac{\cos \varphi}{r} \frac{\partial u}{r \partial \theta} + \frac{3}{4} \frac{\cos \varphi}{r} \left( \frac{\sin \varphi}{r} v - \frac{\partial v}{\partial s} \right) + \left( \frac{\partial^2 w}{r \partial \theta} - \frac{\sin \varphi}{r} \frac{\partial w}{\partial s} \right) \right)$	$\frac{1}{4r} \frac{\partial u}{r \partial \theta} - \frac{3}{4r} \frac{\partial v}{\partial s} + \frac{\partial^2 w}{r \partial \theta}$

(To be continued)

TABLE 2.1. LINEAR STRAINS IN DEGENERATE SHELLS OF REVOLUTION (Continued)

STRAINS	CIRCULAR PLATE	SYMMETRICAL DISPLACEMENTS				LARGE RADIUS	
		GENERAL SHELL	CONE	CYLINDER	PLATE	NON SYM.	SYMM.
$\epsilon_{\langle 11 \rangle}$	$\frac{\partial u}{\partial s}$	$\frac{du}{ds} - w \frac{d\varphi}{ds}$	$\frac{du}{ds}$	$\frac{du}{ds}$	$\frac{du}{ds}$	$\frac{\partial u}{\partial s}$	$\frac{du}{ds}$
$\epsilon_{\langle 22 \rangle}$	$\frac{\partial v}{r \partial \theta} + \frac{u}{r}$	$\frac{u \sin \varphi + w \cos \varphi}{r}$	$\frac{u \sin \varphi + w \cos \varphi}{r}$	$\frac{w}{r}$	$\frac{u}{r}$	$\frac{\partial v}{\partial t}$	0
$\epsilon_{\langle 12 \rangle}$	$\frac{\partial u}{r \partial \theta} - \frac{v}{r}$	0	0	0	0	$\frac{\partial u}{\partial t}$	0
$\epsilon_{\langle 21 \rangle}$	$\frac{\partial v}{\partial s}$	0	0	0	0	$\frac{\partial v}{\partial s}$	0
$\epsilon_{\langle 31 \rangle}$	$\frac{\partial w}{\partial s}$	$u \frac{d\varphi}{ds} + \frac{dw}{ds}$	$\frac{dw}{ds}$	$\frac{dw}{ds}$	$\frac{dw}{ds}$	$\frac{\partial w}{\partial s}$	$\frac{dw}{ds}$
$\epsilon_{\langle 32 \rangle}$	$\frac{\partial w}{r \partial \theta}$	0	0	0	0	$\frac{\partial w}{\partial t}$	0
$-\mathcal{R}_{\langle 11 \rangle}$	$\frac{\partial^2 w}{\partial s^2}$	$\frac{d^2 w}{ds^2} + u \frac{d^2 \varphi}{ds^2} + \frac{du}{ds} \frac{d\varphi}{ds}$	$\frac{d^2 w}{ds^2}$	$\frac{d^2 w}{ds^2}$	$\frac{d^2 w}{ds^2}$	$\frac{\partial^2 w}{\partial s^2}$	$\frac{d^2 w}{ds^2}$
$-\mathcal{R}_{\langle 22 \rangle}$	$\frac{\partial^2 w}{r^2 \partial \theta^2} + \frac{1}{r} \frac{\partial w}{\partial s}$	$\frac{\sin \varphi}{r} \frac{d\varphi}{ds} u + \frac{\sin \varphi}{r} \frac{dw}{ds}$	$\frac{\sin \varphi}{r}$	0	$\frac{1}{r} \frac{dw}{ds}$	$\frac{\partial^2 w}{\partial t^2}$	0
$-\frac{1}{2}(\mathcal{R}_{\langle 12 \rangle} + \mathcal{R}_{\langle 21 \rangle})$	$\frac{\partial^2 w}{r \partial \theta \partial s} - \frac{1}{r} \frac{\partial w}{r \partial \theta}$	0	0	0	0	$\frac{\partial^2 w}{\partial s \partial t}$	0

$$E_{\langle II \rangle} = \frac{du}{ds} + \frac{1}{2} \left( \frac{du}{ds} \right)^2 + \frac{1}{2} \left( \frac{dw}{ds} \right)^2 \quad (2.108)$$

$$\mathcal{K}_{\langle II \rangle} = \frac{d^2 w}{ds^2} \quad (2.109)$$

## 2.4 Effect of Rigid Motions

During recent years, researchers working with finite elements have paid considerable attention to the inclusion of rigid motions in the assumed displacement fields. Sometimes, however, they have failed to recognize an older problem, namely that strain-displacement relationships used in some shell theories give strains under correctly represented rigid motions as explained in the following.

### 2.4.1 Small Motions in Linear Theory

In [15], Cantin compares strain-displacement relationships for cylindrical shells as established by Donnell [26], Flügge [32] (simplified equations), Reissner [101], Novozhilov [94] and Naghdi [84]; he shows that only Novozhilov's and Naghdi's theories lead to strain-free modes for and only for rigid motions.

Meyer [78] makes the same comparison for conical shells; he shows that Flügge's refined and simplified expressions [32] give strains under rigid modes while Novozhilov's equations [94] are correct again; he points out that the latter are rightly used in references [27], [44], [98].

For general shells, a table comparing different theories, from Love [73] to Koiter [66], can also be found in Naghdi [85, page 76].



A detailed study of the effects of rigid motions on Sanders' linearized strains and curvature changes can be found in [106]. In this reference, Sanders introduces the position vector of an arbitrary point P of the middle surface, a constant displacement vector and a constant small rotation vector, all of them described in terms of the normalized curvilinear basis at P

$$\underline{P} = P_{\langle 1 \rangle} \frac{\underline{A}_1}{|\underline{A}_1|} + P_{\langle 2 \rangle} \frac{\underline{A}_2}{|\underline{A}_2|} + P_{\langle N \rangle} \underline{N} \quad (2.110)$$

$$\underline{\Delta} = \Delta_{\langle 1 \rangle} \frac{\underline{A}_1}{|\underline{A}_1|} + \Delta_{\langle 2 \rangle} \frac{\underline{A}_2}{|\underline{A}_2|} + \Delta_{\langle N \rangle} \underline{N} \quad (2.111)$$

$$\underline{\Omega} = \Omega_{\langle 1 \rangle} \frac{\underline{A}_1}{|\underline{A}_1|} + \Omega_{\langle 2 \rangle} \frac{\underline{A}_2}{|\underline{A}_2|} + \Omega_{\langle N \rangle} \underline{N} . \quad (2.112)$$

The displacement vector  $\underline{U}$  of P due to the rigid-body motions  $\underline{\Delta}$  and  $\underline{\Omega}$  is given by

$$\underline{U} = \underline{\Delta} + \underline{\Omega} \times \underline{P} = u \frac{\underline{A}_1}{|\underline{A}_1|} + v \frac{\underline{A}_2}{|\underline{A}_2|} + w \underline{N} \quad (2.113)$$

with

$$\begin{aligned} u &= \Delta_{\langle 1 \rangle} + \Omega_{\langle 2 \rangle} P_{\langle N \rangle} - \Omega_{\langle N \rangle} P_{\langle 2 \rangle} \\ v &= \Delta_{\langle 2 \rangle} + \Omega_{\langle 3 \rangle} P_{\langle 1 \rangle} - \Omega_{\langle 1 \rangle} P_{\langle N \rangle} \\ w &= \Delta_{\langle N \rangle} + \Omega_{\langle 1 \rangle} P_{\langle 2 \rangle} - \Omega_{\langle 2 \rangle} P_{\langle 1 \rangle} . \end{aligned} \quad (2.114)$$

The linear part of the strains (2.84) to (2.86) and the changes of curvature (2.88) to (2.90) vanish when these physical components of displacements are plugged in, which shows that they are insensitive to small rigid-body motions.

Note that Sanders' proof is restricted to small rotations because the vectorial representation assumes that no difference is made between the angles and their sines, and because the rotations are superposed without due regard to the order in which they are applied.

### 2.4.2 Large Motions in Nonlinear Theory

No comparable studies seem to have been made for nonlinear theories. Instead of an elegant and general discussion (perhaps based on tensor analysis), a much simpler approach is chosen here. It consists in taking a typical shell of revolution, giving to it all possible rigid motions and computing the strains. The principal results are summarized hereafter.

- a) Translations along axis  $\hat{i}_1, \hat{i}_2, \hat{i}_3 \equiv$  Translations  $S_1, S_2, S_3$   
(Fig. 2.3 and 2.5).

$$\begin{aligned} u &= S_1 \cos \theta \sin \varphi, & u &= S_2 \sin \theta \sin \varphi, & u &= -S_3 \cos \varphi, \\ v &= -S_1 \sin \theta, & v &= S_2 \cos \theta, & v &= 0, \\ w &= S_1 \cos \theta \cos \varphi, & w &= S_2 \sin \theta \cos \varphi, & w &= S_3 \sin \varphi. \end{aligned} \quad (2.115)$$

$$E_{\langle 11 \rangle} = \epsilon_{\langle 11 \rangle} + \eta_{\langle 11 \rangle} = 0 + 0$$

$$E_{\langle 22 \rangle} = \epsilon_{\langle 22 \rangle} + \eta_{\langle 22 \rangle} = 0 + 0$$

$$\frac{1}{2}(E_{\langle 12 \rangle} + E_{\langle 21 \rangle}) = \frac{1}{2}(\epsilon_{\langle 12 \rangle} + \epsilon_{\langle 21 \rangle}) + \frac{1}{2}(\eta_{\langle 12 \rangle} + \eta_{\langle 21 \rangle}) = 0 + 0$$

$$\mathcal{K}_{\langle 11 \rangle} = 0$$

$$\mathcal{K}_{\langle 22 \rangle} = 0$$

$$\frac{1}{2}(\mathcal{K}_{\langle 12 \rangle} + \mathcal{K}_{\langle 21 \rangle}) = 0.$$

- b) Rotation about the axis of revolution = Rotation  $\beta_3$  (Fig. 2.6)

If the rotation is large,

$$u = r(\cos \beta_3 - 1) \sin \varphi$$

$$v = r \sin \beta_3$$

$$w = r(\cos \beta_3 - 1) \cos \varphi$$

$$E_{\langle 11 \rangle} = (\cos \beta_3 - 1) \sin^2 \varphi - (\cos \beta_3 - 1) \sin^2 \varphi = 0$$

$$E_{\langle 22 \rangle} = (\cos \beta_3 - 1) - (\cos \beta_3 - 1) = 0$$

$$\frac{1}{2}(E_{\langle 12 \rangle} + E_{\langle 21 \rangle}) = 0 + 0$$

If the rotation is small,

$$u = 0$$

$$v = r \beta_3 \quad (2.116)$$

$$w = 0$$

$$E_{\langle 11 \rangle} = 0 + \frac{(\beta_3)^2}{2} \sin^2 \varphi$$

$$E_{\langle 22 \rangle} = 0 + \frac{(\beta_3)^2}{2}$$

$$\frac{1}{2}(E_{\langle 12 \rangle} + E_{\langle 21 \rangle}) = 0 + 0$$

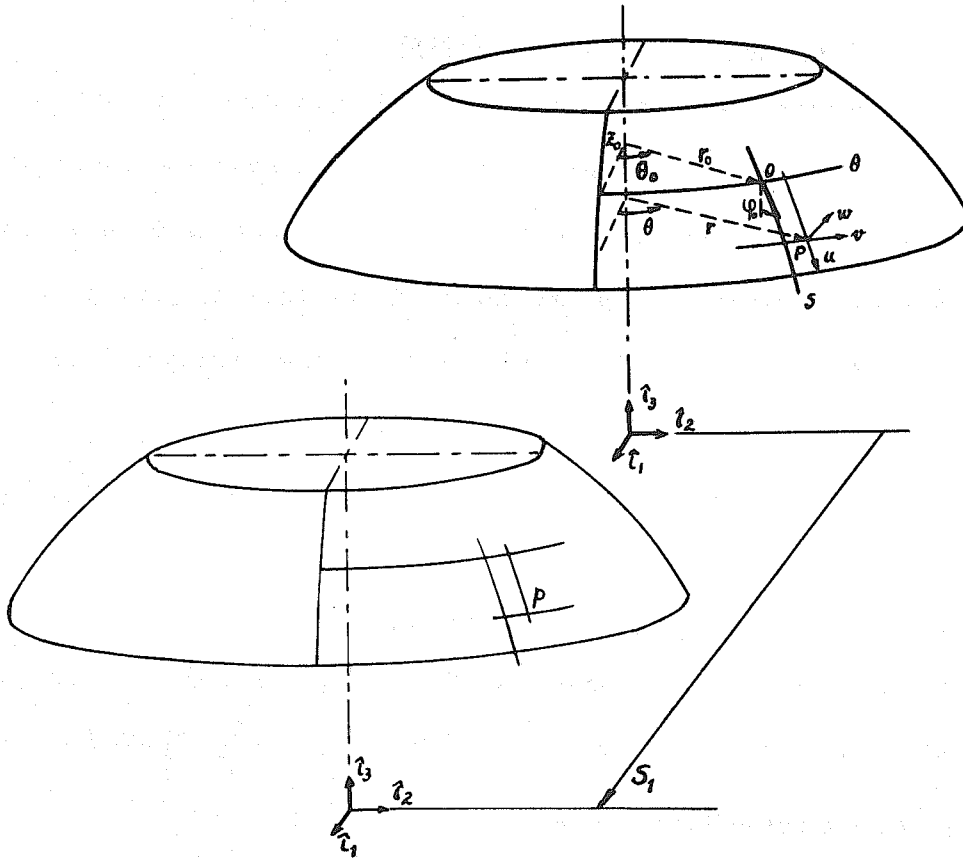


Fig. 2.3. Rigid Translation  $S_1$ .

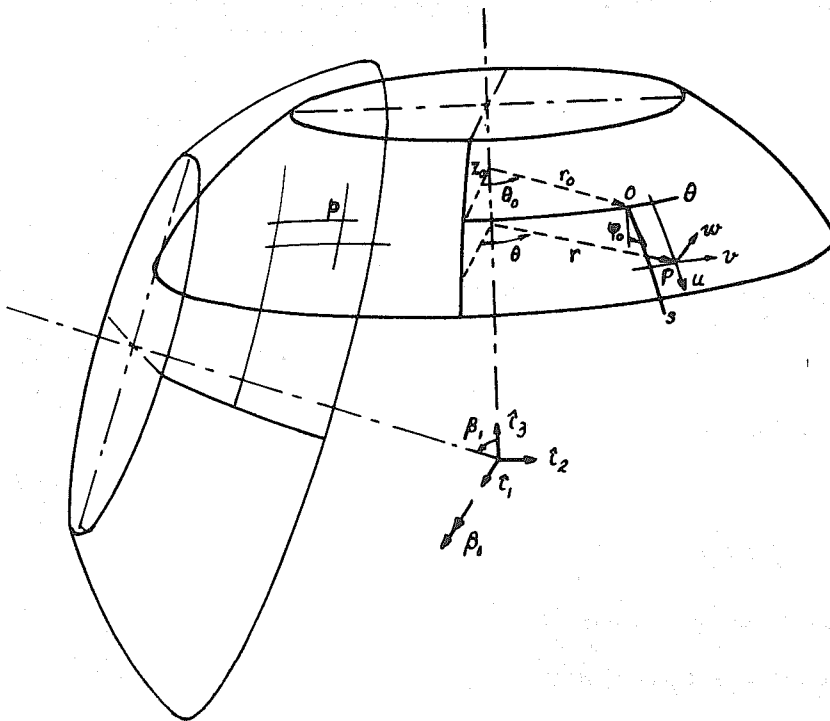


Fig. 2.4. Rigid Rotation  $\beta_1$ .

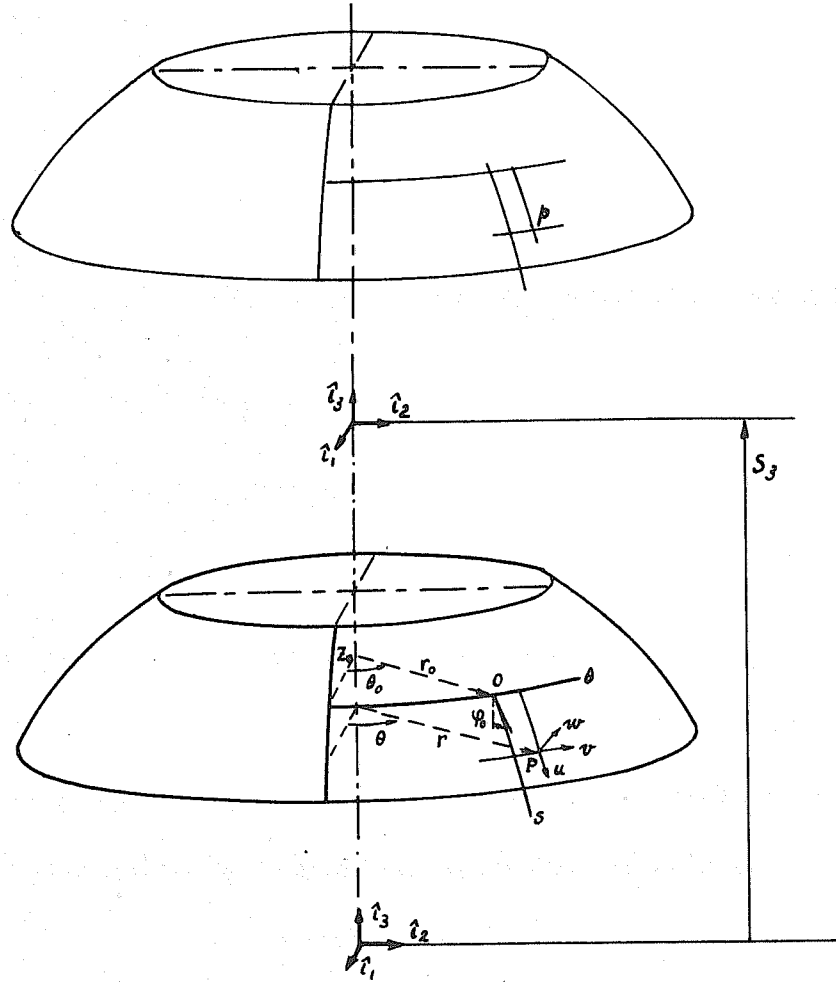


Fig. 2.5. Rigid Translation  $S_3$ .

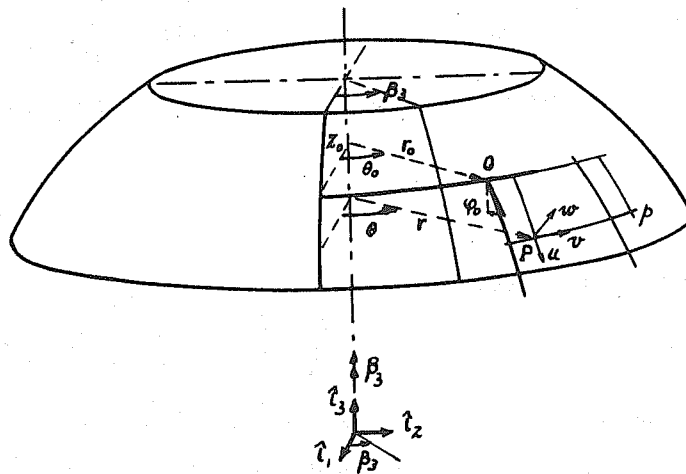


Fig. 2.6. Rigid Rotation  $\beta_3$ .

$$\mathcal{H}_{\langle 11 \rangle} = -(\cos^2 \varphi - \sin^2 \varphi) \frac{\partial \varphi}{\partial s} (\cos \beta_3 - 1) \quad \mathcal{H}_{\langle 11 \rangle} = 0$$

$$\mathcal{H}_{\langle 22 \rangle} = -\sin^2 \varphi \cos^2 \varphi \frac{1}{r} (\cos \beta_3 - 1) \quad \mathcal{H}_{\langle 22 \rangle} = 0$$

$$\frac{1}{2} (\mathcal{H}_{\langle 12 \rangle} + \mathcal{H}_{\langle 21 \rangle}) = 0 \quad \frac{1}{2} (\mathcal{H}_{\langle 12 \rangle} + \mathcal{H}_{\langle 21 \rangle}) = 0$$

c) Tilting about  $\hat{i}_1$  axis  $\equiv$  Rotation  $\beta_1$  (Fig. 2.4)

If the rotation is large,

$$u = (r \sin^2 \theta \sin \varphi - z \cos \varphi) (\cos \beta_1 - 1) - (r \sin \theta \cos \varphi + z \sin \theta \sin \varphi) \sin \beta_1$$

$$v = r \cos \theta \sin \theta (\cos \beta_1 - 1) - z \cos \theta \sin \beta_1 \quad (2.117)$$

$$w = (r \sin^2 \theta \cos \varphi + z \sin \varphi) (\cos \beta_1 - 1) + (r \sin \theta \sin \varphi - z \sin \theta \cos \varphi) \sin \beta_1$$

$$E_{\langle 11 \rangle} = (\sin^2 \theta \sin^2 \varphi + \cos^2 \varphi) (\cos \beta_1 - 1) - (\sin^2 \theta \sin^2 \varphi + \cos^2 \varphi) (\cos \beta_1 - 1) = 0$$

$$E_{\langle 22 \rangle} = \cos^2 \theta (\cos \beta_1 - 1) - \cos^2 \theta (\cos \beta_1 - 1) = 0$$

$$\frac{1}{2} (E_{\langle 12 \rangle} + E_{\langle 21 \rangle}) = \sin \theta \cos \theta \sin \varphi (\cos \beta_1 - 1) - \sin \theta \cos \theta \sin \varphi (\cos \beta_1 - 1) = 0$$

$$2 \mathcal{H}_{\langle 11 \rangle} = -\cos^2 \theta (\sin^2 \varphi - \cos^2 \varphi) \frac{\partial \varphi}{\partial s} (\cos \beta_1 - 1)$$

$$2 \mathcal{H}_{\langle 22 \rangle} = -\frac{\cos \varphi}{r} (\cos^2 \theta \cos^2 \varphi - \sin^2 \theta) (\cos \beta_1 - 1)$$

$$\mathcal{H}_{\langle 12 \rangle} + \mathcal{H}_{\langle 21 \rangle} = -\sin \theta \cos \theta \sin \varphi \left( \frac{\cos \varphi}{r} + \frac{\partial \varphi}{\partial s} \right) (\cos \beta_1 - 1)$$

If the rotation is small,

$$u = -(r \sin \theta \cos \varphi + z \sin \theta \sin \varphi) \beta_1$$

$$v = -z \cos \theta \beta_1 \quad (2.118)$$

$$w = (r \sin \theta \cos \varphi - z \sin \theta \sin \varphi) \beta_1$$

$$E_{\langle 11 \rangle} = 0 + (\cos^2 \theta \cos^2 \varphi + \sin^2 \theta) \frac{(\beta_1)^2}{2}$$

$$E_{\langle 22 \rangle} = 0 + \cos^2 \theta \frac{(\beta_1)^2}{2}$$

$$\frac{1}{2}(E_{\langle 12 \rangle} + E_{\langle 21 \rangle}) = 0 + \sin \theta \cos \theta \sin \varphi \frac{(\beta_1)^2}{2}$$

$$2 \mathcal{K}_{\langle 11 \rangle} = 0$$

$$2 \mathcal{K}_{\langle 22 \rangle} = 0$$

$$\mathcal{K}_{\langle 12 \rangle} + \mathcal{K}_{\langle 21 \rangle} = 0 .$$

- d) Tilting about  $\hat{i}_2$  axis  $\equiv$  Rotation  $\beta_2$ .

The results are the same as above if the origin of  $\theta$  angle is rotated by  $90^\circ$ .

The following conclusions can be drawn from these results.

- a) Linearized strains and curvature changes vanish under any small rigid motion as expected after Sanders' proof.
- b) Translations, no matter how large, produce neither strains (the linear and nonlinear parts vanish separately) nor linearized curvature changes.
- c) Large rotations give zero strains, although the linear and nonlinear parts, taken independently, may be different from zero.
- d) Large rotations give linearized curvature changes of order

$$\cos \beta - 1 \approx -\frac{\beta^2}{2} \quad (2.119)$$

This shows that moderately large rotations will still give small curvature changes and confirms the hypothesis on which (2.71) was obtained.

- e) Small rotations produce nonlinear parts of strains of order  $\beta^2$ ; this is negligible since  $\beta$  is assumed small in the first place.

In another test of rigid motions, not reproduced here, the nonlinearized curvature changes (2.65) were computed for a conical frustum subjected to the six motions described above (the curved element had to be abandoned because of (2.65) complexity). The linear and nonlinear part taken independently do not vanish but their sum is zero. This was expected since no approximation is made to obtain (2.65) except smallness of strain, which is perfectly realized in a rigid motion.

Finally, the motions (2.115) to (2.118) were introduced into Stricklin's strains and changes of curvature [114]. It was found that for small rotations, the linearized change of curvature  $\kappa\langle 12 \rangle + \kappa\langle 21 \rangle$  does not vanish: it is of order  $\beta$ ; i.e. the rotation rigid modes are not present in his formulation. Besides that, neither large nor small rotations give total nonlinear strains equal to zero.

## 2.5 Discussion of Nonlinear Strains

Here, results (2.47) and (2.71) or their physical equivalents (2.84) to (2.86) and (2.88) to (2.90) were considered to be the best. What justifies this choice when compared with results obtained by other authors?

Naghdi and Nordgren [87] derive the absolutely exact expressions for strains within the frame of Kirchhoff assumptions. In material description, they write for the Almansi tensor

$$E_{AB} = \left( a_{\alpha\beta} \frac{\partial x^\alpha}{\partial X^A} \frac{\partial x^\beta}{\partial X^B} - A_{AB} \right) + Z \left( -b_{\alpha\beta} \frac{\partial x^\alpha}{\partial X^A} \frac{\partial x^\beta}{\partial X^B} + B_{AB} \right) + Z^2 \left( b_{\alpha\gamma} b_{\beta}^{\gamma} \frac{\partial x^\alpha}{\partial X^A} \frac{\partial x^\beta}{\partial X^B} - B_{A\gamma} B_B^{\gamma} \right). \quad (2.120)$$

The third term is in  $Z^2$  and contains the difference of third fundamental forms; this term is almost impossible to use in practical computations and could eventually be justified only if an equal level of sophistication was used for the definition of shell forces and constitutive equations. If terms of order "thickness over curvature radius" are neglected in the definition of shell forces and plain Hooke's law is used to find stresses, then Koiter's criteria for consistency [66] show that it is pointless to keep this third term.

The next level of approximation, represented by the first two terms in (2.120) or by Eq. (2.99), is arrived at by Sanders [107], Mushtari [83], Navaratna [91], Novozhilov [93], among others. All of them, although proceeding in different ways, use Kirchhoff assumptions and the "small strain" approximation to find the simplified curvature changes (2.65), the strains (2.97) remaining unchanged. Novozhilov, who, by the way, is using orthogonal curvilinear coordinates and physical components from the start, stops here. His strains and curvature changes are not restricted by the magnitude of rotations but, as shown by (2.66), this form of the curvature change is still too complicated.

What the next approximation should be is not agreed upon. Mushtari specializes his theory: large deflections of shallow or cylindrical shells, partially linearized stability problems, etc.; the approximations are different in each case. Navaratna falls back to Sanders' equations. Stricklin [114] uses Novozhilov's nonlinear results [73] but he reduces the strains to



$$2 \overset{\circ}{E}_{AB} = U_A \parallel_B + U_B \parallel_A - 2 B_{AB} W + \epsilon_A^3 \epsilon_B^3 \quad (2.121)$$

and he simply linearizes the changes of curvature; so doing, he gets a  $\kappa\langle 12 \rangle + \kappa\langle 21 \rangle$  different from the one obtained by Novozhilov himself in his linear theory [94]; these unjustified approximations lead to nonzero strains under some rigid motions!

The most consistent approximation, coming from the nonlinear approach, seems to be Sanders' "small strains, moderately large rotations theory." By this, he means that  $\epsilon$  being a small quantity compared to unity, the strains are of order  $\epsilon^2$  and the rotations of order  $\epsilon$ . He ends up with

$$2 \overset{\circ}{E}_{AB} = U_A \parallel_B + U_B \parallel_A - 2 B_{AB} W + \epsilon_A^3 \epsilon_B^3 + \omega_{A\Gamma} \omega_{\Gamma B} \quad (2.122)$$

for the strains. He acknowledges that the last term is additional with respect to a nonlinear theory derived by Donnell [26], Vlassov [123]. The trouble is that this last term is not equivalent to the term  $\epsilon_A^\Gamma \epsilon_{\Gamma B}$  of (2.47) and, whether it is present or not, some rigid motions contribute nonzero quadratic terms in (2.122). For the changes of curvature, he finds

$$-2 K_{AB} = \epsilon_A^3 \parallel_B + \epsilon_B^3 \parallel_A + B_A^\Gamma \omega_{B\Gamma} + B_B^\Gamma \omega_{A\Gamma} \quad (2.123)$$

i.e. the same completely linear result as obtained by Koiter in his consistent linear theory.

Since no unanimity can be reached for simplified nonlinear strains and since the exact formula (2.47) is relatively easy to use for a shell of revolution, it seems reasonable to choose it. The more so because it will not give any strain under rigid motions, no matter how large they are, and its linear part will not give any strain under small rigid motions. With a computer

application in mind, it does not matter too much that three nonlinear terms are included in each strain when one only could be retained, perhaps, under appropriate simplifications; what makes a difference in computer time and coding difficulty is the fact that a nonlinear part is present or not in a given strain expression; that this nonlinear part contains one term or three terms is almost immaterial.

For the curvature changes, it is very comforting to see that formula (2.71) obtained by pure linearization is as good as any for moderate rotations, does not give any strains under small rigid motions and gives strains of order  $(\cos\beta - 1)$  at most for large rotations. To computer users, the fact that linearized curvature changes are mixed with nonlinear strains must not come as a surprise; this approach has been successfully used for a long time in nonlinear frame analysis where strains

$$E_{||} = \frac{du}{dx} + \frac{1}{2} \left( \frac{dw}{dx} \right)^2, \quad E_{||} = \frac{du}{dx} + \frac{1}{2} \left( \frac{du}{dx} \right)^2 + \frac{1}{2} \left( \frac{dw}{dx} \right)^2 \quad (2.124)$$

are chosen while the nonlinear denominator is always dropped in

$$\frac{1}{\rho} = \frac{\frac{d^2w}{dx^2}}{\left[ 1 + \left( \frac{dw}{dx} \right)^2 \right]^{3/2}} \quad (2.125)$$

Among the references for numerical nonlinear analysis for shells mentioned in the introduction, only Yaghmai [128] considers nonlinear curvature changes; he uses refined expressions because he is studying plastic deformations, can expect large strains and non-negligible volume changes; he is able to do it because he considers axisymmetric problems only.

Now that shell strain-displacement relationships, suitable for a linear or nonlinear analysis, have been found, the purpose of the next chapters will be to set up a shell element using them in the linear range but also capable of extension in the nonlinear range.

### 3. APPLICATION OF THE FINITE ELEMENT METHOD TO SHELLS OF REVOLUTION

#### 3.1 Preliminary Remark on Notations

The indicial notation and summation convention, best suited to shell theory, are now abandoned and replaced by the matricial notation, which is more convenient for finite elements.

Physical quantities referred to the original configuration are used everywhere; letter indices designate element corners; a column vector  $v$  is represented by  $\{v\}$ , its transpose or row vector by  $\{v\}^T = \langle v \rangle$ , a matrix  $A$  by  $[A]$ .

#### 3.2 Representation of the Element Geometry

For shells of revolution, a division into quadrilateral elements along the parallel, and meridians constitutes the most natural grid. The parallel edges, each with a constant radius, are exactly represented; the meridian curves must generally be approximated.

##### 3.2.1 General Meridian Curve

Khojasteh-Bakht [63] studied different ways of idealizing the meridional shape and concluded that a representation within each element by a cubic polynomial matching the coordinates and slopes at the end points is very satisfactory. The quantity being approximated can be either the rise  $\zeta$  above the chord (Fig. 3.1) or the parallel radius  $r$ ; the polynomial variable can be either  $\eta$  along the chord or  $s$  along the arc. There is no significant difference between the different approaches and it must be noted that all of them require a numerical evaluation of the arc length

$l$  sooner or later.

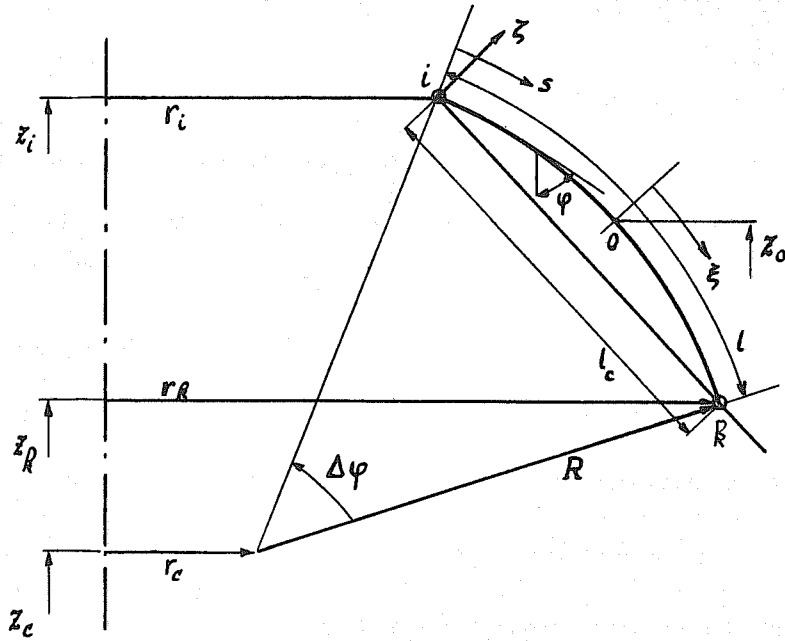


Fig. 3.1. Representation of the Element Geometry.

The method chosen here consists in expressing  $r$  as a function of  $s$  varying between 0 and  $l$  or, equivalently, as a function of the dimensionless variable  $\xi$  defined so that

$$-1 \leq \xi = -1 + \frac{2s}{l} \leq 1. \quad (3.1)$$

The arc length  $l$  is evaluated by assuming an arc of a circle with chord length  $l_c$  and angular opening  $\Delta\varphi$  between  $i$  and  $k$

$$l_c = \sqrt{(z_R - z_i)^2 + (r_R - r_i)^2}, \quad \Delta\varphi = \varphi_i - \varphi_R, \quad (3.2)$$

$$R = \frac{l_c}{2 \sin \frac{\Delta\varphi}{2}}, \quad l \approx |R \Delta\varphi|. \quad (3.3)$$

After fitting the nodal radii and slopes, the cubic polynomial becomes

$$r(\xi) = r_i \left( \frac{1}{2} - \frac{3\xi}{4} + \frac{\xi^3}{4} \right) + r_R \left( \frac{1}{2} + \frac{3\xi}{4} - \frac{\xi^3}{4} \right) \\ + \sin \varphi_i \frac{l}{2} \left( \frac{1}{4} - \frac{\xi}{4} - \frac{\xi^2}{4} + \frac{\xi^3}{4} \right) + \sin \varphi_R \frac{l}{2} \left( -\frac{1}{4} - \frac{\xi}{4} + \frac{\xi^2}{4} + \frac{\xi^3}{4} \right). \quad (3.4)$$

From this, other useful quantities can be derived

$$\sin \varphi = \frac{dr}{ds} = \frac{dr}{d\xi} \frac{d\xi}{ds} \\ = \frac{2}{l} \left[ r_i \left( -\frac{3}{4} + \frac{3\xi^2}{4} \right) + r_R \left( \frac{3}{4} - \frac{3\xi^2}{4} \right) \right. \\ \left. + \sin \varphi_i \frac{l}{2} \left( -\frac{1}{4} - \frac{\xi}{2} + \frac{3\xi^2}{4} \right) + \sin \varphi_R \frac{l}{2} \left( -\frac{1}{4} + \frac{\xi}{2} + \frac{3\xi^2}{4} \right) \right] \quad (3.5)$$

$$\cos \varphi = \sqrt{1 - \sin^2 \varphi} \quad (3.6)$$

$$\frac{d\varphi}{ds} = \frac{d}{ds} \sin^{-1}(\sin \varphi) = \frac{1}{\cos \varphi} \frac{d(\sin \varphi)}{d\xi} \frac{2}{l} \\ = \frac{4}{l^2 \cos \varphi} \left[ r_i \left( \frac{3\xi}{2} \right) + r_R \left( -\frac{3\xi}{2} \right) + \sin \varphi_i \frac{l}{2} \left( -\frac{1}{2} + \frac{3\xi}{2} \right) + \sin \varphi_R \frac{l}{2} \left( \frac{1}{2} + \frac{3\xi}{2} \right) \right] \quad (3.7)$$

$$\frac{d^2\varphi}{ds^2} = \frac{d}{ds} \left( \frac{d\varphi}{ds} \right) = \frac{2}{l \cos \varphi} \frac{d^2(\sin \varphi)}{d\xi^2} + \frac{\sin \varphi}{\cos^2 \varphi} \frac{d\varphi}{ds} \frac{d(\sin \varphi)}{d\xi} \frac{2}{l} \\ = \frac{8}{l^3 \cos \varphi} \left[ r_i \left( \frac{3}{2} \right) + r_R \left( -\frac{3}{2} \right) + \sin \varphi_i \frac{l}{2} \left( \frac{3}{2} \right) + \sin \varphi_R \frac{l}{2} \left( \frac{3}{2} \right) \right] + \frac{\sin \varphi}{\cos \varphi} \left( \frac{d\varphi}{ds} \right)^2. \quad (3.8)$$

The coordinate  $z_0$  which is also necessary for future computation is obtained from

$$z_0 = z_i - \int_{s=0}^{s=\frac{l}{2}} \cos \varphi ds = z_i - \frac{l}{2} \int_{\xi=-1}^{\xi=0} \cos \varphi d\xi \quad (3.9)$$

or

$$z_0 = z_R + \int_{s=\frac{l}{2}}^{s=l} \cos \varphi ds = z_R + \frac{l}{2} \int_{\xi=0}^{\xi=1} \cos \varphi d\xi. \quad (3.10)$$

Both formulas require a numerical integration. In the program, both are used and  $z_0$  is taken as the average of the two results.

### 3.2.2 Particular Cases of Meridian Curves

a) If the element is slightly curved in the meridian direction, the angle

$$\Delta\varphi_{iR} = \varphi_i - \varphi_R \quad (3.11)$$

may be so small that

$$\sin \Delta\varphi_{iR} \approx \Delta\varphi_{iR} \quad , \quad \cos \Delta\varphi_{iR} = 1 - \frac{(\Delta\varphi_{iR})^2}{2} + \dots \approx 1 \quad (3.12)$$

In that case, the interpolation function (3.4), written as

$$\begin{aligned} r = & \left[ \frac{1}{2} (r_i + r_R) + \frac{1}{8} (\sin \varphi_i - \sin \varphi_R) \right] + \left[ \frac{3}{4} (r_R - r_i) - \frac{1}{8} (\sin \varphi_i + \sin \varphi_R) \right] \xi \\ & + \left[ -\frac{1}{8} (\sin \varphi_i - \sin \varphi_R) \right] \xi^2 + \left[ \frac{1}{4} (r_i - r_R) + \frac{1}{8} (\sin \varphi_i + \sin \varphi_R) \right] \xi^3 \end{aligned} \quad (3.13)$$

can be replaced by

$$r = \frac{1}{2} (r_i + r_R) + \frac{1}{8} \cos \varphi_0 \Delta\varphi_{iR} + \frac{1}{2} (r_R - r_i) \xi - \frac{1}{8} \cos \varphi_0 \Delta\varphi_{iR} \xi^2 \quad (3.14)$$

by neglecting terms in  $(\Delta\varphi_{ik})^2$  in front of unity, i.e. by committing approximations similar to (3.12).

b) The conical segment, which includes the cylindrical shell and circular plate as particular cases can be exactly represented

$$\begin{aligned} r &= r_i \frac{1}{2} (1 - \xi) + r_R \frac{1}{2} (1 + \xi) \\ \varphi &= \tan^{-1} \left( \frac{z_R - z_i}{r_R - r_i} \right) \\ \frac{d\varphi}{ds} &= \frac{d^2\varphi}{ds^2} = 0 \\ z_0 &= \frac{z_i + z_R}{2} \end{aligned} \quad (3.15)$$

c) The arc of a circle, of such a frequent use in spherical, toroidal or torispherical shells, also deserves a special representation. In that case, expressions (3.2), (3.3) become exact and

$$\begin{aligned}
 r_o &= r_i - R \cos \varphi_i \\
 z_o &= z_i + R \sin \varphi_i \\
 \varphi &= \varphi_i \frac{1}{2}(1-\xi) + \varphi_R \frac{1}{2}(1+\xi) \\
 r &= r_o + R \cos \varphi \\
 \frac{d\varphi}{ds} &= \frac{\varphi_R - \varphi_i}{l} \\
 \frac{d^2\varphi}{ds^2} &= 0 \\
 z_o &= z_i + R \sin \frac{\varphi_i + \varphi_R}{2} .
 \end{aligned} \tag{3.16}$$

d) The general formulation can give relatively inaccurate values of  $\frac{d\varphi}{ds}$ ,  $\frac{d^2\varphi}{ds^2}$  for an almost flat element with  $\varphi \approx 90^\circ$ . In that case, it may be advantageous to approximate the element by an arc of a circle when the data are input.

### 3.3 Displacement Fields

In elements of revolution, it is customary to take a linear interpolation function of the coordinates for the meridian and parallel displacements  $u$  and  $v$  and a cubic for the transverse displacement  $w$ ; Fourier series are used to represent variations along the coordinate  $\theta$ . In replacing the element of revolution by a quadrilateral and the Fourier series by polynomials, the idea naturally came up to use linear and cubic functions of  $\theta$  for  $u$ ,  $v$  and  $w$ , respectively.



Define the dimensionless variables (Fig. 3.2)

$$-1 \leq \xi = \frac{-(s_i + s_R) + 2s}{s_R - s_i} \leq 1 \quad (3.17)$$

$$-1 \leq \eta = \frac{-(\theta_i + \theta_j) + 2\theta}{\theta_j - \theta_i} \leq 1 \quad (3.18)$$

giving

$$\frac{d\xi}{ds} = \frac{2}{s_R - s_i} = \frac{2}{l} \quad , \quad \frac{d\eta}{d\theta} = \frac{2}{\theta_j - \theta_i} = \frac{2}{a} \quad (3.19)$$

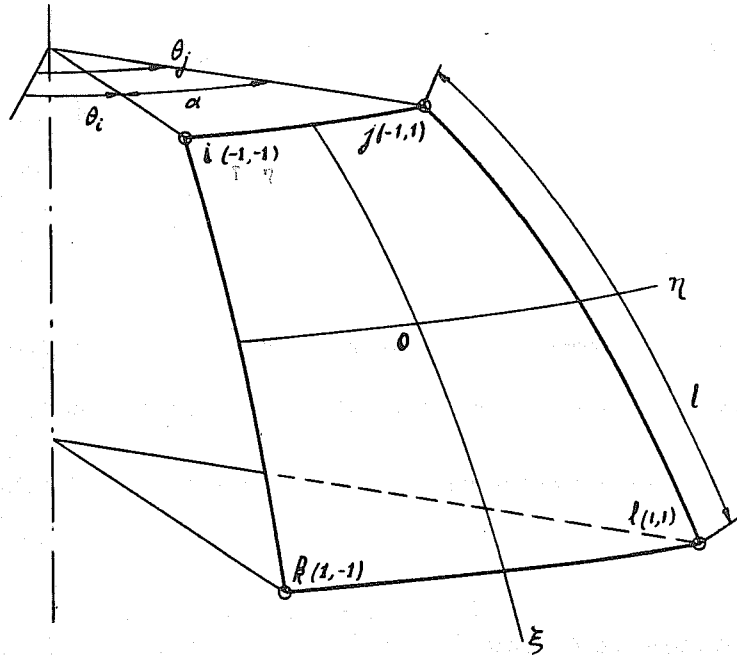


Fig. 3.2. Element Coordinates

Also define the following functions and their derivatives:

$$\begin{aligned} f_1(x) &= \frac{1}{2} - \frac{1}{2}x & , & \quad f_1'(x) = \frac{df_1(x)}{dx} & , \\ f_2(x) &= \frac{1}{2} + \frac{1}{2}x & , & \quad f_2'(x) = \frac{df_2(x)}{dx} & , \end{aligned} \quad (3.20)$$

$$\begin{aligned}
f_3(x) &= \frac{1}{2} - \frac{3}{4}x + \frac{1}{4}x^3, & f_3'(x) &= \frac{df_3(x)}{dx}, & f_3''(x) &= \frac{d^2f_3(x)}{dx^2} \\
f_4(x) &= \frac{1}{2} + \frac{3}{4}x - \frac{1}{4}x^3, & f_4'(x) &= \frac{df_4(x)}{dx}, & f_4''(x) &= \frac{d^2f_4(x)}{dx^2} \\
f_5(x) &= \frac{1}{4} - \frac{x}{4} - \frac{x^2}{4} + \frac{x^3}{4}, & f_5'(x) &= \frac{df_5(x)}{dx}, & f_5''(x) &= \frac{d^2f_5(x)}{dx^2} \\
f_6(x) &= -\frac{1}{4} - \frac{x}{4} + \frac{x^2}{4} + \frac{x^3}{4}, & f_6'(x) &= \frac{df_6(x)}{dx}, & f_6''(x) &= \frac{d^2f_6(x)}{dx^2}.
\end{aligned} \tag{3.20}$$

These functions can be interpreted as Hermite interpolation polynomials extending over the range  $-1, +1$ .

When linear interpolation is used along the meridians, the value of  $u$  anywhere in the element can be described in terms of its values along the meridian through  $i$  and the meridian through  $k$ :

$$u(s, \theta) = u_i(\theta) \frac{1}{2}(1-\xi) + u_k(\theta) \frac{1}{2}(1+\xi). \tag{3.21}$$

When linear interpolation is also used along the parallels,  $u_i(\theta)$  and  $u_k(\theta)$  can be described in terms of the nodal values  $u_i, u_j$  and  $u_k, u_l$  respectively.

$$\begin{aligned}
u_i(\theta) &= u_i \frac{1}{2}(1-\eta) + u_j \frac{1}{2}(1+\eta) \\
u_k(\theta) &= u_k \frac{1}{2}(1-\eta) + u_l \frac{1}{2}(1+\eta).
\end{aligned} \tag{3.22}$$

Hence,

$$\begin{aligned}
u(s, \theta) &= u_i \frac{1}{2}(1-\xi) \frac{1}{2}(1-\eta) + u_j \frac{1}{2}(1-\xi) \frac{1}{2}(1+\eta) \\
&\quad + u_k \frac{1}{2}(1+\xi) \frac{1}{2}(1-\eta) + u_l \frac{1}{2}(1+\xi) \frac{1}{2}(1+\eta) \\
&= u_i f_1(\xi) f_1(\eta) + u_j f_1(\xi) f_2(\eta) + u_k f_2(\xi) f_1(\eta) + u_l f_2(\xi) f_2(\eta). \tag{3.23}
\end{aligned}$$

Similarly,

$$v(s, \theta) = v_i f_1(\xi) f_1(\eta) + v_j f_1(\xi) f_2(\eta) + v_k f_2(\xi) f_1(\eta) + v_l f_2(\xi) f_2(\eta). \tag{3.24}$$

When cubic interpolation is used along the meridians,  $w$  is given by

$$w(s, \theta) = w_i(\theta) f_3(\xi) + w_R(\theta) f_4(\xi) + \left[ \frac{\partial w}{\partial s}(\theta) \right]_i \frac{l}{2} f_5(\xi) + \left[ \frac{\partial w}{\partial s}(\theta) \right]_R \frac{l}{2} f_6(\xi) \quad (3.25)$$

and, if cubic interpolation is used along the parallels too,

$$w_i(\theta) = w_i f_3(\eta) + w_j f_4(\eta) + \left( \frac{\partial w}{\partial s} \right)_i \frac{ar_i}{2} f_5(\eta) + \left( \frac{\partial w}{\partial s} \right)_j \frac{ar_i}{2} f_6(\eta) \quad (3.26)$$

$$\left[ \frac{\partial w}{\partial s}(\theta) \right]_i = \left( \frac{\partial w}{\partial s} \right)_i f_3(\eta) + \left( \frac{\partial w}{\partial s} \right)_j f_4(\eta) + \left( \frac{\partial^2 w}{r \partial \theta \partial s} \right)_i \frac{ar_i}{2} f_5(\eta) + \left( \frac{\partial^2 w}{r \partial \theta \partial s} \right)_j \frac{ar_i}{2} f_6(\eta)$$

and similar expressions, with  $r_k$  instead of  $r_i$ , for  $w_k(\theta)$ ,

$\left[ \frac{\partial w}{\partial s}(\theta) \right]_k$ . After substitution,

$$w(s, \theta) = \left[ w_i f_3(\xi) f_3(\eta) + \left( \frac{\partial w}{\partial s} \right)_i \frac{l}{2} f_5(\xi) f_3(\eta) + \left( \frac{\partial w}{r \partial \theta} \right)_i \frac{ar_i}{2} f_5(\xi) f_5(\eta) + \left( \frac{\partial^2 w}{r \partial \theta \partial s} \right)_i \frac{ar_i l}{4} f_5(\xi) f_5(\eta) \right] + \left[ w_j f_3(\xi) f_4(\eta) + \left( \frac{\partial w}{\partial s} \right)_j \frac{l}{2} f_5(\xi) f_4(\eta) + \left( \frac{\partial w}{r \partial \theta} \right)_j \frac{ar_j}{2} f_5(\xi) f_6(\eta) + \left( \frac{\partial^2 w}{r \partial \theta \partial s} \right)_j \frac{ar_j l}{4} f_5(\xi) f_6(\eta) \right] + \left[ w_R f_4(\xi) f_3(\eta) + \left( \frac{\partial w}{\partial s} \right)_R \frac{l}{2} f_6(\xi) f_3(\eta) + \left( \frac{\partial w}{r \partial \theta} \right)_R \frac{ar_R}{2} f_6(\xi) f_5(\eta) + \left( \frac{\partial^2 w}{r \partial \theta \partial s} \right)_R \frac{ar_R l}{4} f_6(\xi) f_5(\eta) \right] + \left[ w_\rho f_4(\xi) f_4(\eta) + \left( \frac{\partial w}{\partial s} \right)_\rho \frac{l}{2} f_6(\xi) f_4(\eta) + \left( \frac{\partial w}{r \partial \theta} \right)_\rho \frac{ar_\rho}{2} f_6(\xi) f_6(\eta) + \left( \frac{\partial^2 w}{r \partial \theta \partial s} \right)_\rho \frac{ar_\rho l}{4} f_6(\xi) f_6(\eta) \right]. \quad (3.27)$$

When the interpolation functions are introduced as explained above, the choice of the 24 DOF\* to be used follows automatically from the symmetric problem. The bilinear and bicubic interpolation functions used for  $u$ ,  $v$  and  $w$  can also be written

\*Defined in chapter 1 as the abbreviation for Degree of Freedom.

$$\begin{aligned}
u &= a_1 + a_2 \xi + a_3 \eta + a_4 \xi \eta \\
v &= a_5 + a_6 \xi + a_7 \eta + a_8 \xi \eta \\
w &= (a_9) + (a_{10} \xi + a_{11} \eta) + (a_{12} \xi^2 + a_{13} \xi \eta + a_{14} \eta^2) + (a_{15} \xi^3 + a_{16} \xi^2 \eta + a_{17} \xi \eta^2 + a_{18} \eta^3) \\
&\quad + (a_{19} \xi^3 \eta + a_{20} \xi^2 \eta^2 + a_{21} \xi \eta^3) + (a_{22} \xi^3 \eta^2 + a_{23} \xi^2 \eta^3) + (a_{24} \xi^3 \eta^3) .
\end{aligned} \tag{3.28}$$

Under this form, however, it is not so clear which DOF are simplest and easiest to use to determine the 24 unknown  $a_n$  coefficients.

These incomplete polynomials of degree two and six in  $\xi$  and  $\eta$  have been very successful in solving rectangular plate problems [9], [37]; there, the advantage is that they insure continuity of displacements and slopes along interelement boundaries and that they include rigid body modes. Thanks to the choice of displacements, related to the middle surface rather than to a global frame, the interelement compatibility is maintained in the doubly curved element introduced here. Unfortunately, because of this same choice, the rigid body modes are lost; this last point will be discussed thoroughly in chapter 4.

For future use, the interpolation functions are abbreviated as

$$\begin{Bmatrix} u(s, \theta) \\ v(s, \theta) \\ w(s, \theta) \end{Bmatrix} = [\phi(s, \theta)] \{v\} \tag{3.29}$$

with  $[\Phi(x, \theta)]$  and the vector  $\{v\}$  of generalized DOF defined in Table 3.1 on the next page.

Also for future use, one has represented in the same table the vector  $\{S\}$  of generalized forces associated with  $\{v\}$ .

TABLE 3.1. INTERPOLATION MATRIX; DOF; GENERALIZED FORCES.

$$\begin{aligned}
 \left[ \phi_{(3,0)} \right]^T = & \begin{bmatrix} f_1(\xi) f_1(\eta) & 0 & 0 \\ 0 & f_1(\xi) f_1(\eta) & 0 \\ 0 & 0 & f_3(\xi) f_3(\eta) \\ 0 & 0 & \frac{\ell}{2} f_5(\xi) f_5(\eta) \\ 0 & 0 & \frac{\alpha r_i}{2} f_3(\xi) f_5(\eta) \\ 0 & 0 & \frac{\alpha r_i \ell}{4} f_5(\xi) f_5(\eta) \\ f_1(\xi) f_2(\eta) & 0 & 0 \\ 0 & f_1(\xi) f_2(\eta) & 0 \\ 0 & 0 & f_3(\xi) f_4(\eta) \\ 0 & 0 & \frac{\ell}{2} f_5(\xi) f_4(\eta) \\ 0 & 0 & \frac{\alpha r_i}{2} f_3(\xi) f_6(\eta) \\ 0 & 0 & \frac{\alpha r_i \ell}{4} f_5(\xi) f_6(\eta) \\ f_2(\xi) f_1(\eta) & 0 & 0 \\ 0 & f_2(\xi) f_1(\eta) & 0 \\ 0 & 0 & f_4(\xi) f_3(\eta) \\ 0 & 0 & \frac{\ell}{2} f_6(\xi) f_3(\eta) \\ 0 & 0 & \frac{\alpha r_R}{2} f_4(\xi) f_5(\eta) \\ 0 & 0 & \frac{\alpha r_R \ell}{4} f_6(\xi) f_5(\eta) \\ f_2(\xi) f_2(\eta) & 0 & 0 \\ 0 & f_2(\xi) f_2(\eta) & 0 \\ 0 & 0 & f_4(\xi) f_4(\eta) \\ 0 & 0 & \frac{\ell}{2} f_6(\xi) f_4(\eta) \\ 0 & 0 & \frac{\alpha r_R}{2} f_4(\xi) f_6(\eta) \\ 0 & 0 & \frac{\alpha r_R \ell}{4} f_6(\xi) f_6(\eta) \end{bmatrix} ; \{V\} = \begin{bmatrix} u_i \\ v_i \\ w_i \\ w_i' = \left( \frac{\partial w}{\partial s} \right)_i \\ w_i'' = \left( \frac{\partial w}{r \partial \theta} \right)_i \\ w_i''' = \left( \frac{\partial^2 w}{r \partial \theta \partial s} \right)_i \\ u_j \\ v_j \\ w_j \\ w_j' = \left( \frac{\partial w}{\partial s} \right)_j \\ w_j'' = \left( \frac{\partial w}{r \partial \theta} \right)_j \\ w_j''' = \left( \frac{\partial^2 w}{r \partial \theta \partial s} \right)_j \\ u_R \\ v_R \\ w_R \\ w_R' = \left( \frac{\partial w}{\partial s} \right)_R \\ w_R'' = \left( \frac{\partial w}{r \partial \theta} \right)_R \\ w_R''' = \left( \frac{\partial^2 w}{r \partial \theta \partial s} \right)_R \\ u_\ell \\ v_\ell \\ w_\ell \\ w_\ell' = \left( \frac{\partial w}{\partial s} \right)_\ell \\ w_\ell'' = \left( \frac{\partial w}{r \partial \theta} \right)_\ell \\ w_\ell''' = \left( \frac{\partial^2 w}{r \partial \theta \partial s} \right)_\ell \end{bmatrix} ; \{S\} = \begin{bmatrix} F_{u_i} \\ F_{v_i} \\ F_{w_i} \\ F_{w_i'} \\ F_{w_i''} \\ F_{w_i'''} \\ F_{u_j} \\ F_{v_j} \\ F_{w_j} \\ F_{w_j'} \\ F_{w_j''} \\ F_{w_j'''} \\ F_{u_R} \\ F_{v_R} \\ F_{w_R} \\ F_{w_R'} \\ F_{w_R''} \\ F_{w_R'''} \\ F_{u_\ell} \\ F_{v_\ell} \\ F_{w_\ell} \\ F_{w_\ell'} \\ F_{w_\ell''} \\ F_{w_\ell'''} \end{bmatrix}
 \end{aligned}$$

### 3.4 Derivation of the Element Stiffness

#### 3.4.1 Strains

When the displacement fields (3.29) are introduced into the strains for general shells of revolution derived in chapter 2 (Table 2.1), one finds

$$\begin{Bmatrix} E \end{Bmatrix}_{6 \times 1} = \begin{bmatrix} B \end{bmatrix}_{6 \times 24} \begin{Bmatrix} V \end{Bmatrix}_{24 \times 1} \quad (3.30)$$

where

$$\langle E \rangle = \langle E_{\langle 11 \rangle} \quad E_{\langle 22 \rangle} \quad \frac{1}{2}(E_{\langle 12 \rangle} + E_{\langle 21 \rangle}) \quad -\nu E_{\langle 11 \rangle} \quad -\nu E_{\langle 22 \rangle} \quad -\frac{1}{2}(\nu E_{\langle 12 \rangle} + \nu E_{\langle 21 \rangle}) \rangle \quad (3.31)$$

[B] is given in transposed form (24 × 6) in Table 3.2 on the next page.

#### 3.4.2 Strain Energy

The formula for the strain energy U of a thin linear elastic shell in terms of the deformation measures  $\epsilon$  and  $K$  is given by

$$U = \frac{1}{2} \int_A \langle E \rangle [D] \{ E \} dA \quad (3.32)$$

with

$$[D] = \frac{Eh}{1-\nu^2} \begin{bmatrix} 1 & \nu & 0 & 0 & 0 & 0 \\ \nu & 1 & 0 & 0 & 0 & 0 \\ 0 & 0 & 2(1-\nu) & 0 & 0 & 0 \\ 0 & 0 & 0 & \frac{h^2}{12} & \frac{\nu h^2}{12} & 0 \\ 0 & 0 & 0 & \frac{\nu h^2}{12} & \frac{h^2}{12} & 0 \\ 0 & 0 & 0 & 0 & 0 & 2(1-\nu) \frac{h^2}{12} \end{bmatrix} \quad (3.33)$$



Although all of the assumptions on which this relationship is based are widely accepted in linear shell theory, some of them are worth recalling.

- a) The usual Hooke's law for linear isotropic materials holds; this should be reconsidered if nonlinear strains were used.
- b) This law is transformed for plane stress; but the condition of zero transverse strain was used in (2.53).
- c) The strain across the thickness can be expressed in terms of middle surface strains and curvature changes only; this is true because terms in  $Z^2$  were neglected in (2.44).
- d) The integral over the shell volume is approximated by [66]

$$\int_V dV = \int_{-\frac{h}{2}}^{+\frac{h}{2}} \int_A \left(1 - \frac{Z}{R_1} - \frac{Z}{R_2} + \frac{Z^2}{R_1 R_2}\right) dZ dA \approx \int_{-\frac{h}{2}}^{+\frac{h}{2}} \int_A dZ dA$$

In terms of the nodal degrees of freedom, (3.32) becomes

$$U = \frac{1}{2} \langle V \rangle \int_A [B^T][D][B] dA \{V\}. \quad (3.35)$$

### 3.4.3 Virtual Work Principle

If one designates  $\{S\}$  the vector of generalized forces associated with the nodal DOF (see Table 3.1), an application of the virtual displacements principle gives immediately

$$\langle \delta V \rangle \{S\} = \langle \delta V \rangle \int_A [B^T][D][B] dA \{V\} \quad (2.38)$$

$$\{S\} = [K]\{V\} \quad (3.37)$$

with the element stiffness  $[K]$  defined as

$$[K] = \int_A [B^T][D][B] dA. \quad (3.38)$$



### 3.4.4 Numerical Integration

When the triple matricial product  $[B^T][D][B]$  is performed, a typical term appearing under the integral sign may contain the different following factors in  $\xi$ :

Factor	Approximate or Exact Representation		
	General Shell	Toroidal Shell	Conical Shell
$f_1(\xi), f_2(\xi)$	polyn. 1st deg.	polyn. 1st deg.	polyn. 1st deg.
$f_3(\xi), \dots, f_6(\xi)$	polyn. 3rd deg.	polyn. 3rd deg.	polyn. 3rd deg.
$r(\xi)$	polyn. 3rd deg.	trigon. funct.	polyn. 1st deg.
$\frac{1}{r(\xi)}$	$\frac{1}{\text{polyn. 3rd deg.}}$	$\frac{1}{\text{trigon. funct.}}$	$\frac{1}{\text{polyn. 1st deg.}}$
$\sin\varphi = \frac{\partial r}{\partial s}$	polyn. 2nd deg.	trigon. funct.	constant
$\cos\varphi = \sqrt{1 - \sin^2\varphi}$	irrat. funct.	trigon. funct.	constant
$\frac{\partial\varphi}{\partial s} = \frac{\partial(\sin\varphi)/\partial s}{\cos\varphi}$	polyn. 1st deg. irrat. funct.	linear in $\xi$	0

The variable  $\eta$  appears only through  $f_1(\eta)$  to  $f_6(\eta)$  i.e. through polynomials of degree one to three in  $\eta$ .

For instance, the energy term  $\left( \epsilon_{11} \frac{Eh}{1-\nu^2} \epsilon_{11} \right)$  will contribute the following dot product to the component  $K_{11}$  of the stiffness matrix

$$\int_A \langle B_{11} \ B_{21} \ \dots \ B_{241} \rangle \frac{Eh}{1-\nu^2} \langle B_{11} \ B_{21} \ \dots \ B_{241} \rangle^T dA \quad (3.39)$$

where the subscripts are now used to represent row and column numbers in matrices; in particular, the last term of the dot product writes

$$\int_A B_{24} \frac{Eh}{1-\nu^2} B_{24} dA = \frac{Eh}{1-\nu^2} \frac{\alpha^2 r_0^2 l^2}{16} \int_{-1}^{+1} [f_6(\eta)]^2 d\eta \int_{-1}^{+1} \frac{\partial \varphi}{\partial s} [f_6(\xi)]^2 r(\xi) d\xi \quad (3.40)$$

The integrand in  $\eta$  is a polynomial of degree 6; considering  $\frac{\partial \varphi}{\partial s}$  as linear in  $\xi$  (torus), the integrand in  $\xi$  is a polynomial of degree 11. If one assumes that the elements are small enough so that the trigonometric and irrational functions can also be approximated by polynomials, a similar study can be conducted for all diagonal components of [K], which are likely to give the highest products. One finds that degree 6 in  $\eta$  and approximate degree 11 in  $\xi$  are the highest polynomials to be expected for a general shell of revolution; for a cylindrical shell, degree 6 can be expected in both  $\xi$  and  $\eta$ .

Formal integration of all 300 components of one half stiffness matrix is theoretically feasible, but very tedious, for the circular plate, the cylindrical and conical shells. For more general cases, numerical integration is necessary.

It is known that Gaussian integration with  $n$  points will give exact results for polynomials of degree up to  $(2n-1)$ . Therefore, in the present case 4 points seem required in the  $\eta$  direction and 4 to 6 points in the  $\xi$  direction depending on the type of shell.

In practice, numerical integration with  $6 \times 6$  and  $4 \times 4$  points were found to give almost equivalent stiffnesses for a spherical element. But significant differences were found when it was attempted to use 3 and 4 points on the  $\eta$  and  $\xi$  directions respectively. Therefore, a  $4 \times 4$  grid was adopted.

It must be noted that comparison of stiffnesses was based on their 24 eigenvalues rather than their components. Besides the advantage of having to look at 24 values instead of 300, the sensitivity of the eigenvalue problem makes more obvious differences in accuracy of the numerical integration process.

### 3.4.5 Interpretation of Stiffness Terms

While the stiffness matrix was being checked, a puzzling problem arose; although its solution turned out to be trivial, it seems worth mentioning because it is representative of the surprises to be expected with curvilinear coordinates.

For simplicity sake, this problem is explained on a circular ring which can be considered as degenerated from the cylindrical shell by choosing the loading and the elastic coefficients such that the variable  $u$  can be neglected. The DOF reduce to (Fig. 3.3).

$$\langle V \rangle = \langle v_i \ w_i \ w_i \ v_j \ w_j \ w_j \rangle \quad (3.41)$$

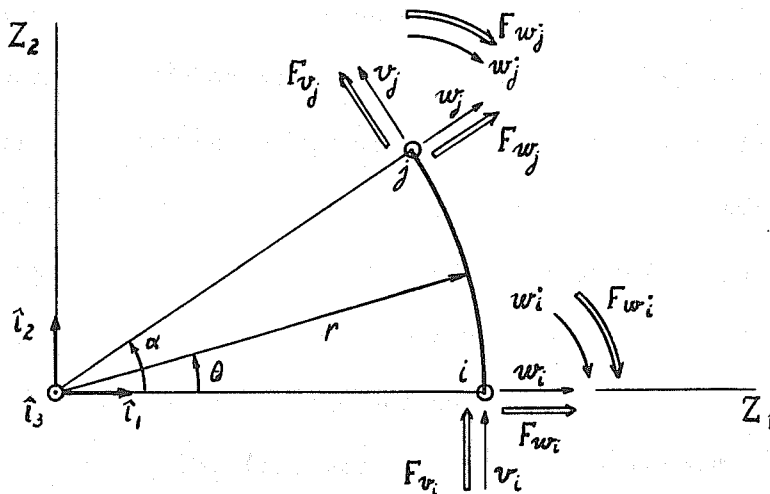


Fig. 3.3. Circular Ring DOF.

In the resulting stiffness matrix, the first column, for instance, can be interpreted as the set of generalized forces required to maintain a deformed configuration in which  $v_i = 1$ , all others DOF being blocked. Hence, for this particular deformation

$$\begin{aligned} K_{11} &= Fv_i & , & & K_{21} &= Fw_i & , & & K_{31} &= Fw_i^* & , & & \\ K_{41} &= Fv_j & , & & K_{51} &= Fw_j & , & & K_{61} &= Fw_j^* & . & & \end{aligned} \quad (3.42)$$

A preliminary check of correctness for  $[K]$  consists in verifying that this first column satisfies translational and rotational equilibriums. Similar interpretation and identical checks can be performed on every column of  $[K]$ .

The natural tendency would be to write for the translation check along  $Z_2$  and rotation check about 0

$$Fv_i + Fv_j \cos \alpha + Fw_j \sin \alpha = 0 \quad (3.43)$$

$$-Fw_i - Fw_j + rFv_i + rFv_j = 0. \quad (3.44)$$

It turns out that none of these equilibriums is satisfied! A closer look reveals that a translation  $S_2$  along  $Z_2$  produces

$$\begin{aligned} v(\theta) &= S_2 \cos \theta & , & & v_i &= S_2 & , & & v_j &= S_2 \cos \alpha \\ w(\theta) &= S_2 \sin \theta & , & & w_i &= 0 & , & & w_j &= S_2 \sin \alpha \\ w^*(\theta) &= \frac{S_2}{r} \cos \theta & , & & w_i^* &= \frac{S_2}{r} & , & & w_j^* &= \frac{S_2}{r} \cos \alpha \end{aligned} \quad (3.45)$$

and a small rotation  $\beta_3$  about 0 gives

$$\begin{aligned} v(\theta) &= \beta_3 r & , & & v_i &= \beta_3 r & , & & v_j &= \beta_3 r \\ w(\theta) &= 0 & , & & w_i &= 0 & , & & w_j &= 0 \\ w^*(\theta) &= 0 & , & & w_i^* &= 0 & , & & w_j^* &= 0 \end{aligned} \quad (3.46)$$

An application of the virtual displacement principle to translation  $S_2$  and small rotation  $\beta_3$  gives

$$S_2 F_{v_i} + \frac{S_2}{r} F_{w_i} + S_2 \cos \alpha F_{v_j} + S_2 \sin \alpha F_{w_j} + \frac{S_2}{r} \cos \alpha F_{w_j} = 0 \quad (3.47)$$

$$\beta_3 r F_{v_i} + \beta_3 r F_{v_j} = 0 \quad (3.48)$$

from which one obtains the correct equilibrium equations

$$F_{v_i} + F_{v_j} \cos \alpha + F_{w_j} \sin \alpha + \frac{1}{r} F_{w_i} + \frac{\cos \alpha}{r} F_{w_j} = 0 \quad (3.49)$$

$$F_{v_i} + F_{v_j} = 0. \quad (3.50)$$

The error implicitly committed in (3.43) and (3.44) was to consider  $F_{w_i}$  and  $F_{w_j}$  as bending moments. They are not bending moments because  $w_i$  and  $w_j$  are not physical rotations. The real physical rotations are

$$\gamma_i = w_i - \frac{v_i}{r}, \quad \gamma_j = w_j - \frac{v_j}{r}. \quad (3.51)$$

The second term is due to the rotation of the curvilinear basis from point to point and would come from Christoffel symbols if the indicial notation was still used.

If the  $\gamma$ 's were taken as nodal degrees of freedom, the resulting stiffness matrix would avoid the pitfalls explained in this section. They are not chosen however, because they are less convenient to use in the displacement interpolation functions.

Another important remark ought to be made here. Even the correct equilibrium equations (3.49) and (3.50) will not be satisfied by the stiffness matrix (3.38) for a general element of revolution; this can be explained as follows.

Because they are not exactly represented in the displacement interpolation functions, the rigid modes produce some strains when they are imposed on the element. The left hand sides in Eqs. (3.47) and (3.48) represent the virtual work of the external loading, replaced by nodal generalized forces, in rigid motions  $S_2$  and  $\beta_3$ . If the rigid motions produce strains, these left hand sides should be equated to the internal work or internal energy variation produced during these displacements, then the right hand sides are not zeros and (3.49), (3.50) are no longer satisfied.

This point will be discussed again in chapter 4. But it may already be mentioned that when the rigid body modes are introduced in  $[K]$ , Eqs. (3.49) and (3.50) are finally satisfied.

### 3.5 Generalized Nodal Forces

The concept of tributary area is sometimes used to replace the distributed load externally applied to the element by concentrated nodal forces. In the virtual work approach, on the other hand, generalized forces are associated with each DOF by the condition that they produce the same work as the external load under any possible deformation pattern.

The reliability of these methods depends essentially on the type of element. The tributary area may be satisfactory for plane stress or plane stress elements with displacement DOF only. The generalized forces seem preferable in plate bending elements with rotation DOF (the tributary area will not associate any forces with those). But the generalized moments may in turn be

detrimental if the flat plate elements are an approximation of a curved shell, as experienced by Johnson [21].

In the element being developed here, half of the DOF are displacement derivatives without clear physical significance; the tributary area concept which would not associate forces with any of these seems unsafe.

The generalized forces  $\{F\}$  are obtained from the virtual displacements expressions

$$\langle \delta V \rangle \{F\} = \int_A \langle \delta u \ \delta v \ \delta w \rangle \begin{Bmatrix} f_u \\ f_v \\ f_w \end{Bmatrix} dA = \langle \delta V \rangle \int_A [\phi^T] \begin{Bmatrix} f_u \\ f_v \\ f_w \end{Bmatrix} dA \quad (3.52)$$

where  $f_u$ ,  $f_v$ ,  $f_w$  are distributed loads in the  $u$ ,  $v$ ,  $w$  directions.

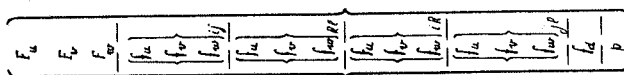
Table 3.3 on next page contains the generalized forces  $\{F\}$  for the following loading cases:

- a) Concentrated loads  $\langle F_u, F_v, F_w \rangle$  applied at coordinates  $\xi, \eta$ ,
- b) Uniform line loads  $\langle f_u, f_v, f_w \rangle_{ij}$  along the parallel  $ij$ ,
- c) Uniform line loads  $\langle f_u, f_v, f_w \rangle_{kl}$  along the parallel  $kl$ ,
- d) Uniform line loads  $\langle f_u, f_v, f_w \rangle_{ik}$  along the meridian  $ik$ ,
- e) Uniform line loads  $\langle f_u, f_v, f_w \rangle_{jl}$  along the meridian  $jl$ ,
- f) Uniform dead load  $f_d$  directed along the axis of revolution,
- g) Uniform inner pressure  $p$ .

Numerical integration must be used again wherever the integral signs have been left.

TABLE 3.3 GENERALIZED EXTERNAL FORCES

$F_{u_1}$	$f_1(\xi) f_1(\eta)$	0	0	0	0	0	0	0	0	0	0	0	0	0	0	0	0	0	$\frac{a_1}{4} \int_{-1}^{+1} \int_{-1}^{+1} r \cos \varphi f_1(\xi) f_1(\eta) d\xi d\eta$	$\frac{a_1}{4} \int_{-1}^{+1} \int_{-1}^{+1} r f_1(\xi) f_1(\eta) d\xi d\eta$
$F_{v_1}$	$f_1(\xi) f_1(\eta)$	0	0	0	0	0	0	0	0	0	0	0	0	0	0	0	0	0	0	0
$F_{w_1}$	0	0	0	0	0	0	0	0	0	0	0	0	0	0	0	0	0	0	0	0
$F_{u_2}$	0	0	0	0	0	0	0	0	0	0	0	0	0	0	0	0	0	0	0	0
$F_{v_2}$	0	0	0	0	0	0	0	0	0	0	0	0	0	0	0	0	0	0	0	0
$F_{w_2}$	0	0	0	0	0	0	0	0	0	0	0	0	0	0	0	0	0	0	0	0
$F_{u_3}$	$f_1(\xi) f_1(\eta)$	0	0	0	0	0	0	0	0	0	0	0	0	0	0	0	0	0	0	0
$F_{v_3}$	0	0	0	0	0	0	0	0	0	0	0	0	0	0	0	0	0	0	0	0
$F_{w_3}$	0	0	0	0	0	0	0	0	0	0	0	0	0	0	0	0	0	0	0	0
$F_{u_4}$	0	0	0	0	0	0	0	0	0	0	0	0	0	0	0	0	0	0	0	0
$F_{v_4}$	0	0	0	0	0	0	0	0	0	0	0	0	0	0	0	0	0	0	0	0
$F_{w_4}$	0	0	0	0	0	0	0	0	0	0	0	0	0	0	0	0	0	0	0	0
$F_{u_5}$	0	0	0	0	0	0	0	0	0	0	0	0	0	0	0	0	0	0	0	0
$F_{v_5}$	0	0	0	0	0	0	0	0	0	0	0	0	0	0	0	0	0	0	0	0
$F_{w_5}$	0	0	0	0	0	0	0	0	0	0	0	0	0	0	0	0	0	0	0	0
$F_{u_6}$	0	0	0	0	0	0	0	0	0	0	0	0	0	0	0	0	0	0	0	0
$F_{v_6}$	0	0	0	0	0	0	0	0	0	0	0	0	0	0	0	0	0	0	0	0
$F_{w_6}$	0	0	0	0	0	0	0	0	0	0	0	0	0	0	0	0	0	0	0	0
$F_{u_7}$	0	0	0	0	0	0	0	0	0	0	0	0	0	0	0	0	0	0	0	0
$F_{v_7}$	0	0	0	0	0	0	0	0	0	0	0	0	0	0	0	0	0	0	0	0
$F_{w_7}$	0	0	0	0	0	0	0	0	0	0	0	0	0	0	0	0	0	0	0	0
$F_{u_8}$	0	0	0	0	0	0	0	0	0	0	0	0	0	0	0	0	0	0	0	0
$F_{v_8}$	0	0	0	0	0	0	0	0	0	0	0	0	0	0	0	0	0	0	0	0
$F_{w_8}$	0	0	0	0	0	0	0	0	0	0	0	0	0	0	0	0	0	0	0	0
$F_{u_9}$	0	0	0	0	0	0	0	0	0	0	0	0	0	0	0	0	0	0	0	0
$F_{v_9}$	0	0	0	0	0	0	0	0	0	0	0	0	0	0	0	0	0	0	0	0
$F_{w_9}$	0	0	0	0	0	0	0	0	0	0	0	0	0	0	0	0	0	0	0	0
$F_{u_{10}}$	0	0	0	0	0	0	0	0	0	0	0	0	0	0	0	0	0	0	0	0
$F_{v_{10}}$	0	0	0	0	0	0	0	0	0	0	0	0	0	0	0	0	0	0	0	0
$F_{w_{10}}$	0	0	0	0	0	0	0	0	0	0	0	0	0	0	0	0	0	0	0	0





### 3.6 Structure Stiffness

The structural stiffness can be formed from the element stiffnesses by means of the direct stiffness method. The geometry idealization maintains continuity of slopes between adjacent elements; on the other hand, the chosen DOF are referred to the middle surface; therefore, at one given nodal point, the DOF are the same no matter which element they are supposed to belong to. No transformation to a new global system of reference is necessary before assemblage into the structural system; this is an advantage to be credited to the curvilinear coordinates.

The load vector can also be formed by direct addition of the generalized forces contributed by neighboring elements to a given nodal point.

## 4. REPRESENTATION OF THE RIGID MODES

### 4.1 General

In chapter 3, two facts concerning the derivation of the stiffness matrices were mentioned: first, that the rigid body modes were not included in the assumed displacement fields and, second, that the columns of the stiffness matrix did not satisfy equilibrium precisely because of the lack of these rigid body modes. This topic will be further discussed in the present chapter.

The exact small rigid motions for the quadrilateral curved element are derived in Section 4.2. It is shown that they cannot be represented in general by the set of chosen interpolation functions, except in the limit, when the element is almost flat, or in certain degenerate cases.

A study of the eigenvalues permits one to find how many rigid modes, if any, are already present in the displacement field, but not to decide which ones should still be added. In Section 4.5, it is explained first, how to add all rigid body modes and second, how to determine which ones are redundant. The technique is demonstrated on a cylindrical shell element and later applied to other types of elements of revolution.

The chapter concludes with the computation of shell forces in the presence of rigid body motions.

## 4.2 Exact Small Rigid Motions for the Quadrilateral Element

### 4.2.1 Relationships Between Bases

The normalized curvilinear basis at an arbitrary point P can be expressed in terms of the general Cartesian basis (Fig. 4.1) as

$$\begin{Bmatrix} \frac{A_1}{|A_1|} \\ \frac{A_2}{|A_2|} \\ \underline{N} \end{Bmatrix}_P = \begin{bmatrix} \sin \varphi \cos \theta & \sin \varphi \sin \theta & -\cos \varphi \\ -\sin \theta & \cos \theta & 0 \\ \cos \varphi \cos \theta & \cos \varphi \sin \theta & \sin \varphi \end{bmatrix} \begin{Bmatrix} \hat{i}_1 \\ \hat{i}_2 \\ \hat{i}_3 \end{Bmatrix} \quad (4.1)$$

The same relationship holds at the element center O when  $\varphi$  and  $\theta$  are replaced by  $\varphi_0$  and  $\theta_0$ . Its inverse at O is given by

$$\begin{Bmatrix} \hat{i}_1 \\ \hat{i}_2 \\ \hat{i}_3 \end{Bmatrix} = \begin{bmatrix} \sin \varphi_0 \cos \theta_0 & -\sin \theta_0 & \cos \varphi_0 \cos \theta_0 \\ \sin \varphi_0 \sin \theta_0 & \cos \theta_0 & \cos \varphi_0 \sin \theta_0 \\ -\cos \varphi_0 & 0 & \sin \varphi_0 \end{bmatrix} \begin{Bmatrix} \frac{A_1}{|A_1|} \\ \frac{A_2}{|A_2|} \\ \underline{N} \end{Bmatrix}_O \quad (4.2)$$

From (4.1) and (4.2), it is possible to find the relationship between the normalized curvilinear bases at O and P:

$$\begin{Bmatrix} \frac{A_1}{|A_1|} \\ \frac{A_2}{|A_2|} \\ \underline{N} \end{Bmatrix}_O = \begin{bmatrix} \sin \varphi_0 \sin \varphi \cos \theta + \cos \varphi_0 \cos \varphi & -\sin \varphi_0 \sin \theta & \sin \varphi_0 \cos \varphi \cos \theta - \cos \varphi_0 \sin \varphi \\ \sin \varphi \sin \theta & \cos \theta & \cos \varphi \sin \theta \\ \cos \varphi_0 \sin \varphi \cos \theta - \sin \varphi_0 \cos \varphi & -\cos \varphi_0 \sin \theta & \cos \varphi_0 \cos \varphi \cos \theta + \sin \varphi_0 \sin \varphi \end{bmatrix} \begin{Bmatrix} \frac{A_1}{|A_1|} \\ \frac{A_2}{|A_2|} \\ \underline{N} \end{Bmatrix}_P \quad (4.3)$$

in which  $(\theta - \theta_0)$  has been reduced to  $\theta$  by assuming that O belongs to the plane defined by  $\hat{i}_1$  and  $\hat{i}_3$ . In matrix form

$$\left\{ \frac{A}{|A|} \right\}_O = \left[ T_P^T \right] \left\{ \frac{A}{|A|} \right\}_P \quad (4.4)$$

with

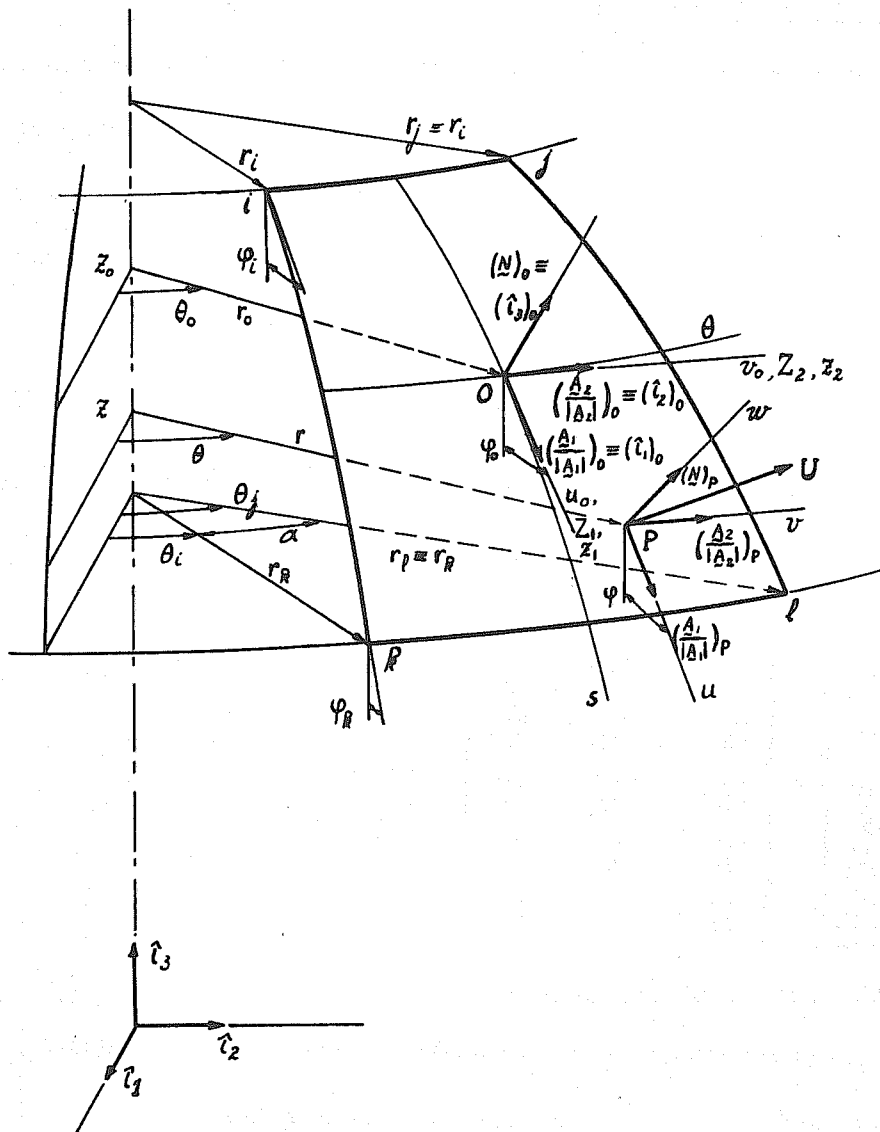


Fig. 4.1. Quadrilateral Shell Element.

$$\left[ T_P^T \right] = \begin{bmatrix} T_{11} & T_{21} & T_{31} \\ T_{12} & T_{22} & T_{32} \\ T_{13} & T_{23} & T_{33} \end{bmatrix} \quad (4.5)$$

#### 4.2.2 Translations

Assume that the element undergoes a translation described by the vector  $\underline{U}$  whose components are  $u_o, v_o, w_o$  with respect to the normalized curvilinear basis at element center 0. The displacement is also described by  $\underline{U}$  at an arbitrary point P but its components with respect to the normalized basis at P are

$$\langle u \ v \ w \rangle = \langle u_o \ v_o \ w_o \rangle \left[ T_P^T \right] \quad (4.6)$$

For future purposes, it is also interesting to compute the derivatives of  $w$  so that, finally,

$$\left\{ \begin{array}{l} u \\ v \\ w \\ \frac{\partial w}{\partial s} \\ \frac{\partial w}{r \partial \theta} \\ \frac{\partial^2 w}{r \partial \theta \partial s} \end{array} \right\} = \begin{bmatrix} T_{11} & T_{12} & T_{13} \\ T_{21} & T_{22} & T_{23} \\ T_{31} & T_{32} & T_{33} \\ T_{31}' & T_{32}' & T_{33}' \\ T_{31}'' & T_{32}'' & T_{33}'' \\ T_{31}''' & T_{32}''' & T_{33}''' \end{bmatrix} \left\{ \begin{array}{l} u_o \\ v_o \\ w_o \end{array} \right\} \quad (4.7)$$

with the matrix of T's detailed here below.

$$\left[ \begin{array}{ccc} \sin \varphi_o \sin \varphi \cos \theta + \cos \varphi_o \cos \varphi & \sin \varphi \sin \theta & \cos \varphi_o \sin \varphi \cos \theta - \sin \varphi_o \cos \varphi \\ -\sin \varphi_o \sin \theta & \cos \theta & -\cos \varphi_o \sin \theta \\ \sin \varphi_o \cos \varphi \cos \theta - \cos \varphi_o \sin \varphi & \cos \varphi_o \sin \theta & \cos \varphi_o \cos \varphi \cos \theta + \sin \varphi_o \sin \varphi \\ -\sin \varphi_o \sin \varphi \cos \theta \frac{\partial \varphi}{\partial s} - \cos \varphi_o \cos \varphi \frac{\partial \varphi}{\partial s} & -\sin \varphi \sin \theta \frac{\partial \varphi}{\partial s} & -\cos \varphi_o \sin \varphi \cos \theta \frac{\partial \varphi}{\partial s} + \sin \varphi_o \cos \varphi \frac{\partial \varphi}{\partial s} \\ -\sin \varphi_o \cos \varphi \sin \theta \frac{1}{r} & \cos \varphi \cos \theta \frac{1}{r} & -\cos \varphi_o \cos \varphi \sin \theta \frac{1}{r} \\ \sin \varphi_o \sin \varphi \sin \theta \frac{\partial \varphi}{\partial s} \frac{1}{r} & -\sin \varphi \cos \theta \frac{\partial \varphi}{\partial s} \frac{1}{r} & \cos \varphi_o \sin \varphi \sin \theta \frac{1}{r} \frac{\partial \varphi}{\partial s} \end{array} \right] \quad (4.8)$$

### 4.2.3 Small Rigid Rotations

Consider the normalized basis at 0 as a local Cartesian basis fixed in space.

$$\{\hat{r}\}_0 = \{\underline{A}/|\underline{A}|\}_0 \quad (4.9)$$

Assume that the rotations  $\beta_1, \beta_2, \beta_3$  about the three basis directions at 0 are so small that, for each of them,

$$\cos \beta \approx 1, \quad \sin \beta \approx \beta \quad (4.10)$$

and that they can be superposed without paying attention to the order of rotation.

Take an arbitrary point P; its coordinates  $\{Z\}$  or rotation radii  $\{P\}$  with respect to the local Cartesian basis are

$$\begin{Bmatrix} Z_1 \\ Z_2 \\ Z_3 \end{Bmatrix} = \begin{Bmatrix} \sin \varphi_0 (r \cos \theta - r_0) - \cos \varphi_0 (z - z_0) \\ r \sin \theta \\ \cos \varphi_0 (r \cos \theta - r_0) + \sin \varphi_0 (z - z_0) \end{Bmatrix} \equiv \begin{Bmatrix} P_1 \\ P_2 \\ P_3 \end{Bmatrix} \quad (4.11)$$

When the element rotates while the local Cartesian basis remains fixed, the coordinates of P become

$$\begin{Bmatrix} z_1 \\ z_2 \\ z_3 \end{Bmatrix} = \begin{bmatrix} 1 & -\beta_3 & \beta_2 \\ \beta_3 & 1 & -\beta_1 \\ -\beta_2 & \beta_1 & 1 \end{bmatrix} \begin{Bmatrix} Z_1 \\ Z_2 \\ Z_3 \end{Bmatrix} \quad (4.12)$$

The difference between coordinates after and before rotation gives the components of the displacement vector at P referred to the Cartesian basis at 0.

$$\begin{Bmatrix} z_1 - Z_1 \\ z_2 - Z_2 \\ z_3 - Z_3 \end{Bmatrix} = \begin{bmatrix} 0 & -\beta_3 & \beta_2 \\ \beta_3 & 0 & -\beta_1 \\ -\beta_2 & \beta_1 & 0 \end{bmatrix} \begin{Bmatrix} Z_1 \\ Z_2 \\ Z_3 \end{Bmatrix} = \begin{bmatrix} 0 & P_3 & -P_2 \\ -P_3 & 0 & P_1 \\ P_2 & -P_1 & 0 \end{bmatrix} \begin{Bmatrix} \beta_1 \\ \beta_2 \\ \beta_3 \end{Bmatrix} \quad (4.13)$$

When the displacement vector is referred to the normalized basis at P, one gets

$$\langle u \ v \ w \rangle = \langle x_1 - Z_1 \ x_2 - Z_2 \ x_3 - Z_3 \rangle \left[ T_P^T \right] \quad (4.14)$$

and finally,

$$\begin{pmatrix} u \\ v \\ w \\ \frac{\partial w}{\partial s} \\ \frac{\partial w}{r \partial \theta} \\ \frac{\partial^2 w}{r \partial \theta \partial s} \end{pmatrix} = \begin{pmatrix} -T_{12} P_3 + T_{13} P_2 & T_{11} P_3 - T_{13} P_1 & -T_{11} P_2 + T_{12} P_1 \\ -T_{22} P_3 + T_{23} P_2 & T_{21} P_3 - T_{23} P_1 & -T_{21} P_2 + T_{22} P_1 \\ -T_{32} P_3 + T_{33} P_2 & T_{31} P_3 - T_{33} P_1 & -T_{31} P_2 + T_{32} P_1 \\ -T_{32}' P_3 - T_{32} P_3' + T_{33}' P_2 + T_{33} P_2' & T_{31}' P_3 + T_{31} P_3' - T_{33}' P_1 - T_{33} P_1' & -T_{31}' P_2 - T_{31} P_2' + T_{32}' P_1 + T_{32} P_1' \\ -T_{32}'' P_3 - T_{32} P_3'' + T_{33}'' P_2 + T_{33} P_2'' & T_{31}'' P_3 + T_{31} P_3'' - T_{33}'' P_1 - T_{33} P_1'' & -T_{31}'' P_2 - T_{31} P_2'' + T_{32}'' P_1 + T_{32} P_1'' \\ -T_{32}''' P_3 - T_{32} P_3''' - T_{32}'' P_3' - T_{32} P_3'' & T_{31}''' P_3 + T_{31} P_3''' + T_{31}'' P_3' + T_{31} P_3'' & -T_{31}''' P_2 - T_{31} P_2''' - T_{31}'' P_2' - T_{31} P_2'' \\ + T_{33}' P_2 + T_{33} P_2' + T_{33}'' P_2 + T_{33} P_2'' & -T_{33}' P_1 - T_{33} P_1' - T_{33}'' P_1 - T_{33} P_1'' & + T_{32}'' P_1 + T_{32} P_1'' + T_{32}' P_1' + T_{32} P_1' \end{pmatrix} \begin{pmatrix} \beta_1 \\ \beta_2 \\ \beta_3 \end{pmatrix} \quad (4.15)$$

with  $T_{11}, \dots, T_{33}$  and  $P_1, P_2, P_3$  defined by (4.5) and (4.10), respectively, and their derivatives given by

$$\begin{aligned} P_1' &= \frac{\partial P_1}{\partial s} = T_{11} & , & \quad T_{31}' = \frac{\partial T_{31}}{\partial s} = -T_{11} \frac{\partial \varphi}{\partial s} \\ P_2' &= \frac{\partial P_2}{\partial s} = T_{12} & , & \quad T_{32}' = \frac{\partial T_{32}}{\partial s} = -T_{12} \frac{\partial \varphi}{\partial s} \\ P_3' &= \frac{\partial P_3}{\partial s} = T_{13} & , & \quad T_{33}' = \frac{\partial T_{33}}{\partial s} = -T_{13} \frac{\partial \varphi}{\partial s} \\ P_1'' &= \frac{\partial P_1}{r \partial \theta} = -\sin \varphi_0 \sin \theta & , & \quad T_{31}'' = \frac{\partial T_{31}}{r \partial \theta} = -\frac{1}{r} \sin \varphi_0 \cos \varphi \sin \theta \\ P_2'' &= \frac{\partial P_2}{r \partial \theta} = \cos \theta & , & \quad T_{32}'' = \frac{\partial T_{32}}{r \partial \theta} = \frac{1}{r} \cos \varphi \cos \theta \\ P_3'' &= \frac{\partial P_3}{r \partial \theta} = -\cos \varphi_0 \sin \theta & , & \quad T_{33}'' = \frac{\partial T_{33}}{r \partial \theta} = -\frac{1}{r} \cos \varphi_0 \cos \varphi \sin \theta \\ P_1''' &= \frac{\partial^2 P_1}{r \partial \theta \partial s} = -\frac{1}{r} \sin \varphi_0 \sin \varphi \sin \theta & , & \quad T_{31}''' = \frac{\partial^2 T_{31}}{r \partial \theta \partial s} = -P_1''' \frac{\partial \varphi}{\partial s} \\ P_2''' &= \frac{\partial^2 P_2}{r \partial \theta \partial s} = \frac{1}{r} \sin \varphi \cos \theta & , & \quad T_{32}''' = \frac{\partial^2 T_{32}}{r \partial \theta \partial s} = -P_2''' \frac{\partial \varphi}{\partial s} \\ P_3''' &= \frac{\partial^2 P_3}{r \partial \theta \partial s} = -\frac{1}{r} \cos \varphi_0 \sin \varphi \sin \theta & , & \quad T_{33}''' = \frac{\partial^2 T_{33}}{r \partial \theta \partial s} = -P_3''' \frac{\partial \varphi}{\partial s} \end{aligned} \quad (4.16)$$

#### 4.2.4 Summary

For future use, define

$$\begin{Bmatrix} u(s, \theta) \\ v(s, \theta) \\ w(s, \theta) \end{Bmatrix} = \left[ \phi_R(s, \theta) \right] \{U_R\} \quad (4.17)$$

where

$$\left[ \phi_R(s, \theta) \right] = \begin{bmatrix} T_{11} & T_{12} & T_{13} & -T_{12}P_3 + T_{13}P_2 & T_{11}P_3 - T_{13}P_1 & -T_{11}P_2 + T_{12}P_1 \\ T_{21} & T_{22} & T_{23} & -T_{22}P_3 + T_{23}P_2 & T_{21}P_3 - T_{23}P_1 & -T_{21}P_2 + T_{22}P_1 \\ T_{31} & T_{32} & T_{33} & -T_{32}P_3 + T_{33}P_2 & T_{31}P_3 - T_{33}P_1 & -T_{31}P_2 + T_{32}P_1 \end{bmatrix} \quad (4.18)$$

$$\langle U_R \rangle = \langle u_0 \quad v_0 \quad w_0 \quad ; \quad \beta_1 \quad \beta_2 \quad \beta_3 \rangle \quad (4.19)$$

Also introduce

$$\{V_R\} = [T_R] \{U_R\} \quad (4.20)$$

where  $\{V_R\}$  is the rigid part of the usual 24 displacement DOF vector and  $[T_R]$  is a  $(24 \times 6)$  matrix obtained by applying results (4.7) and (4.15) successively at

- a) corner i :  $\theta = -\frac{\alpha}{2}$  ,  $\varphi = \varphi_i$  ,  $\frac{\partial \varphi}{\partial s} = \left(\frac{\partial \varphi}{\partial s}\right)_i$  ,  $r = r_i$  ,
- b) corner j :  $\theta = \frac{\alpha}{2}$  ,  $\varphi = \varphi_i$  ,  $\frac{\partial \varphi}{\partial s} = \left(\frac{\partial \varphi}{\partial s}\right)_i$  ,  $r = r_i$  ,
- c) corner k :  $\theta = -\frac{\alpha}{2}$  ,  $\varphi = \varphi_R$  ,  $\frac{\partial \varphi}{\partial s} = \left(\frac{\partial \varphi}{\partial s}\right)_R$  ,  $r = r_R$  ,
- d) corner l :  $\theta = \frac{\alpha}{2}$  ,  $\varphi = \varphi_R$  ,  $\frac{\partial \varphi}{\partial s} = \left(\frac{\partial \varphi}{\partial s}\right)_R$  ,  $r = r_R$  .

#### 4.3 Representation of the Rigid Modes by the Displacement Functions

The results (4.7) and (4.15) show that  $u(s, \theta)$ ,  $v(s, \theta)$  and  $w(s, \theta)$ , due to small rigid-body modes, are not polynomial functions of the coordinates  $s$ ,  $\theta$  or their dimensionless equivalents  $\xi$  and  $\eta$ . The dependency on  $\theta$  is in the form of trigonometric functions and  $s$  indirectly appears through  $r$ ,  $z$ ,  $\sin \varphi$ ,  $\cos \varphi$ ,



of which only the first one is a polynomial. So there is no possibility to represent a rigid-body motion by a combination of the polynomials defined in Section 2.3. This conclusion must be revised in two special cases discussed hereafter:

- a) the finite element mesh is so refined that the elements are almost flat,
- b) the shell is a degenerate form

#### 4.3.1 Almost Flat Elements

If the following approximations are made

$$\cos \theta \approx 1, \quad \sin \theta \approx \theta, \quad (4.21)$$

$$\sin \varphi = \sin(\varphi_0 + \Delta\varphi) \approx \sin \varphi_0 + \Delta\varphi \cos \varphi_0, \quad (4.22)$$

$$\cos \varphi = \cos(\varphi_0 + \Delta\varphi) \approx \cos \varphi_0 - \Delta\varphi \sin \varphi_0.$$

the transformation matrix  $[T_p]$  and the displacements due to a rigid translation of element center 0 are given by

$$\begin{Bmatrix} u(s, \theta) \\ v(s, \theta) \\ w(s, \theta) \end{Bmatrix} = \begin{bmatrix} 1 & \theta (\sin \varphi_0 + \Delta\varphi \cos \varphi_0) & \Delta\varphi \\ -\theta \sin \varphi_0 & 1 & -\theta \cos \varphi_0 \\ -\Delta\varphi & \theta (\cos \varphi_0 - \Delta\varphi \sin \varphi_0) & 1 \end{bmatrix} \begin{Bmatrix} u_0 \\ v_0 \\ w_0 \end{Bmatrix} \quad (4.23)$$

The displacements due to small rigid rotations  $\beta_1, \beta_2, \beta_3$  are given by

$$\begin{Bmatrix} u(s, \theta) \\ v(s, \theta) \\ w(s, \theta) \end{Bmatrix} = \begin{Bmatrix} -\theta (\sin \varphi_0 + \Delta\varphi \cos \varphi_0) [\cos \varphi_0 (r - r_0) + \sin \varphi_0 (z - z_0)] + \Delta\varphi (r\theta) \\ -[\cos \varphi_0 (r - r_0) + \sin \varphi_0 (z - z_0)] - \theta \cos \varphi_0 (r\theta) \\ -\theta (\cos \varphi_0 - \Delta\varphi \sin \varphi_0) [\cos \varphi_0 (r - r_0) + \sin \varphi_0 (z - z_0)] + (r\theta) \end{Bmatrix} \beta_1$$

$$+ \begin{Bmatrix} \dots \\ \dots \\ \dots \end{Bmatrix}$$

$$\begin{aligned}
& \dots \left. \begin{aligned}
& \left[ \cos \varphi_0 (r-r_0) + \sin \varphi_0 (z-z_0) \right] - \Delta \varphi \left[ \sin \varphi_0 (r-r_0) - \cos \varphi_0 (z-z_0) \right] \\
& - \theta \sin \varphi_0 \left[ \cos \varphi_0 (r-r_0) + \sin \varphi_0 (z-z_0) \right] + \theta \cos \varphi_0 \left[ \sin \varphi_0 (r-r_0) - \cos \varphi_0 (z-z_0) \right] \\
& - \Delta \varphi \left[ \cos \varphi_0 (r-r_0) + \sin \varphi_0 (z-z_0) \right] - \left[ \sin \varphi_0 (r-r_0) - \cos \varphi_0 (z-z_0) \right]
\end{aligned} \right\} \beta_2 \\
& + \left. \begin{aligned}
& -(r\theta) + \theta (\sin \varphi_0 + \Delta \varphi \cos \varphi_0) \left[ \sin \varphi_0 (r-r_0) - \cos \varphi_0 (z-z_0) \right] \\
& \theta \sin \varphi_0 (r\theta) + \left[ \sin \varphi_0 (r-r_0) - \cos \varphi_0 (z-z_0) \right] \\
& \Delta \varphi (r\theta) + \theta (\cos \varphi_0 - \Delta \varphi \sin \varphi_0) \left[ \sin \varphi_0 (r-r_0) - \cos \varphi_0 (z-z_0) \right]
\end{aligned} \right\} \beta_3
\end{aligned} \tag{4.24}$$

The coordinate  $\theta$  now appears linearly and the small rigid motions will be correctly represented by linear polynomials as far as the variable  $\theta$  is concerned. But the variable  $s$  appears through  $\Delta \varphi$  in the translation part of  $u$  and  $w$ , through  $r$ ,  $z$  in the rotation part of  $v$ , and through the products  $r\Delta \varphi$ ,  $z\Delta \varphi$  in the rotation part of  $u$ ,  $w$ . This shows that the linear polynomial in  $s$  used to interpolate the displacement  $u$  will not represent correctly the translations unless  $\Delta \varphi \approx \sin \varphi$  be considered as linear in  $s$ ; it will not represent correctly the rotations unless  $r$ ,  $z$  and  $\Delta \varphi$  be considered as linear and constant in  $s$ . The cubic polynomials used for  $w$ , on the other hand, are accurate enough for the translations and will be correct for rotations if  $r$ ,  $z$  and  $\Delta \varphi$  are quadratic and linear in  $s$ , respectively.

The result (3.14) shows that a quadratic representation of  $r$  and its consequences, linear  $\Delta \varphi$ , quadratic  $Z$ , are reasonable approximations for elements with slightly curved meridian. Therefore the conditions imposed by  $w$  on  $r$ ,  $z$ ,  $\Delta \varphi$  are not really restrictive and the correct  $w$  under rigid motions will be recovered in the limit when the finite element mesh is refined. But the

condition imposed by  $u$ , namely that  $r$  be linear in  $s$ , is much more restrictive. It means either that  $\Delta\varphi$  is zero, i.e. the shell is conical, or  $\Delta\varphi$  is neglected with respect to unity, which is a rougher assumption than (4.22). Hence, the correct  $u$  under rigid motion will be recovered in the limit much more slowly than the  $w$ .

This reveals a disadvantage of choosing polynomials of lower degree for  $u$ ,  $v$  than for  $w$ . This choice was based on the understanding that smaller values and smaller gradients are expected for the "membrane" displacements  $u$  and  $v$  than for the "plate" displacement  $w$ . However, the above discussion shows that  $u$ ,  $v$ ,  $w$  deserve equal treatment as far as rigid motions are concerned.

#### 4.3.2 Degenerate Shells

Only the case of a cylindrical shell, which exhibits most of the interesting features of degeneracy, will be described here.

It is characterized by

$$\begin{aligned} \varphi(s) &= \varphi_0 = 0, & \cos\varphi &= 1, & \sin\varphi &= 0, \\ r(s) &= r_0 = R_2, & z(s) &= z_0 - s. \end{aligned} \quad (4.25)$$

Hence, rigid motions are described by

$$\begin{pmatrix} u \\ v \\ w \end{pmatrix} = \begin{bmatrix} 1 & 0 & 0 & 0 & r_0(\cos\theta-1) - r_0\sin\theta \\ 0 & \cos\theta & -\sin\theta & r_0(\cos\theta-1) & s\sin\theta & s\cos\theta \\ 0 & \sin\theta & \cos\theta & r_0\sin\theta & -s\cos\theta & s\sin\theta \end{bmatrix} \begin{pmatrix} u_0 \\ v_0 \\ w_0 \\ \beta_1 \\ \beta_2 \\ \beta_3 \end{pmatrix} \quad (4.26)$$

The linear and cubic interpolation functions chosen for  $u$ ,  $v$  and  $w$  obviously include the translation along the revolution axis giving

$u(s, \theta) = u_0$  everywhere. But they seem unable to represent any other motion since they can only approximate the trigonometric functions.

If, however, one considers a small rigid rotation  $\gamma_3$  about the axis of revolution, it can be considered as the superposition of a translation  $v_0 = +\gamma_3 r_0$  and a small rotation  $\beta_1 = -\gamma_3$  at element center  $O$  (Fig. 4.2). And, as such, it gives

$$\begin{Bmatrix} u \\ v \\ w \end{Bmatrix} = \begin{Bmatrix} 0 \\ r_0 \cos \theta - r_0 \cos \theta + r_0 \\ r_0 \sin \theta - r_0 \sin \theta \end{Bmatrix} \gamma_3 = \begin{Bmatrix} 0 \\ \gamma_3 r_0 \\ 0 \end{Bmatrix} \quad (4.27)$$

which is also representable by the chosen interpolation functions.

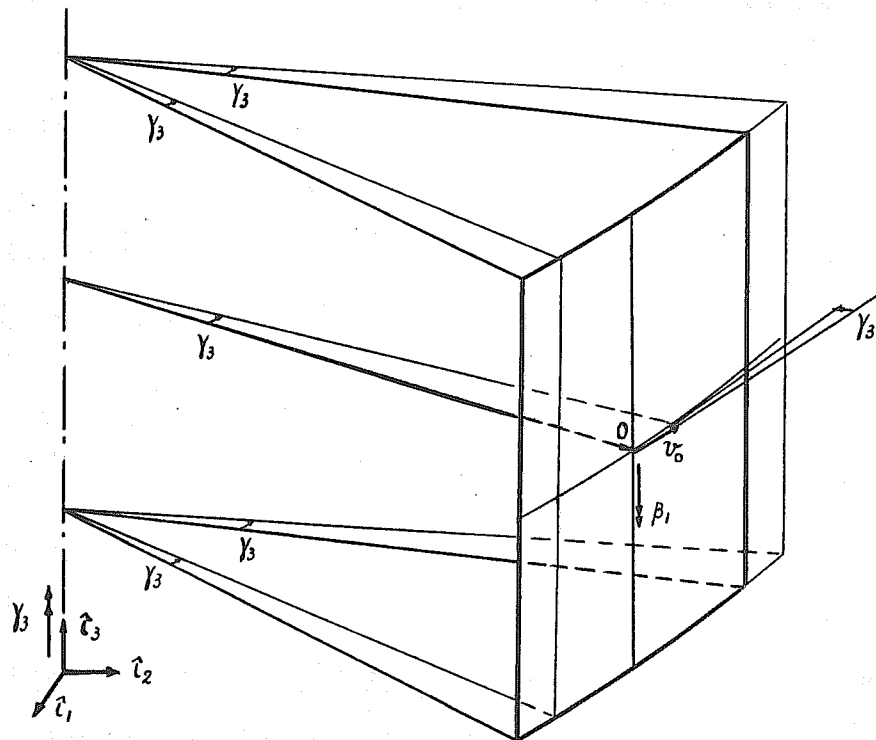


Fig. 4.2. Rotation of a Cylinder About Revolution Axis.

Therefore, even if the selected six rigid motions are not included in the displacement functions, linear combinations of some of them may still be present; there may be fewer missing modes than suspected at first sight.

In the case of the cylinder, also notice that, for a mesh refined in the  $\theta$  direction,

$$\begin{Bmatrix} u \\ v \\ w \end{Bmatrix} = \begin{bmatrix} 1 & 0 & 0 & 0 & 0 & -r_0\theta \\ 0 & 1 & -\theta & 0 & s\theta & s \\ 0 & \theta & 1 & r_0\theta & -s & s\theta \end{bmatrix} \begin{Bmatrix} u_0 \\ v_0 \\ w_0 \\ \beta_1 \\ \beta_2 \\ \beta_3 \end{Bmatrix} \quad (4.28)$$

All rigid body modes are comprised in linear displacement functions. The same conclusion holds for the cone, cylinder and plate with very large radii  $r$  and small central angle  $\theta$ .

The cylindrical shell is a simple example. For other elements, it may not be so easy to determine how many rigid modes, or combination of them, if any, are present. A more general procedure is required for this purpose and will be explained in the next section.

#### 4.4 Eigenvalues and Rigid Body Modes

Physically, an eigenvalue  $\lambda_n$  of an element stiffness matrix can be interpreted as the energy stored in the element while it is deformed in the associated mode shape  $\{W_n\}$ . A mode of deformation in which no energy is stored, i.e. the associated eigenvalue is zero, is called a rigid mode.

To illustrate this property of the eigenvalues and the previous discussion of rigid modes, three examples are presented in Table 4.1.

The first example is a large element cut along the diameter of a spherical shell ( $\alpha = 22.5^\circ$ ,  $0 \leq \varphi \leq 22.5^\circ$ ) (Fig. 4.3). The first column of Table 4.1 shows that no rigid modes are present: the six last eigenvalues are far from being zeros; eigenvalues 19 and 20, corresponding to "rigid modes" are just as big as eigenvalue 18, which is supposed to represent a "straining mode."

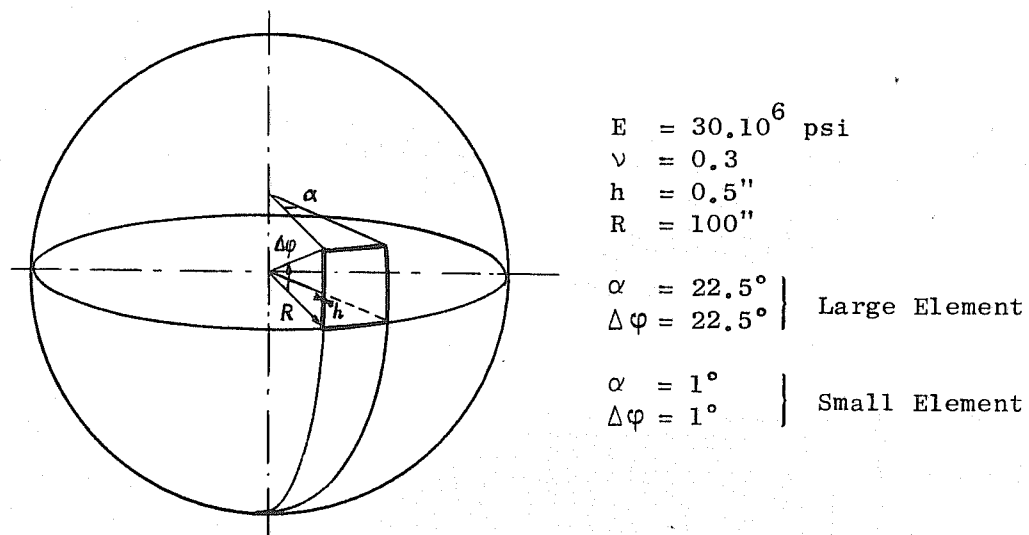


Fig. 4.3. Spherical Elements.

When a much smaller element ( $\alpha = 1^\circ$ ,  $0^\circ \leq \varphi \leq 1^\circ$ ) is cut from the same sphere the second column of Table 4.1 shows that a gap is opening between the "straining" and "rigid" modes. Considering the 15 digits accuracy of the computations, the last eigenvalue can be thought of as a perfect zero. This indicates that some modes are recovered faster than others in the limiting process.

TABLE 4.1  
EIGENVALUES AND EIGENVECTORS OF ELEMENT STIFFNESS MATRICES.

	LARGE SPHERICAL ELMT 24 EIGENVALUES	SMALL SPHERICAL ELMT 24 EIGENVALUES	LARGE CYLINDER ELEMNT 24 EIGENVALUES	LARGE CYLINDER ELEMNT EIGENVECTOR 23	LARGE CYLINDER ELEMNT EIGENVECTOR 24
1	4176722566.0162964	21431976.9577730	1909569765.0057983	.4829755	-.1228002
2	681131495.3889008	11538780.3087630	347279762.9251404	.1293625	.4846857
3	666937346.7416115	11538779.1628980	345696794.6368294	.0000002	.0000004
4	113928345.7404699	7419184.0735210	66679420.4683249	-.0000000	.0000000
5	203922287.1506830	7418604.0043053	16306890.1810810	-.0000000	.0000000
6	13708293.1141230	3477962.1370814	11540424.8459910	.0000000	-.0000000
7	11811164.4737060	2736780.6693152	10557390.1861330	.4829755	-.1228000
8	11728879.1116000	2736392.2466839	8007935.5352491	.1293624	.4846856
9	11679675.5296810	530209.9575731	7912059.9049824	.0000002	.0000004
10	10683975.3890720	339373.3830795	5887909.6943662	.0000000	-.0000000
11	4106475.6220745	339344.4633820	4791332.8843170	.0000000	.0000000
12	4086550.2059630	336543.1373246	2037486.4815816	.0000000	-.0000000
13	2026405.8903123	240439.3304099	1167351.5573968	.4829755	-.1228002
14	2021952.0157398	206285.5476790	1141631.2134812	.1293625	.4846856
15	1848139.7597253	44033.7270108	872737.0874942	.0000002	.0000004
16	1442861.0959006	30727.8869371	820024.6951047	.0000000	.0000000
17	491403.9297666	30726.9029130	362569.6975316	.0000000	-.0000000
18	36497.2618524	13585.1198616	20727.7244014	.0000000	.0000000
19	35429.7352569	243.7016549	18810.4700137	.4829755	-.1228000
20	30812.1009661	243.6766947	16181.3150266	.1293624	.4846855
21	2393.3498376	.0112231	22.5560385	.0000002	.0000004
22	1542.6481350	.0055772	1.2179351	.0000000	-.0000000
23	329.6969117	.0028224	-.0000013	.0000000	-.0000000
24	38.4541142	.0000009	-.0000047	.0000000	-.0000000

If they happen to be the important modes because the others are already included or not needed in the problem under consideration, the element is said "to contain the rigid body modes for all practical purposes." This conclusion was reached by Stricklin for curved segments of revolution with  $\Delta\varphi \leq 2^\circ$  [49] and by Schmit et al. for a specialized element [108].

The next example is a cylindrical shell element (Fig. 4.4).

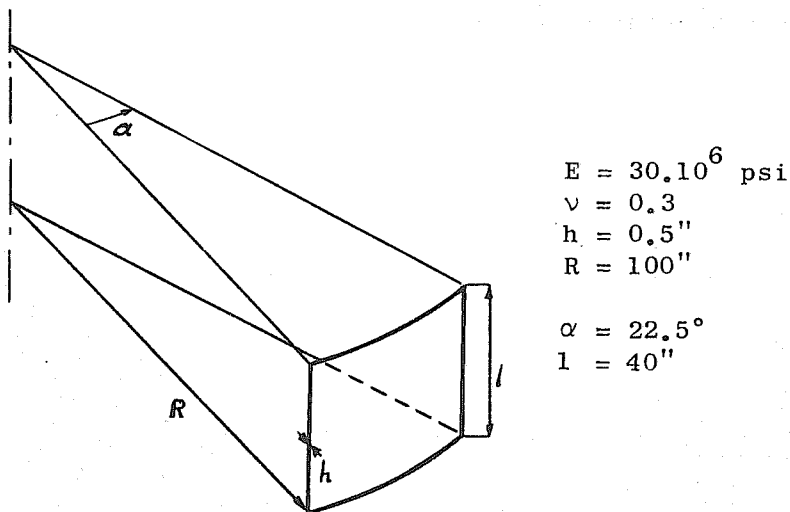


Fig. 4.4. Cylindrical Element.

As expected, the column 3 in Table 4.1 exhibits two zero eigenvalues (the minus sign and the residual figures in eigenvalues 23 and 24 are due to roundoff errors). The corresponding eigenvectors can both be considered as linear combinations of a vertical translation

$$\begin{aligned}
 u_i &= u_j = u_R = u_\theta = u_o \\
 w &= \frac{\partial w}{\partial s} = \frac{\partial w}{r \partial \theta} = \frac{\partial^2 w}{r \partial \theta \partial s} \quad \text{at } i, j, R, \theta.
 \end{aligned}
 \tag{4.29}$$



and a rotation about the axis of revolution

$$\begin{aligned} v_i &= v_j = v_R = v_\theta = \frac{1}{3} r_0 \\ w &= \frac{\partial w}{\partial s} = \frac{\partial w}{r \partial \theta} = \frac{\partial^2 w}{r \partial \theta \partial s} \quad \text{at } i, j, R, \theta. \end{aligned} \quad (4.30)$$

Again, in the cylindrical case, it is easy to find the rigid modes by inspection of the eigenvectors. But the fact that they represent linear combinations of the modes derived in Section 4.2 makes them difficult to identify in a general case. Also, the straining modes, imperfectly uncoupled from the rigid modes in this approximate representation, can inject some components in the "rigid modes" eigenvectors and make the interpretation even more difficult.

Therefore, an eigenvalue study can tell how many modes are present but not identify them in general. An easy way to identify them will be explained later.

#### 4.5 Determination of the Represented Rigid Modes

##### 4.5.1 Addition of Rigid Body Modes

Assume that the displacement functions do not include any rigid body modes.

The total displacements  $\langle u \ v \ w \rangle_T$  and the total 24 displacement DOF  $\{V_T\}$  can be divided into a deformation part and a rigid part such that

$$\begin{Bmatrix} u \\ v \\ w \end{Bmatrix}_T = \begin{Bmatrix} u \\ v \\ w \end{Bmatrix}_D + \begin{Bmatrix} u \\ v \\ w \end{Bmatrix}_R = \begin{bmatrix} \phi_D & \phi_R \end{bmatrix} \begin{Bmatrix} V_D \\ V_R \end{Bmatrix} \quad (4.31)$$

$$\begin{matrix} \{V_T\} \\ 24 \times 1 \end{matrix} = \begin{matrix} \{V_D\} \\ 24 \times 24 \end{matrix} + \begin{matrix} \{V_R\} \\ 24 \times 6 \end{matrix} = \begin{matrix} [I] \\ [T_R] \end{matrix} \begin{matrix} \left\{ \begin{matrix} V_D \\ U_R \end{matrix} \right\} \\ 30 \times 1 \end{matrix} \quad (4.32)$$

where  $[I]$  is an identity matrix,  $[\bar{\phi}_D]$ ,  $[\bar{\phi}_R]$ ,  $[T_R]$  are given by (3.29), (4.18) and (4.20) respectively.

As emphasized in Chapter 2, the selected strain-displacement relationships do not produce strains under rigid motion. therefore

$$\{E\} = [B \mid 0] \begin{matrix} \left\{ \begin{matrix} V_D \\ U_R \end{matrix} \right\} \end{matrix} \quad (4.33)$$

One can proceed as before to derive the stiffness matrix. Virtual displacements produce the internal work

$$\langle \delta V_D \mid \delta U_R \rangle \begin{matrix} \left[ \int_A [B^T] [D] [B] dA \mid 0 \right] \\ \left[ \begin{matrix} \phantom{\int_A} \\ 0 \phantom{\int_A} \end{matrix} \right] \end{matrix} \begin{matrix} \left\{ \begin{matrix} V_D \\ U_R \end{matrix} \right\} \end{matrix} = \langle \delta V_D \mid \delta U_R \rangle \begin{matrix} \left[ \begin{matrix} K \mid 0 \\ 0 \mid 0 \end{matrix} \right] \end{matrix} \begin{matrix} \left\{ \begin{matrix} V_D \\ U_R \end{matrix} \right\} \end{matrix} \quad (4.34)$$

The external work can be written in any of the three following ways:

$$\langle \delta V_T \rangle \{S_T\} = \langle \delta V_D \mid \delta U_R \rangle \begin{matrix} \left[ \begin{matrix} I \\ T_R^T \end{matrix} \right] \end{matrix} \{S_T\} = \langle \delta V_D \mid \delta U_R \rangle \begin{matrix} \left\{ \begin{matrix} S_D \\ S_R \end{matrix} \right\} \end{matrix} \quad (4.35)$$

After equating the internal and external work one gets

$$\begin{matrix} \left[ \begin{matrix} I \\ T_R^T \end{matrix} \right] \end{matrix} \{S_T\} = \begin{matrix} \left\{ \begin{matrix} S_D \\ S_R \end{matrix} \right\} \end{matrix} = \begin{matrix} \left[ \begin{matrix} K \mid 0 \\ 0 \mid 0 \end{matrix} \right] \end{matrix} \begin{matrix} \left\{ \begin{matrix} V_D \\ U_R \end{matrix} \right\} \end{matrix} \quad (4.36)$$

from which some predictable conclusions can be drawn:

a) the stiffness matrix  $[K]$  previously derived is a deformation stiffness,

b) all generalized forces associated with rigid modes vanish

$$[T_R^T] \{S_T\} = \{S_R\} = 0 \quad (4.37)$$

c) the generalized forces associated with total or deformation DOF are identical

$$[I] \{S_T\} = \{S_D\} \quad (4.38)$$

In the solution process, the deformation DOF  $\{V_D\}$  do not present any interest as such; one would like to replace them by the total displacements  $\{V_T\}$ . To this purpose, use

$$\{V_D\} = \begin{bmatrix} I \\ T_R \end{bmatrix} \begin{Bmatrix} V_T \\ -U_R \end{Bmatrix} \quad (4.39)$$

and the above conclusions to perform the following transformations

$$\{S_D\} = [K_D] \{V_D\} \quad (4.40)$$

$$\begin{bmatrix} I \\ T_R^T \end{bmatrix} \{S_D\} = \begin{bmatrix} I \\ T_R^T \end{bmatrix} [K_D] \begin{bmatrix} I \\ T_R \end{bmatrix} \begin{Bmatrix} V_T \\ -U_R \end{Bmatrix}$$

$$\begin{Bmatrix} S_D \\ 0 \end{Bmatrix} = \begin{bmatrix} K_D & K_D T_R \\ T_R^T K_D & T_R^T K_D T_R \end{bmatrix} \begin{Bmatrix} V_T \\ -U_R \end{Bmatrix} \equiv \begin{bmatrix} K_{DD} & K_{DR} \\ K_{RD} & K_{RR} \end{bmatrix} \begin{Bmatrix} V_T \\ -U_R \end{Bmatrix} \quad (4.41)$$

which is the result usually obtained when a deformation stiffness is transformed into a complete stiffness by a congruent transformation. In the following, the new stiffness will be called the "augmented matrix;" its different parts  $K_{DD}$ ,  $K_{DR}$ ,  $K_{RD}$ ,  $K_{RR}$  are defined by (4.41).

#### 4.5.2 Static Condensation of Rigid Modes

The rigid body modes  $\{U_R\}$  need not be compatible between adjacent elements; they can be considered as internal degrees of freedom and eliminated by static condensation. Using (4.41),

$$\{-U_R\} = -[K_{RR}^{-1}] [K_{RD}] \{V_T\} \quad (4.42)$$

$$\{S_T\} = [K_T] \{V_T\} \quad (4.43)$$

with

$$\{S_T\} = \{S_D\} \quad (4.44)$$

$$[K_T] = [K_{DD}] - [K_{DR}][K_{RR}^{-1}][K_{RD}]. \quad (4.45)$$

The structure stiffness is formed by assembling Eq. (4.43), written for each element, and the global system is solved to find  $\{V_T\}$ . The rigid motions  $\{U_R\}$  and nodal deformation DOF  $\{V_D\}$  can then be recovered by means of (4.42) and (4.39):

Now, the nodal displacement  $\{V_T\}$  will be compatible, i.e., at a given corner, the total displacements will be the same no matter which of the adjacent element this corner is supposed to belong to. But, the rigid motions being discontinuous from one element to the next one, different values of

$$\{V_R\} = [T_R] \{U_R\}, \quad \{V_D\} = \{V_T\} - \{V_R\} \quad (4.46)$$

will be obtained at the same corner, depending on which element is used to compute them. Furthermore, between the nodal points, the deformation part of the displacement will be represented by polynomial functions, while the rigid part will be represented by functions including trigonometric functions of  $\theta$  and  $s$ :

$$\begin{Bmatrix} u(s, \theta) \\ v(s, \theta) \\ w(s, \theta) \end{Bmatrix} = [\phi_D(s, \theta)] \{V_D\}, \quad \begin{Bmatrix} u(s, \theta) \\ v(s, \theta) \\ w(s, \theta) \end{Bmatrix} = [\phi_R(s, \theta)] \{U_R\}. \quad (4.47)$$

Therefore, the total displacement will be discontinuous between adjacent elements, the compatibility being recovered at the nodal points only for the considered DOF.

The static condensation does not usually produce this difficulty because, unlike the present case, the displacement fields

associated with the eliminated DOF often vanish on the element contour. Wilson [127], however, has developed elements rendered incompatible by static condensation of midside DOF; these elements compare favorably, in computational efficiency, with compatible elements possessing the same total number of DOF. Therefore, incompatibility, per se, does not invalidate a solution; its main drawback is the loss of the lower bound characteristic for the finite element solution based on displacement functions and stiffness matrices.

Additional comments will be made about incompatibility in Section 5.8. They are delayed until then because they are better understood in the light of numerical examples.

#### 4.5.3 Determination of the Rigid Modes Included in the Displacement Functions

So far it has been assumed that no rigid modes were included in the displacement functions

If one of them is present, it was previously explained that it can be considered as the eigenvector  $\{W_n\}$  associated with the eigenvalue  $\lambda_n = 0$  of the stiffness matrix  $[K]$ . If its presence is not detected, one may try to add it again: one column of  $[T_R]$  will be identical to  $\{W_n\}$  save for a constant proportionality factor. For that particular column,

$$\begin{aligned}
 [K_{DR}] &= [K_D][T_R] & \rightarrow [K_D]\{W_n\} &= \lambda_n \{W_n\} = \{0\} \\
 [K_{RD}] &= [T_R^T][K_D] & \rightarrow \langle W_n \rangle [K_D] &= \lambda_n \langle W_n \rangle = \langle 0 \rangle \\
 [K_{RR}] &= [T_R^T][K_D][T_R] & \rightarrow \langle W_n \rangle [K_D] \{W_n\} &= \lambda_n = 0
 \end{aligned} \tag{4.48}$$

i.e. one row and column, including the diagonal term, will be all zeros in the augmented matrix, which makes the rigid mode already represented easy to identify.

Note that, in practice, due to roundoff errors, the zeros are replaced by small quantities. Experience has shown that, even though  $[K_{RR}]$  is singular, its inversion during the static condensation process does not stop the computer!

Suppose now that none of rigid body modes  $\{U_R\}$  is present but a linear combination of some, representing another rigid mode, is included in the displacement functions. Say, for instance, that columns p and q of  $[T_R]$  can be combined to give the rigid mode  $\{W_n\}$ :

$$\{T_R\}_p + \alpha \{T_R\}_q = \{W_n\} \quad (4.49)$$

Then, column p and q of  $[K_{DR}]$  are given by

$$\begin{aligned} \{K_{DR}\}_p &= [K] \{T_R\}_p = [K] (\{W_n\} - \alpha \{T_R\}_q) = -\alpha [K] \{T_R\}_q \\ \{K_{DR}\}_q &= [K] \{T_R\}_q \end{aligned} \quad (4.50)$$

Typical elements rp, rq, pp and pq in  $[K_{RR}]$  are given by

$$\begin{aligned} (K_{RR})_{rp} &= \langle T_R \rangle_r [K] \{T_R\}_p = -\alpha \langle T_R \rangle_r [K] \{T_R\}_q \\ (K_{RR})_{rq} &= \langle T_R \rangle_r [K] \{T_R\}_q \\ (K_{RR})_{pp} &= \langle T_R \rangle_p [K] \{T_R\}_p = \alpha^2 \langle T_R \rangle_q [K] \{T_R\}_q \\ (K_{RR})_{pq} &= \langle T_R \rangle_p [K] \{T_R\}_q = -\alpha \langle T_R \rangle_q [K] \{T_R\}_q \end{aligned} \quad (4.51)$$

which shows that two columns in the augmented matrix, those corresponding to the rigid modes p and q, will differ only by the proportionality factor - $\alpha$ ; because the augmented matrix is symmetric, the corresponding rows are also proportional and a very

small pivot, theoretically zero, will appear again during the inversion of  $[K_{RR}]$  performed for the static condensation.

Once a rigid mode already present has been identified, it must be removed from  $\{U_R\}$  before applying the augmentation and static condensation processes.

If a linear combination of two modes is included, like in (4.49), one of them must be removed. What must finally be represented in the stiffness matrix is a basis of six linearly independent vectors capable of combining into any rigid translation or small rotation. Since  $\{W_n\}$  is already present,  $\{T_R\}_p$  and  $\{T_R\}_q$  cannot both be kept, but  $\{W_n\}$  and  $\{T_R\}_p$  or  $\{W_n\}$  and  $\{T_R\}_q$  are two acceptable pairs of base vectors for the rigid motions.

#### 4.5.4 Example of Cylindrical Shell

This type of shell was already discussed from a theoretical standpoint in Section 4.3. Numerical results are now exhibited for an element whose dimensions have been shown on Fig. 4.4

The augmented matrix is reproduced in Table 4.2. It can be observed that:

- a) the rigid body mode  $u_o$ , already present, gives a zero row and column,
- b) the rows and columns corresponding to  $v_o$  and  $\beta_1$  differ only by a factor  $r_o = 100$  because a small rotation  $\gamma_3$  about the revolution axis, equivalent to a translation  $v_o = -\gamma_3 r_o$  followed by a rotation  $\beta_1 = \gamma_3$ , is already present.

TABLE 4.2  
CYLINDRICAL ELEMENT. AUGMENTED STIFFNESS MATRIX

.735E+07	.768F+07	-.340E+06	-.227E+07	-.191E+07	-.127E+08	.738E+06	.206E+06	-.146E+06	-.971E+06	.127E+07	.847E+07
.248E+07	-.748F+07	-.115E+07	-.659E+07	-.755E+07	-.432E+08	-.206E+06	-.445E+07	-.115E+07	-.659E+07	.755E+07	-.432E+08
-.340E+06	-.115E+07	.360E+06	.204E+07	.201E+07	.114E+08	-.146E+06	.115E+07	.122E+06	.693E+06	-.115E+07	-.653E+07
-.277E+07	-.659E+07	.204E+07	-.153E+08	-.115E+08	.857E+08	-.971E+06	.659E+07	.693E+06	.509E+07	-.653E+07	-.404E+08
-.191E+07	-.755E+07	.201E+07	.115E+08	-.148E+08	.843E+08	-.127E+07	.755E+07	.115E+07	.653E+07	-.104E+08	-.591E+08
-.127E+08	-.432E+08	-.114E+08	.857E+08	.843E+08	.640E+09	-.847E+07	.432E+08	.653E+07	.484E+08	-.591E+08	-.444E+09
.738E+06	.206E+06	-.146E+06	-.971E+06	.127E+07	.847E+07	.735E+07	-.268E+07	-.340E+06	-.227E+07	.191E+07	-.127E+08
.248E+07	-.748E+07	-.115E+07	-.659E+07	-.755E+07	-.432E+08	-.206E+06	-.445E+07	-.115E+07	-.659E+07	.755E+07	-.432E+08
-.340E+06	-.115E+07	.360E+06	.204E+07	.201E+07	.114E+08	-.146E+06	.115E+07	.122E+06	.693E+06	-.115E+07	-.653E+07
-.277E+07	-.659E+07	.204E+07	-.153E+08	-.115E+08	.857E+08	-.971E+06	.659E+07	.693E+06	.509E+07	-.653E+07	-.404E+08
-.191E+07	-.755E+07	.201E+07	.115E+08	-.148E+08	.843E+08	-.127E+07	.755E+07	.115E+07	.653E+07	-.104E+08	-.591E+08
-.127E+08	-.432E+08	-.114E+08	.857E+08	.843E+08	.640E+09	-.847E+07	.432E+08	.653E+07	.484E+08	-.591E+08	-.444E+09
.706E+06	-.465E+07	.115E+07	.659E+07	.755E+07	.432E+08	.268E+07	.748E+07	.115E+07	.659E+07	-.755E+07	-.432E+08
-.146E+06	.115E+07	.122E+06	.693E+06	.115E+07	.653E+07	-.340E+06	.115E+07	.360E+06	.204E+07	-.201E+07	-.114E+08
-.971E+06	.659E+07	.693E+06	.509E+07	.653E+07	.484E+08	-.127E+07	.659E+07	.204E+07	.153E+08	-.115E+08	-.857E+08
.127E+07	.755E+07	-.115E+07	-.653E+07	-.104E+08	-.591E+08	.191E+07	-.755E+07	-.201E+07	-.115E+08	.148E+08	.843E+08
-.847E+07	.432E+08	-.653E+07	-.484E+08	-.591E+08	-.444E+09	.127E+08	.432E+08	-.114E+08	-.857E+08	.843E+08	.640E+09
-.441E+07	.268E+07	.340E+06	.227E+07	.191E+07	.127E+08	-.368E+07	.268E+07	.146E+06	.971E+06	.127E+07	-.847E+07
-.268E+07	.910E+06	-.495E+06	-.440E+07	-.324E+07	-.288E+08	.268E+07	-.374E+07	-.494E+06	.440E+07	.324E+07	-.288E+08
-.340E+06	-.495E+06	.122E+06	.117E+07	.681E+06	.654E+07	-.146E+06	.494E+06	.428E+05	.404E+06	-.397E+06	-.378E+07
-.227E+07	.440E+07	-.117E+07	-.108E+08	-.654E+07	-.603E+08	.971E+06	.440E+07	-.404E+06	.366E+07	.378E+07	-.344E+08
-.191E+07	-.324E+07	.681E+06	.654E+07	-.492E+07	-.477E+08	-.127E+07	.324E+07	.397E+06	.378E+07	-.352E+07	-.338E+08
-.127E+08	.288E+08	-.654E+07	-.603E+08	-.477E+08	-.445E+09	.847E+07	-.288E+08	.378E+07	.344E+08	-.338E+08	-.312E+09
-.368E+07	-.268E+07	.146E+06	.971E+06	.127E+07	-.847E+07	-.441E+07	-.206E+06	.340E+06	.227E+07	.191E+07	-.127E+08
-.268E+07	.910E+06	-.495E+06	.440E+07	.324E+07	.288E+08	.206E+06	.910E+06	.495E+06	.440E+07	-.324E+07	-.288E+08
-.340E+06	-.495E+06	.428E+05	.404E+06	.397E+06	.378E+07	-.340E+06	.495E+06	.122E+06	.117E+07	.681E+06	-.654E+07
-.227E+07	.440E+07	-.404E+06	-.366E+07	-.378E+07	-.344E+08	.227E+07	-.440E+07	-.117E+07	-.108E+08	.654E+07	.603E+08
-.191E+07	-.324E+07	.681E+06	.654E+07	-.492E+07	-.477E+08	-.191E+07	-.324E+07	.681E+06	.654E+07	.492E+07	-.477E+08
-.127E+08	.288E+08	-.654E+07	-.603E+08	-.477E+08	-.445E+09	.127E+08	.288E+08	.654E+07	.603E+08	.477E+08	-.444E+09
-.104E+06	0.	-.279E+08	-.745E+08	.298E+07	.119E+08	.596E+07	.130E+07	-.186E+08	.149E+07	-.224E+07	0.
.633E+05	-.427E+07	-.109E+03	-.213E+02	-.166E+06	.111E+07	-.633E+05	-.512E+07	-.109E+03	-.213E+02	-.166E+06	.111E+07
-.320E+02	.109E+03	-.213E+02	.166E+06	.111E+07	.119E+08	.512E+07	-.109E+03	.213E+02	-.166E+06	.111E+07	-.320E+02
.633E+07	-.358E+06	.737E+07	-.171E+03	.405E+06	.135E+07	.633E+05	-.512E+07	-.109E+03	-.213E+02	-.166E+06	.111E+07
-.358E+06	.737E+07	-.171E+03	.405E+06	.135E+07	.443E+07	-.148E+07	.145E+07	-.405E+06	-.135E+07	.133E+07	.443E+07
-.148E+07	.145E+07	-.405E+06	-.135E+07	.133E+07	.443E+07	0.	0.	0.	0.	0.	0.
-.441E+07	-.206E+06	-.340E+06	.227E+07	-.191E+07	.127E+08	-.368E+07	-.268E+07	-.146E+06	.971E+06	.127E+07	-.847E+07
.206E+06	.340E+06	.227E+07	-.191E+07	.127E+08	.288E+08	-.268E+07	-.374E+07	-.494E+06	.440E+07	.324E+07	-.288E+08
-.340E+06	-.227E+07	.191E+07	-.127E+08	.847E+07	.843E+08	-.268E+07	.374E+07	.494E+06	.428E+05	.404E+06	-.397E+06
-.268E+07	.374E+07	.494E+06	.428E+05	.404E+06	.397E+06	.971E+06	.440E+07	-.404E+06	.366E+07	.378E+07	-.344E+08
-.268E+07	.910E+06	-.495E+06	.440E+07	.324E+07	.288E+08	-.127E+07	.324E+07	.397E+06	.378E+07	-.352E+07	-.338E+08
-.340E+06	-.495E+06	.428E+05	.404E+06	.397E+06	.378E+07	-.127E+07	.324E+07	.397E+06	.378E+07	-.352E+07	-.338E+08
-.227E+07	.440E+07	-.404E+06	-.366E+07	-.378E+07	-.344E+08	.847E+07	-.288E+08	.378E+07	.344E+08	-.338E+08	-.312E+09
-.191E+07	-.324E+07	.681E+06	.654E+07	-.492E+07	-.477E+08	-.191E+07	-.324E+07	.681E+06	.654E+07	.492E+07	-.477E+08
-.127E+08	.288E+08	-.654E+07	-.603E+08	-.477E+08	-.445E+09	.127E+08	.288E+08	.654E+07	.603E+08	.477E+08	-.444E+09
-.104E+06	0.	-.279E+08	-.745E+08	.298E+07	.119E+08	.596E+07	.130E+07	-.186E+08	.149E+07	-.224E+07	0.
.633E+05	-.427E+07	-.109E+03	-.213E+02	-.166E+06	.111E+07	-.633E+05	-.512E+07	-.109E+03	-.213E+02	-.166E+06	.111E+07
-.320E+02	.109E+03	-.213E+02	.166E+06	.111E+07	.119E+08	.512E+07	-.109E+03	.213E+02	-.166E+06	.111E+07	-.320E+02
.633E+07	-.358E+06	.737E+07	-.171E+03	.405E+06	.135E+07	.633E+05	-.512E+07	-.109E+03	-.213E+02	-.166E+06	.111E+07
-.358E+06	.737E+07	-.171E+03	.405E+06	.135E+07	.443E+07	-.148E+07	.145E+07	-.405E+06	-.135E+07	.133E+07	.443E+07
-.148E+07	.145E+07	-.405E+06	-.135E+07	.133E+07	.443E+07	0.	0.	0.	0.	0.	0.
-.441E+07	-.206E+06	-.340E+06	.227E+07	-.191E+07	.127E+08	-.368E+07	-.268E+07	-.146E+06	.971E+06	.127E+07	-.847E+07
.206E+06	.340E+06	.227E+07	-.191E+07	.127E+08	.288E+08	-.268E+07	-.374E+07	-.494E+06	.440E+07	.324E+07	-.288E+08
-.340E+06	-.227E+07	.191E+07	-.127E+08	.847E+07	.843E+08	-.268E+07	.374E+07	.494E+06	.428E+05	.404E+06	-.397E+06
-.268E+07	.374E+07	.494E+06	.428E+05	.404E+06	.397E+06	.971E+06	.440E+07	-.404E+06	.366E+07	.378E+07	-.344E+08
-.268E+07	.910E+06	-.495E+06	.440E+07	.324E+07	.288E+08	-.127E+07	.324E+07	.397E+06	.378E+07	-.352E+07	-.338E+08
-.340E+06	-.495E+06	.428E+05	.404E+06	.397E+06	.378E+07	-.127E+07	.324E+07	.397E+06	.378E+07	-.352E+07	-.338E+08
-.227E+07	.440E+07	-.404E+06	-.366E+07	-.378E+07	-.344E+08	.847E+07	-.288E+08	.378E+07	.344E+08	-.338E+08	-.312E+09
-.191E+07	-.324E+07	.681E+06	.654E+07	-.492E+07	-.477E+08	-.191E+07	-.324E+07	.681E+06	.654E+07	.492E+07	-.477E+08
-.127E+08	.288E+08	-.654E+07	-.603E+08	-.477E+08	-.445E+09	.127E+08	.288E+08	.654E+07	.603E+08	.477E+08	-.444E+09
-.104E+06	0.	-.279E+08	-.745E+08	.298E+07	.119E+08	.596E+07	.130E+07	-.186E+08	.149E+07	-.224E+07	0.
.633E+05	-.427E+07	-.109E+03	-.213E+02	-.166E+06	.111E+07	-.633E+05	-.512E+07	-.109E+03	-.213E+02	-.166E+06	.111E+07
-.320E+02	.109E+03	-.213E+02	.166E+06	.111E+07	.119E+08	.512E+07	-.109E+03	.213E+02	-.166E+06	.111E+07	-.320E+02
.633E+07	-.358E+06	.737E+07	-.171E+03	.405E+06	.135E+07	.633E+05	-.512E+07	-.109E+03	-.213E+02	-.166E+06	.111E+07
-.358E+06	.737E+07	-.171E+03	.405E+06	.135E+07	.443E+07	-.148E+07	.145E+07	-.405E+06	-.135E+07	.133E+07	.443E+07
-.148E+07	.145E+07	-.405E+06	-.135E+07	.133E+07	.443E+07	0.	0.	0.	0.	0.	0.
-.441E+07	-.206E+06	-.340E+06	.227E+07	-.191E+07	.127E+08	-.368E+07	-.268E+07	-.146E+06	.971E+06	.127E+07	-.847E+07
.206E+06	.340E+06	.227E+07	-.191E+07	.127E+08	.288E+08	-.268E+07	-.374E+07	-.494E+06	.440E+07	.324E+07	-.288E+08
-.340E+06	-.227E+07	.191E+07	-.127E+08	.847E+07	.843E+08	-.268E+07	.374E+07	.494E+06	.428E+05	.404E+06	-.397E+06
-.268E+07	.374E+07	.494E+06	.428E+05	.404E+06	.397E+06	.971E+06	.440E+07	-.404E+06	.366E+07	.378E+07	-.344E+08
-.268E+07	.910E+06	-.495E+06	.440E+07	.324E+07	.288E+08	-.127E+07	.324E+07	.397E+06	.378E+07	-.352E+07	-.338E+08
-.340E+06	-.495E+06	.428E+05	.404E+06	.397E+06	.378E+07	-.127E+07	.324E+07	.397E+06	.378E+07	-.352E+07	-.338E+08
-.227E+07	.440E+07	-.404E+06	-.366E+07	-.378E+07	-.344E+08	.847E+07	-.288E+08	.378E+07	.344E+08	-.338E+08	-.312E+09
-.191E+07	-.324E+07	.681E+06	.654E+07	-.492E+07	-.477E+08	-.191E+07	-.324E+07	.681E+06	.654E+07	.492E+07	-.477E+08
-.127E+08	.288E+08	-.654E+07	-.603E+08	-.477							



The matrix after static condensation is reproduced in Table

#### 4.3. Notice

- a) the small pivot in the  $u_0$  row,
- b) the additional small pivot appearing in the  $v_0$  row after a backward Gaussian elimination has been applied to rows  $v_0$  and  $\beta_1$ ,
- c) the important changes between the element stiffnesses  $[K_D]$  and  $[K_T]$ .

The matrices  $[K_{RD}]$  and  $[K_{RR}]$ , obtained before and after static condensation when 4 rigid modes only are added, namely  $v_0$ ,  $w_0$ ,  $\beta_2$  and  $\beta_3$ , are reproduced in Table 4.4. They no longer contain zero lines or zero pivots.

The eigenvalues of the matrix  $[K_T]$  obtained either from the (30 x 30) or from the (28 x 28) augmented matrix are reproduced in Table 4.5 together with the eigenvalues of the original  $[K_D]$  matrix. Observe now the reduction of all eigenvalues and the presence of six rigid body modes. The equality of eigenvalues obtained by adding and condensing out 6 or 4 rigid modes shows that, in this particular case, it did not hurt to invert a "singular" (6 x 6) matrix  $[K_{RR}]$ . Nevertheless, it is preferable to add the minimum possible number of rigid modes to save on operations and avoid potential troubles with very small pivots.

It is sometimes considered that a reduction in the trace, a reduction of the maximum eigenvalue or the eigenvalue sum are measures of the improvements brought to a stiffness matrix. In all these respects, going from  $[K_D]$  to  $[K_T]$  represents an improvement; but this favorable opinion must be tempered because

TABLE 4.3  
CYLINDRICAL ELEMENT. AUGMENTED STIFFNESS AFTER STATIC CONDENSATION

Table with 16 columns and 32 rows of numerical data in scientific notation, representing augmented stiffness values.

Table with 16 columns and 32 rows of numerical data in scientific notation, representing augmented stiffness values.

Table with 6 columns and 16 rows of numerical data in scientific notation, representing augmented stiffness values.

NODE i  
NODE j  
NODE k  
NODE l  
RIGID MODE

u<sub>0</sub>    v<sub>0</sub>    w<sub>0</sub>    β<sub>1</sub>    β<sub>2</sub>    β<sub>3</sub>

TABLE 4.4  
CYLINDRICAL ELEMENT. MATRICES  $[K_{RD}]$ ,  $[K_{RR}]$  AFTER AUGMENTATION

.633E+05	-.427E-07	-.507E+05	-.338E+06	-.166E+06	-.111E+07	-.633E+05	-.652E-08	.507E+05	.338E+06	-.166E+06	-.111E+07
.320E+02	.109E+03	-.213E+02	-.142E+03	.107E+05	.712E+05	.320E+02	-.109E+03	-.213E+02	-.142E+03	.107E+05	.712E+05
.864E-07	.737E+07	-.171E+03	-.569E+03	.870E+05	.285E+06	.315E-06	-.737E+07	-.171E+03	-.569E+03	.870E+05	.285E+06
.148E+07	.145E+07	.405E+06	.133E+07	.133E+07	.443E+07	-.148E+07	.145E+07	.405E+06	.133E+07	.133E+07	.443E+07
-.633E+05	.373E-08	-.507E+05	.338E+06	-.166E+06	.111E+07	.633E+05	.512E-07	.507E+05	.338E+06	-.166E+06	.111E+07
-.320E+02	.109E+03	-.213E+02	.142E+03	.107E+05	-.712E+05	-.320E+02	-.109E+03	-.213E+02	.142E+03	.107E+05	-.712E+05
-.354E-06	-.737E+07	.171E+03	-.569E+03	-.870E+05	.285E+06	-.137E-06	.737E+07	.171E+03	-.569E+03	-.870E+05	.285E+06
.148E+07	-.145E+07	-.405E+06	.133E+07	-.133E+07	.443E+07	-.148E+07	-.145E+07	-.405E+06	.133E+07	-.133E+07	.443E+07
.330E+05	.972E-08	.580E-06	.399E-05	RIGID MODES							
.972E-08	.844E+02	.473E-06	-.182E-06								
.580E-06	.473E-06	.115E+09	-.104E-04								
.399E-05	-.182E-06	-.104E-04	.589E+07								

$V_0$        $W_0$        $\beta_2$        $\beta_3$

CYLINDRICAL ELEMENT. MATRICES  $[K_{RD}]$ ,  $[K_{RR}]$  AFTER STATIC CONDENSATION

.192E+01	-.326E-10	-.153E+01	-.102E+02	-.503E+01	-.335E+02	-.192E+01	-.285E-10	.153E+01	.102E+02	-.503E+01	-.335E+02
.379E+00	.129E+01	-.253E+00	.168E+01	.126E+03	.843E+03	.379E+00	.129E+01	-.253E+00	.168E+01	.126E+03	.843E+03
.234E-13	.641E-01	-.148E-05	-.494E-05	.756E-03	.248E-02	-.199E-13	-.641E-01	.148E-05	-.494E-05	.756E-03	.248E-02
.251E+00	.246E+00	.688E-01	.230E+00	.228E+00	.752E+00	-.251E+00	.246E+00	.688E-01	.230E+00	.228E+00	.752E+00
-.192E+01	.304E-10	-.153E+01	.102E+02	-.503E+01	.335E+02	.192E+01	.306E-10	.153E+01	.102E+02	-.503E+01	.335E+02
-.379E+00	.129E+01	-.253E+00	.168E+01	.126E+03	.843E+03	-.379E+00	.129E+01	-.253E+00	.168E+01	.126E+03	.843E+03
.196E-13	-.641E-01	.148E-05	-.494E-05	-.756E-03	.248E-02	-.238E-13	.641E-01	.148E-05	-.494E-05	.756E-03	.248E-02
.251E+00	-.246E+00	-.688E-01	.230E+00	-.228E+00	.752E+00	-.251E+00	-.246E+00	-.688E-01	.230E+00	-.228E+00	.752E+00
.330E+05	.972E-08	.580E-06	.399E-05	RIGID MODES							
.972E-08	.844E+02	.473E-06	-.182E-06								
.580E-06	.473E-06	.115E+09	-.104E-04								
.399E-05	-.182E-06	-.104E-04	.589E+07								

$V_0$        $W_0$        $\beta_2$        $\beta_3$

TABLE 4.5  
EIGENVALUES AND TRACE OF ELEMENT STIFFNESS MATRICES.

	LARGE CYLINDER ELEM 24 EIGV WITHOUT RIG.	LARGE CYLINDER ELEM 24 EIGV WITH 6 RIG.	LARGE CYLINDER ELEM 24 EIGV WITH 4 RIG.	LARGE CYLINDER ELEM TRACE ORIGIN. STIFF.	LARGE CYLINDER ELEM TRACE CONDENS. STIFF.
1	1909569765.0057983	1670548054.9383011	1670548054.7860031	7353049.2442492	6861087.6112278
2	347279762.9251404	345692232.4835300	345692232.4835396	7484654.2034075	6655295.3710720
3	345696794.6368294	184802772.3600597	184802772.3600597	359787.1106961	254148.1877135
4	66679420.4689249	52322561.6776841	52322561.6776841	15308960.8258380	11543797.6344690
5	16306890.1810810	15562582.3934880	15562582.3934880	14789289.8039400	12303495.9608070
6	11540424.8459910	9349192.8309811	9349192.8305725	639776066.3830299	539289811.0604286
7	10557390.1861330	7874610.0993414	7874610.0323139	7353049.2442493	6861087.6112290
8	8007935.5352491	7223372.6791601	7223372.6791547	7484654.2034075	6655295.3710742
9	7512059.9049824	6867370.5814301	6867370.5814298	359787.1106961	254148.1877133
10	5887909.6943662	2173535.7973595	2173535.7973601	15308960.8258390	11543797.6344660
11	4791332.8843170	1562451.2533276	1562451.2499390	14789289.8039400	12303495.9608520
12	2037486.4815816	1534283.8349459	1534283.8349445	639776066.3830299	539289811.0618782
13	1167351.5573948	821044.6009340	821044.6009310	7353049.2442492	6861087.6112191
14	1141631.2134812	506804.0014362	506804.0014228	7484654.2034076	6655295.3710735
15	872737.0874942	391614.9937828	391614.9917382	359787.1106961	254148.1877150
16	820024.6951047	290005.7513694	290005.7513700	15308960.8258390	11543797.6345060
17	362569.697316	106629.5453928	106629.5444051	14789289.8039400	12303495.9608390
18	20727.7244014	1223.7102142	1223.7100799	639776066.3830299	539289811.0612793
19	18910.4700137	.0000030	.0000002	7353049.2442492	6861087.6112196
20	16181.3150266	.0000002	.0000000	7484654.2034076	6655295.3710748
21	22.5560385	.0000000	.0000001	359787.1106961	254148.1877149
22	1.2179351	-.0000001	-.0000003	15308960.8258390	11543797.6345040
23	-.0000013	-.0000017	-.0000016	14789289.8039400	12303495.9608460
24	-.0000047	-.0000038	-.0000050	639776066.3830299	539289811.0616989

incompatibilities are also introduced in this process!

#### 4.6 Rigid Modes to be Added for Different Types of Shells of Revolution

The procedure of finding which rigid body modes need to be added has been applied to several different types of shell elements. The following conclusions can be drawn from numerical results obtained in these studies and from theoretical considerations.

1. For a doubly curved element, all six rigid modes need to be added.
2. For a cylindrical shell, the translation along and the rotation about the axis of revolution are already present, only four modes, either  $\langle v_o \ w_o \ \beta_2 \ \beta_3 \rangle$  or  $\langle w_o \ \beta_1 \ \beta_2 \ \beta_3 \rangle$  need to be added.
3. For a conical shell the following five rigid motions are of interest

$$\begin{Bmatrix} u \\ v \\ w \end{Bmatrix} = \begin{bmatrix} \sin^2 \varphi_o \cos \theta + \sin^2 \varphi_o & \sin \varphi_o \sin \theta & \cos \varphi_o \sin \varphi_o (\cos \theta - 1) \\ -\sin \varphi_o \sin \theta & \cos \theta & -\cos \varphi_o \sin \theta \\ \sin \varphi_o \cos \varphi_o (\cos \theta - 1) & \cos \varphi_o \sin \theta & \cos^2 \varphi_o \cos \theta + \sin^2 \varphi_o \end{bmatrix} \begin{Bmatrix} u_o \\ v_o \\ w_o \end{Bmatrix} \quad (4.52)$$

$$\begin{Bmatrix} u \\ v \\ w \end{Bmatrix} = \begin{bmatrix} 0 & -r_o \sin \theta \\ -r \cos \varphi_o + r \cos \varphi_o \cos \theta & r \sin \varphi_o - r \sin \varphi_o \cos \theta + s \cos \theta \\ r_o \sin \theta + s \sin \varphi \sin \theta & s \cos \varphi_o \sin \theta \end{bmatrix} \begin{Bmatrix} \beta_1 \\ \beta_3 \end{Bmatrix} \quad (4.53)$$

A translation  $S_3$  along the revolution axis is equivalent to the superposition of translations

$$u_o = -\cos \varphi_o \quad , \quad w_o = \sin \varphi_o \quad (4.54)$$

while a rotation  $\gamma_3$  about this revolution axis is the superposition of

$$v_0 = r_0 \gamma_3, \quad \beta_1 = -\gamma_3 \cos \varphi, \quad \beta_3 = \gamma_3 \sin \varphi \quad (4.55)$$

resulting in

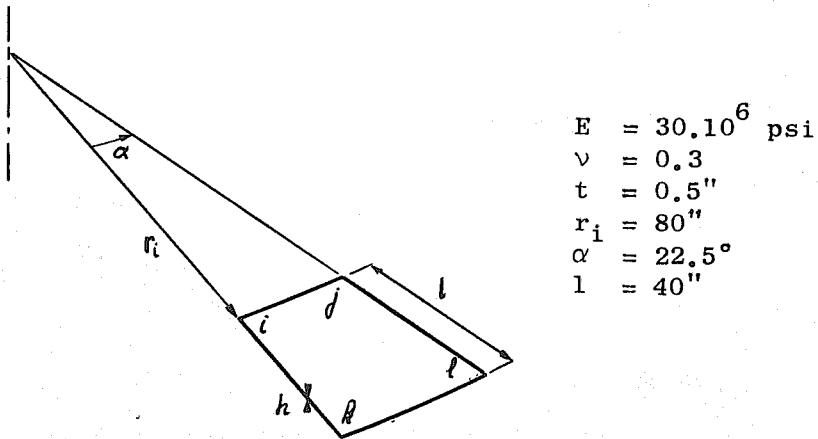
$$\begin{Bmatrix} u \\ v \\ w \end{Bmatrix} = \begin{bmatrix} -\cos \varphi_0 & 0 \\ 0 & r \\ \sin \varphi_0 & 0 \end{bmatrix} \begin{Bmatrix} \gamma_3 \\ \gamma_3 \end{Bmatrix} \quad (4.56)$$

These two modes are represented by the displacement functions and only four others,  $\langle v_0, w_0, \beta_2, \beta_3 \rangle$  for instance, need to be added.

4. The circular plate is another interesting example. The rigid modes reduce to

$$\begin{Bmatrix} u \\ v \\ w \end{Bmatrix} = \begin{bmatrix} \cos \theta & \sin \theta & 0 & 0 & 0 & -r_0 \sin \theta \\ -\sin \theta & \cos \theta & 0 & 0 & 0 & r - r_0 \cos \theta \\ 0 & 0 & 1 & r \sin \theta & -(r \cos \theta - r_0) & 0 \end{bmatrix} \begin{Bmatrix} u_0 \\ v_0 \\ w_0 \\ \beta_1 \\ \beta_2 \\ \beta_3 \end{Bmatrix} \quad (4.57)$$

The translation along and the rotation about the revolution axis, respectively represented by  $w_0$  and a superposition of  $v_0 = \gamma_3 r$ ,  $\beta_3 = \gamma_1$ , are present in the displacement functions. If one attempts to add them in the plate whose dimensions are described in Fig. 4.5, they give pivots of order  $10^{-10}$  and  $10^{-7}$  in  $[K_{RR}]$ ; these can be considered as very small compared with the "nonzero" pivots which are of order  $10^5$  or more. Moreover, besides these two "very small" pivots, two other "small" pivots appear: one of order  $10^{-2}$  in the  $\beta_1$  row, the other of order  $10^1$  in the  $\beta_2$  row. They represent the order of approximation by a cubic polynomial of the



$$\begin{aligned}
 E &= 30.10^6 \text{ psi} \\
 \nu &= 0.3 \\
 t &= 0.5'' \\
 r_i &= 80'' \\
 \alpha &= 22.5^\circ \\
 l &= 40''
 \end{aligned}$$

Fig. 4.5 Circular Plate Element

trigonometric functions  $\sin \theta$  and  $\cos \theta$ , respectively, with  $-\pi/8 \leq \theta \leq \pi/8$ . An examination of the eigenvalues shows that, for practical purposes,  $\beta_1$  but not  $\beta_2$  can be considered as already included. The three modes still to be added can be chosen as  $\langle u_0 \beta_2 \beta_3 \rangle$ .

5. For a toroidal shell with very large parallel radii, the rotation about the axis of revolution is included and  $\langle u_0 w_0 \beta_1 \beta_2 \beta_3 \rangle$  must be added.
6. For a cone, cylinder or plate element with very large radii of revolution and very small parallel opening, such that  $rd\theta = dt$ , all six rigid modes

$$\begin{Bmatrix} u \\ v \\ w \end{Bmatrix} = \begin{bmatrix} 1 & 0 & 0 & 0 & 0 & -t \\ 0 & 1 & 0 & 0 & 0 & s \\ 0 & 0 & 1 & t & -s & 0 \end{bmatrix} \begin{Bmatrix} u_0 \\ v_0 \\ w_0 \\ \beta_1 \\ \beta_2 \\ \beta_3 \end{Bmatrix} \quad (4.58)$$

are present; none need be added.

#### 4.7 Computation of Shell Forces

The interpretation of stress resultants in a finite element analysis based on the displacement method poses certain difficulties. The methods most frequently used to compute stresses are:

- a) direct computation of forces from the element stiffness matrix,
- b) computation of strains and then stress resultants from the assumed displacement field.

Other methods have sometimes been proposed [90] but do not seem to improve much over the former ones.

Whatever method is used to compute the shell forces, it must make use of the deformation displacements. Therefore, the first step, if rigid modes have been added and condensed out, is to recover the rigid modes through

$$\{-U_R\} = -[K_{RR}^{-1}][K_{RD}]\{V_T\} \quad (4.59)$$

and the deformation DOF

$$\{V_D\} = \begin{bmatrix} I \\ T_R \end{bmatrix} \begin{Bmatrix} V_T \\ U_R \end{Bmatrix} \quad (4.60)$$

When the element stiffness is used directly, the results

$$\{S_D\} = [K_D]\{V_D\} \quad (4.61)$$

represent the generalized concentrated forces associated with the generalized DOF. Even in the simple case of a rectangular plate, some of these forces are not quite straightforward to interpret: Buffer and Stein [13] have shown that  $\partial^2 w / \partial s \partial t$  is associated a bimoment defined as (Fig. 4.6)



$$\mathcal{M} = \lim_{\substack{\epsilon \rightarrow 0 \\ F \rightarrow \infty}} (\epsilon^2 F) \quad (4.62)$$

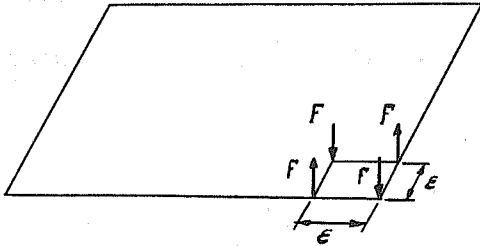


Fig. 4.6 Definition of Bimoment.

When curvilinear coordinates are used, the physical interpretation of these forces is even more complicated as was already shown in Section 3.4.5. This method of computing forces will nevertheless be used in the ring example to be discussed later: in this case it is relatively easy to relate the generalized nodal forces to well-known quantities such as bending moments, normal and shear forces.

In the second method of computing the stress resultants, the interpolation functions for the displacements and the linearized strain displacement relationships are combined to compute the strains

$$\{E\} = [B] \{V_D\} \quad (3.25)$$

at any point within the element. The shell forces, measured per unit length of the middle surface, are defined as the integrals over the shell surface of the stresses and stress moments

$$\begin{aligned}
N_{\langle 11 \rangle} &= \int_{-\frac{h}{2}}^{\frac{h}{2}} \sigma_{\langle 11 \rangle} dZ, & M_{\langle 11 \rangle} &= \int_{-\frac{h}{2}}^{\frac{h}{2}} \sigma_{\langle 11 \rangle} Z dZ \\
N_{\langle 22 \rangle} &= \int_{-\frac{h}{2}}^{\frac{h}{2}} \sigma_{\langle 22 \rangle} dZ, & M_{\langle 22 \rangle} &= \int_{-\frac{h}{2}}^{\frac{h}{2}} \sigma_{\langle 22 \rangle} Z dZ \\
N_{\langle 12 \rangle} &= \int_{-\frac{h}{2}}^{\frac{h}{2}} \sigma_{\langle 12 \rangle} dZ, & M_{\langle 12 \rangle} &= \int_{-\frac{h}{2}}^{\frac{h}{2}} \sigma_{\langle 12 \rangle} Z dZ \\
N_{\langle 21 \rangle} &= \int_{-\frac{h}{2}}^{\frac{h}{2}} \sigma_{\langle 21 \rangle} dZ, & M_{\langle 21 \rangle} &= \int_{-\frac{h}{2}}^{\frac{h}{2}} \sigma_{\langle 21 \rangle} Z dZ
\end{aligned} \tag{4.63}$$

with

$$N_{\langle 12 \rangle} = N_{\langle 21 \rangle}, \quad M_{\langle 12 \rangle} = M_{\langle 21 \rangle} \tag{4.64}$$

because the shear strain and torsion are defined as

$$\frac{1}{2} (\epsilon_{\langle 12 \rangle} + \epsilon_{\langle 21 \rangle}), \quad \frac{1}{2} (\mathcal{X}_{\langle 12 \rangle} + \mathcal{X}_{\langle 21 \rangle}) \tag{4.65}$$

It is easy to show that the shell forces are related to the strains by

$$\begin{Bmatrix} N_{\langle 11 \rangle} \\ N_{\langle 22 \rangle} \\ N_{\langle 12 \rangle} \end{Bmatrix} = \frac{Eh}{1-\nu^2} \begin{bmatrix} 1 & \nu & 0 \\ \nu & 1 & 0 \\ 0 & 0 & (1-\nu) \end{bmatrix} \begin{Bmatrix} \epsilon_{\langle 11 \rangle} \\ \epsilon_{\langle 22 \rangle} \\ \frac{1}{2} (\epsilon_{\langle 12 \rangle} + \epsilon_{\langle 21 \rangle}) \end{Bmatrix} \tag{4.66}$$

$$\begin{Bmatrix} M_{\langle 11 \rangle} \\ M_{\langle 22 \rangle} \\ M_{\langle 12 \rangle} \end{Bmatrix} = \frac{Eh^3}{12(1-\nu^2)} \begin{bmatrix} 1 & \nu & 0 \\ \nu & 1 & 0 \\ 0 & 0 & (1-\nu) \end{bmatrix} \begin{Bmatrix} \mathcal{X}_{\langle 11 \rangle} \\ \mathcal{X}_{\langle 22 \rangle} \\ \frac{1}{2} (\mathcal{X}_{\langle 12 \rangle} + \mathcal{X}_{\langle 21 \rangle}) \end{Bmatrix} \tag{4.67}$$

In practice, these shell forces are computed at the element center, where the displacement method and the interpolation functions are supposed to give the best results, and at the four corners. Even when rigid body modes are not added, the "membrane"

displacements  $u$  and  $v$  but not their derivative are continuous at the nodal points, the "plate" displacement  $w$  and its first but not its second derivatives are continuous at the nodal points. Therefore, the strains, curvature changes and, consequently, the shell forces will have four different values at the same corner depending on which of the four adjacent elements is used to compute them. The average of these four values is also considered a good measure of the shell forces.

## 5. NUMERICAL EXAMPLES

### 5.1 General

A computer program written to test the new shell element is first briefly described.

Then several examples are solved and discussed. They were selected and arranged to exhibit the various levels of importance of the rigid body modes and the incompatibility they introduce. This ordering coincides with a classification based on purely geometric considerations.

- a) In rectangular plates, the rigid body modes are not necessary and therefore, not added.
- b) In circular plates, the rigid body modes may be added or not; they do not play any significant role.
- c) In shells with zero Gaussian curvature, exemplified by cylinders, the rigid modes are extremely beneficial; they must be added.
- d) In shells with positive or negative Gaussian curvature, such as spheres and hyperboloids of revolution, the incompatibility defects predominate; the rigid modes cannot be added.

The chapter concludes with a short discussion of the incompatibilities introduced by the rigid modes.

### 5.2 Computer Program

#### 5.2.1 Description

The concepts described in Chapters 3 and 4 were incorporated in a program called NADESOR (Non Axisymmetric Deflections of Elastic Shells of Revolution) run on the CDC 6400 of the

University of California at Berkeley. A succinct flow chart is given on Fig. 5.1. Although the program performs linear analysis, a few extensions directed towards solution of nonlinear problems are mentioned in the description here below.

NADESOR, the primary overlay, directs the program towards one of the three secondary overlays.

ENTER prepares all data and preliminary results by means of the following subroutines:

- 1) INCARDS reads all data cards and automatically generates the parallel coordinates for intermediate segments evenly spaced along a straight or circular meridian.
- 2) NUMELEM automatically numbers the elements and nodal points to produce the minimum bandwidth.
- 3) BOCOVEC translates the boundary conditions imposed on meridians, parallels or nodal points into numbers of restricted DOF.
- 4) APPGEOM approximates an arbitrary meridian by a cubic curve and computes geometric data at Gaussian integration points.
- 5) DELTAFI computes the strain-displacement matrix [B] at integration points.
- 6) ELASTIF forms the linear elastic stiffness using a grid of  $4 \times 4$  Gaussian integration points.
- 7) RIGIMAT forms the rigid motion matrices.
- 8) LOADVEC assembles the load vector; all elements at the same segment level are scanned for nonsymmetrical loading; if present, such a loading is computed by ELTLOAD.

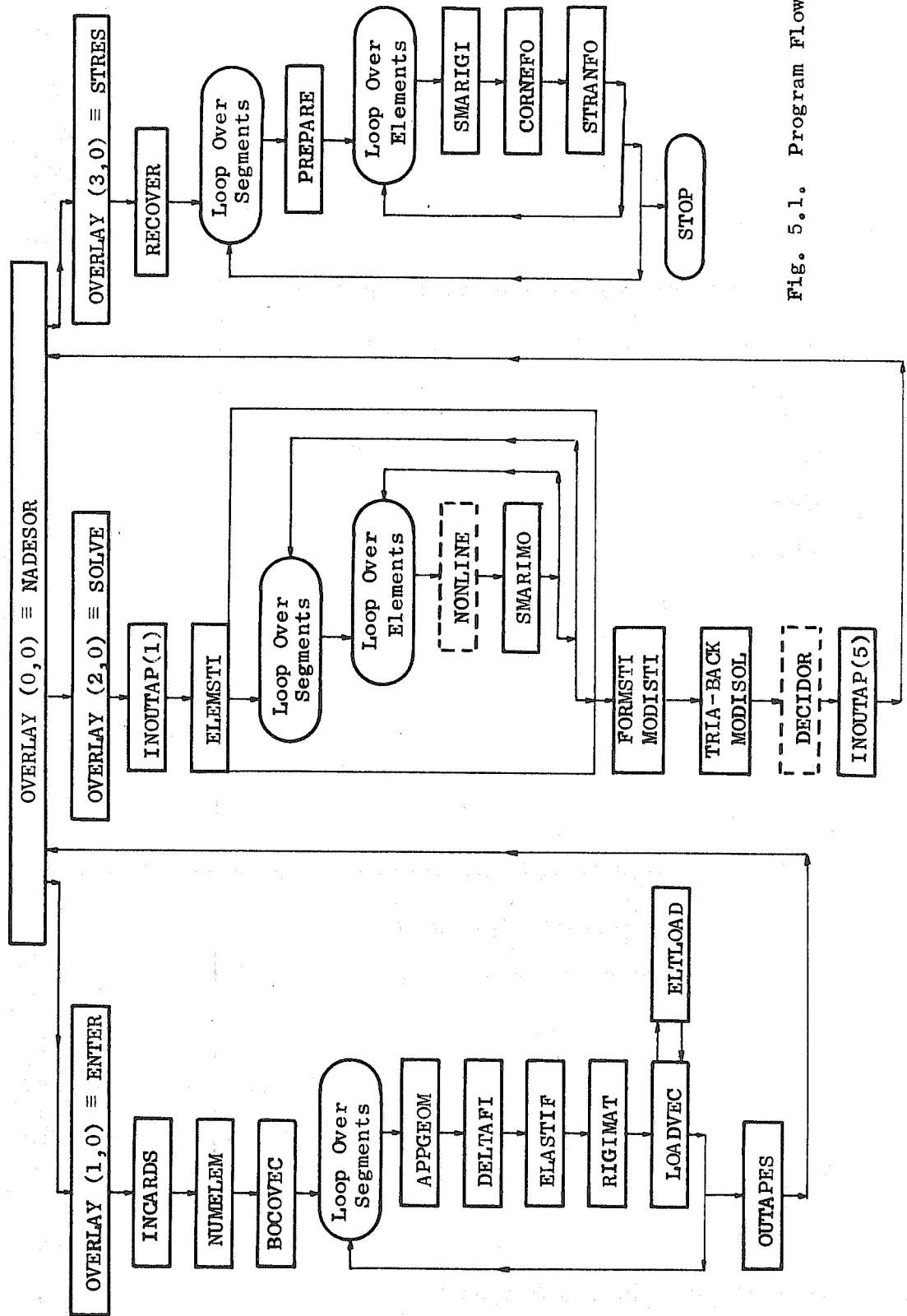


Fig. 5.1. Program Flowchart

- 9) OUTAPES saves on tape all results of the first overlay if execution is stopped at this point.

SOLVE forms and solves the global stiffness relationships of the system.

- 1) INOUTAP(1) retrieves results of ENTER or, in nonlinear cases, the last results of SOLVE if execution is restarted.
- 2) ELEMSTI loops over elements to augment the stiffness and condense out the appropriate small rigid body modes by means of SMARIMO; eventually, a nonlinear modification of the stiffness will have been performed at this stage by NONLINE.
- 3) FORMSTI forms one half band of the symmetric stiffness and MODISTI modifies it in correspondence with the boundary conditions.
- 4) TRIA triangularizes the stiffness, BACK backsubstitutes and MODISOL modifies the solution if boundary conditions require it.
- 5) DECIDOR decides the orientation of the program in a nonlinear analysis.
- 6) INOUTAP(5) saves on tape all results of the second overlay if execution is stopped at this point.

STRES computes the stresses at the element center and four corners.

- 1) RECOVER retrieves results of SOLVE if execution is restarted.
- 2) PREPARE computes the strain displacement matrix [B] at points  $o, i, j, k, l$ .
- 3) SMARIGI recovers the small rigid motions and the deformation part of the nodal displacements.

- 4) CORNEFO directly uses the element stiffness to find corner forces.
- 5) STRANFO computes the strains and shell forces by means of the displacement interpolation functions.

### 5.2.2 Additional Comments

A very severe limitation is imposed on the number of elements in this program: the total storage space occupied by the stiffness halfband cannot exceed 35700 words, which corresponds roughly to a 6X12, 7X10 or 8X9 finite element mesh. This is because TRIA and BACK work entirely in core: only small examples are expected to be solved by this experimental program and an equation solver using tapes would be prohibitively slow when the nonlinear possibility is introduced and the equation system has to be solved again and again. The division in overlays is introduced partially to alleviate this space problem by keeping in core the minimum number of instructions while the equation system is set up and solved.

Thanks to the overlay feature and the data saving subroutine, the program can stop at the end of ENTER or SOLVE and be restarted from the stopping point. This allows the user to check data after the first overlay or to look at results before computing stresses; this latter capability would be most useful after any step or iteration in a nonlinear problem.

The different cases of automatic numbering programmed into NUMELEM are illustrated by the annular plate of Fig. 5.2.



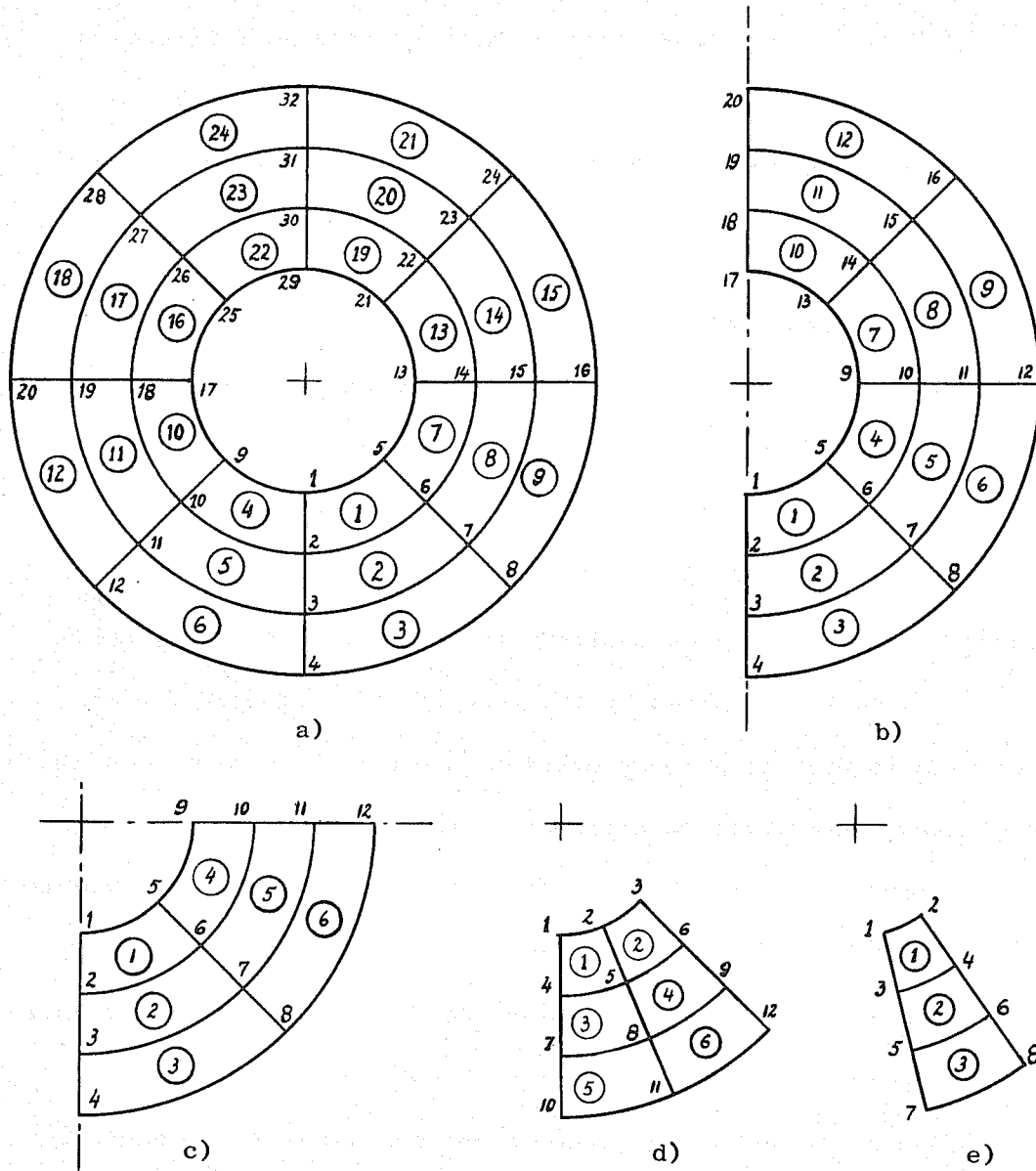


Fig. 5.2. Automatic Node Numbering.

- a) No symmetry plane; a complete circumference is required.
- b) One symmetry plane.
- c) Two symmetry planes.
- d) Complete symmetry of revolution.
- e) The structure to be studied is a sector only of a shell of revolution.

Note the numbering along the meridian or parallel first to

produce minimum bandwidth.

The complete symmetry of revolution requires only 6 DOF per segment.  $\langle u_i w_i (dw/ds)_i u_k w_k (dw/ds)_k \rangle$ . The program is inefficient in this case since 24 DOF are used; the superfluous DOF are eliminated, however, before solving the structural system.

If the shell has a pole, i.e.  $r = 0$ , strain expressions become singular at this point. Special strain expressions [47] or special elements [128] can be derived to take care of this difficulty. No such provisions are incorporated in the present program: to handle the singularity problem, a small hole with free edge boundary condition is introduced at the pole.

### 5.3 Rectangular Plate Examples

#### 5.3.1 Rectangular Plate Under Uniform Load

A simply supported plate of dimensions 8" X 16" is approximated by a portion of an annular plate (see Fig. 5.3a). The circular edges have length of 7.9936" and 8.0064" and the annulus width is 16". As in the case of the real plate, "symmetry" conditions make it possible to study a quarter of the plate only; a 1X1, 2X2 or 4X4 finite element mesh are used over this quarter.

The convergence with mesh refinement of deflection at the plate center and the bending moment  $M_\theta$  along the radial centerline are shown on Fig. 5.3b and c. These results are identical to those obtained by Bogner et al. [10].

Several conclusions can be drawn from this example:

- a) The "large radius, small angle" approximation is satisfactory: when  $r$  is so large and  $\alpha$  so small that  $rd\theta$  can be replaced by

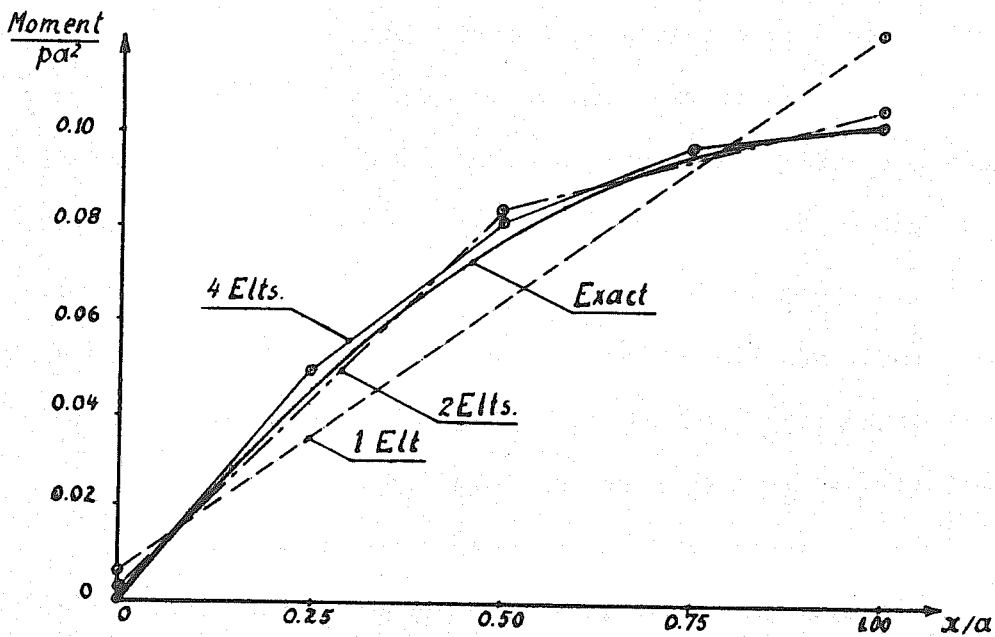
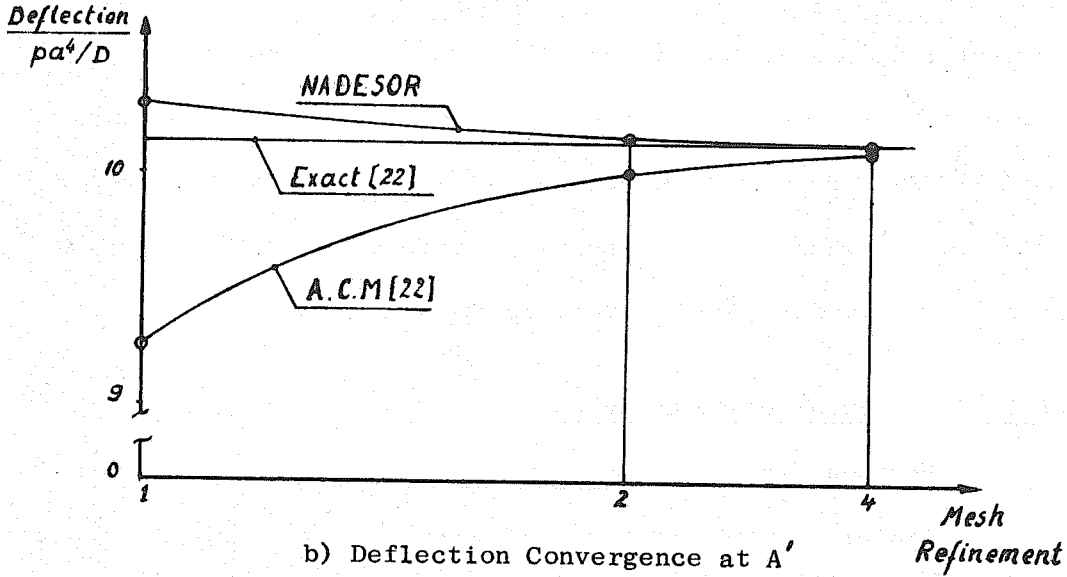
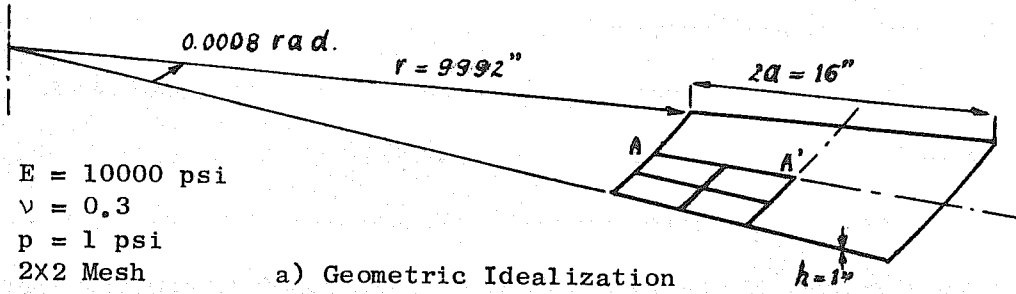


Fig. 5.3. Rectangular Plate Approximation.

dt as defined in (2.107), the sector of annular plate constitutes a good approximation of a rectangular plate. With  $r \approx 10000''$  and  $\alpha$  varying between 0.0001 and 0.0004 radians, all present results are within 0.1% of those obtained with the perfectly rectangular plate. On a computer using 15 significant digits in simple precision, the loss of accuracy that could result from differences of large radii was never experienced.

- b) In the "large radius, small angle" case no rigid modes are added. The fast convergence of results shows that they are indeed not necessary.
- c) The Bogner, Fox, Schmit plate element compares very favorably with other plate elements with similar number of DOF. This can be verified by comparing curves 5.13b and c with equivalent curves plotted by Clough and Tocher [22]. Of course, one must remember that the present rectangular element does not offer the same versatility as many quadrilateral and triangular elements discussed in [22] or developed later [30].

One final remark ought to be made about this example. The central displacement converges from above while convergence from below is expected in a displacement analysis using a compatible element! But as recalled by Bogner et al. [10], the minimum energy and not the displacement at a single point should be examined in assessing the convergence; when the work done by the uniform load acting on the whole plate is evaluated, the proper convergence is recovered.

### 5.3.2 Twisted Square Plate

A plate of dimensions 8" x 8", with the same thickness and elastic properties as in the above example, is simply supported at three corners and loaded at the fourth by a transversal point load of 5 lbs. It is again approximated by an annular plate of mean radius 10000". The results obtained with different meshes are as follows:

Mesh	Deflection Under Load (in.)	Deflection at Plate Center (in.)	Torsion Moments at Element Centers (lb.-in./in.)
1X1	0.2498	0.06246	5.004
2X2	0.2498	0.06246	5.003, 5.002, 5.003, 5.001
4X4	0.2498	0.06246	5.004 to 5.000

Besides confirming conclusions a) and b) of the first example, this shows that a constant twisting mode is included in the present element (it comes from the  $xy$  term in the displacement functions). The lack of it plagued some elements studied in [22].

## 5.4 Circular Plate Examples

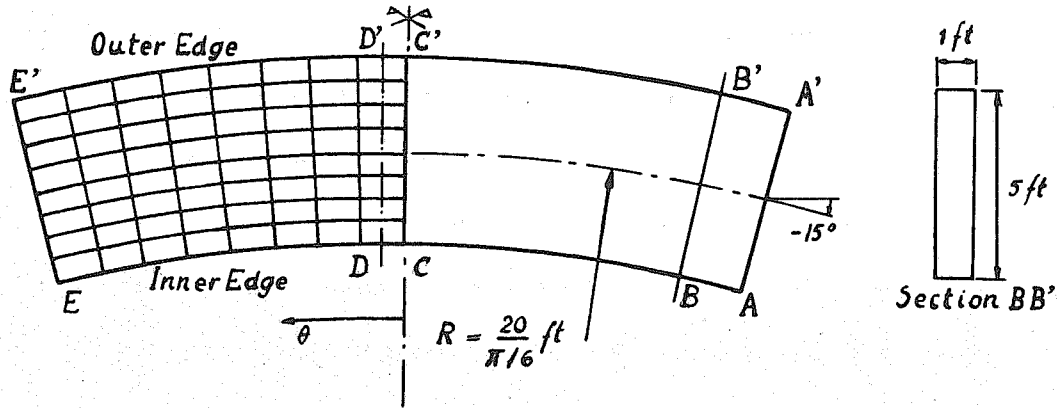
### 5.4.1 Curved Slab

An annular plate, with 30° central opening, 20 ft. span, simply supported along the radial edges and subjected to uniform load is portrayed on Fig. 5.4a. It can be thought of as a slab used in a curved foot-bridge. The symmetry makes it possible to study one half of the structure.

When a refined mesh of  $8 \times 8$  is used to model this system, it does not matter whether rigid body modes are added or not. The finite element results are compared in Fig. 5.4 and 5.5 with the exact solution in Fourier series given by Timoshenko [119], [69] and programmed by Meyer [78]. Comments on these results follow.

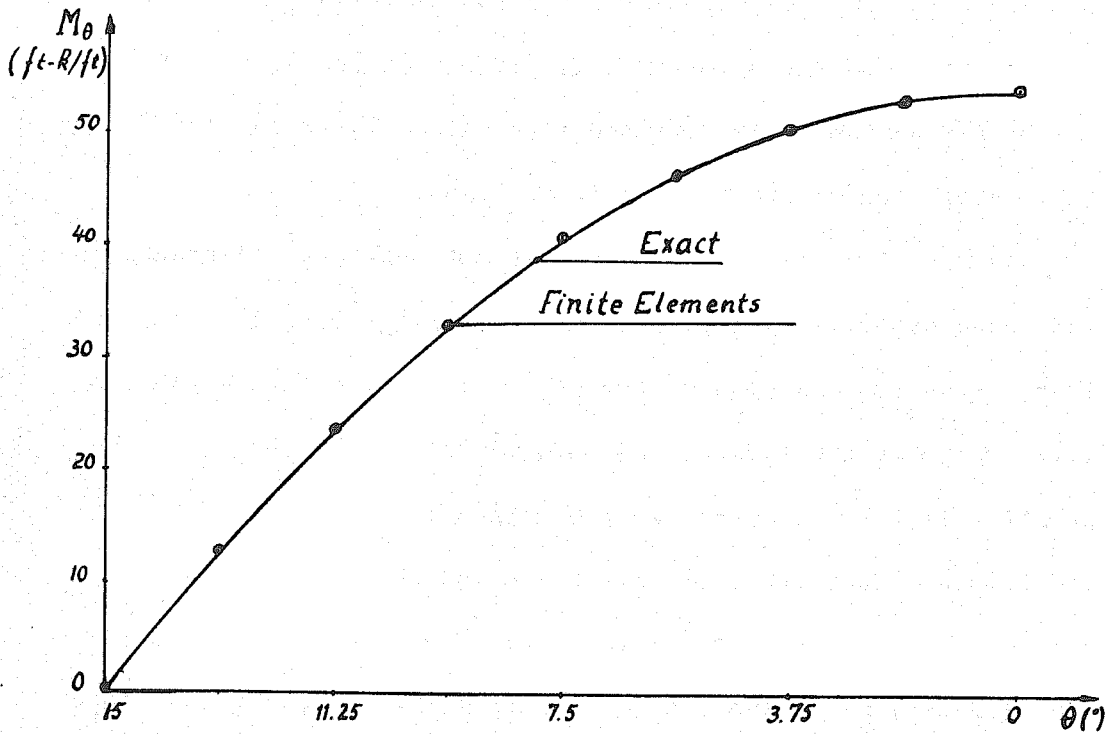
- a) Curves of displacements were not plotted because they coincide with the exact ones.
- b) Values of  $M_\theta$ , obtained by averaging corner values based on strains, agree with exact results; a plot along the inner edge is shown on Fig. 5.4b.
- c) Moments  $M_r$ , also obtained by averaging corner values, do not agree so well, as may be seen in the curves along the axis of the slab and the symmetry axis (Fig. 5.5a and 5.5b). But better agreement is obtained when values based on element center strains are plotted (Fig. 5.5c).

The fact that rigid body modes do not make any difference in this case deserves an explanation. In Section 4.6, it was shown that, for a circular plate element, only the radial translation, rotation about the normal, and rotation about the tangent to the parallel line at element center  $O$  needed to be added. Because of the loading conditions, the first two modes do not play any role here. It was shown in the same section 4.6 that the interpolation function approximates the third mode to the order  $\theta^4$  (difference between  $\cos \theta - 1$  and a cubic in  $\theta$ ); here,  $\theta$  varies between  $\pm 0.0164$  radians within each element; therefore, the third mode is quite well represented already and its addition does not modify the solution significantly.



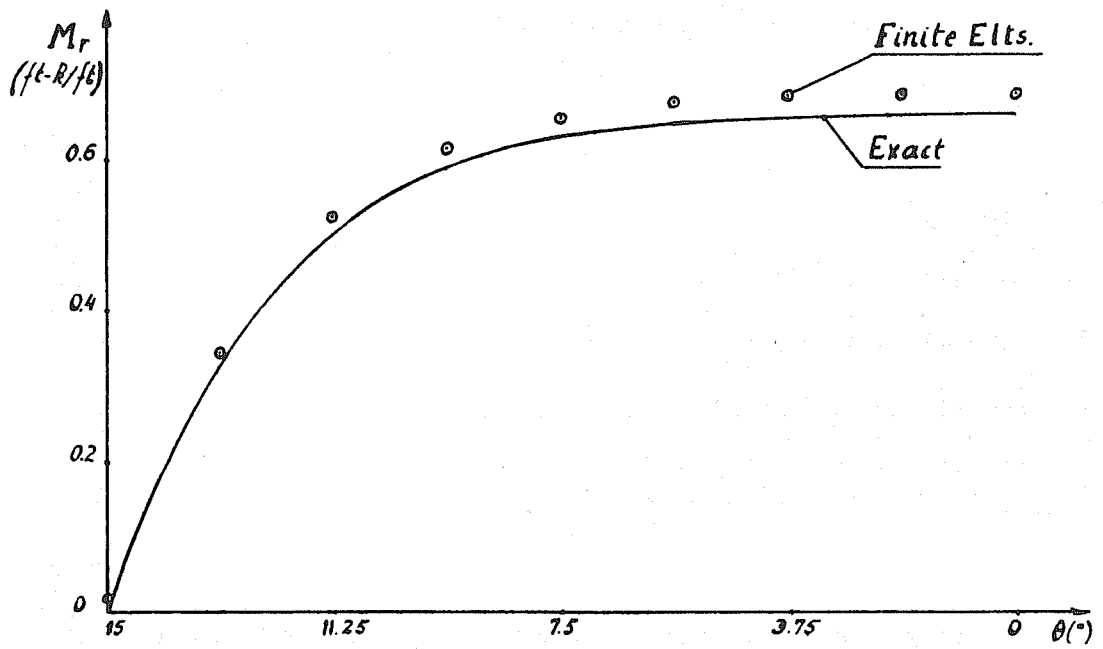
AA', EE' Simple Supports      E = 432000 ksf  
 Span Along Axis = 20 Ft.      nu = 0.15  
 Uniform Load = 1 ksf          8x8 Mesh

a) Problem Description and Finite Element Idealization.

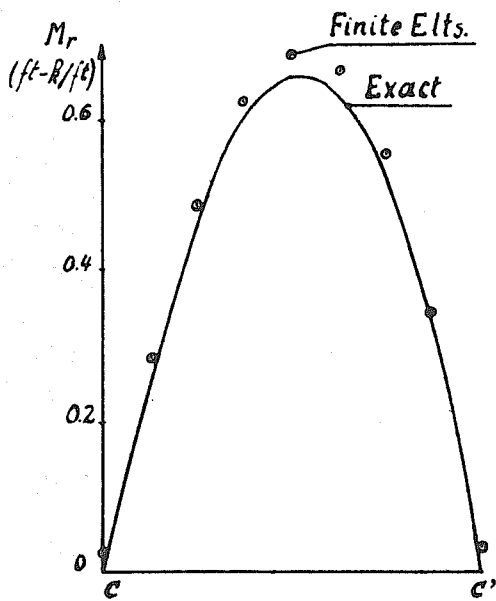


b) Moment  $M_\theta$  Along Inner Edge.

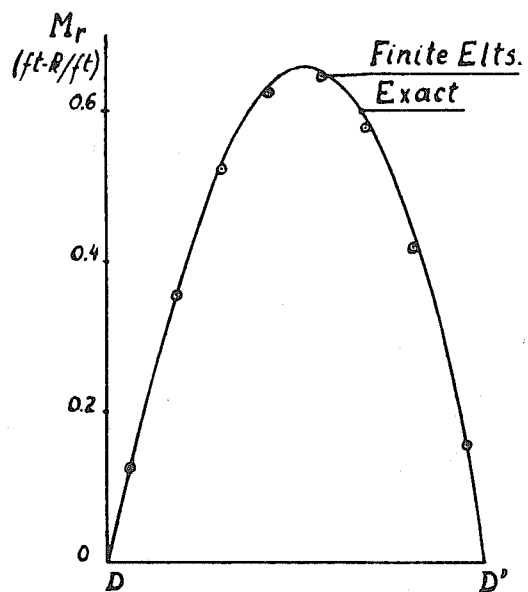
Fig. 5.4. Simply Supported Curved Slab.



a)  $M_r$  Along Axis.



b)  $M_r$  Along Section CC



c)  $M_r$  Along Section DD

Fig. 5.5. Simply Supported Curved Slab.



The lessons to be drawn from this example are obvious.

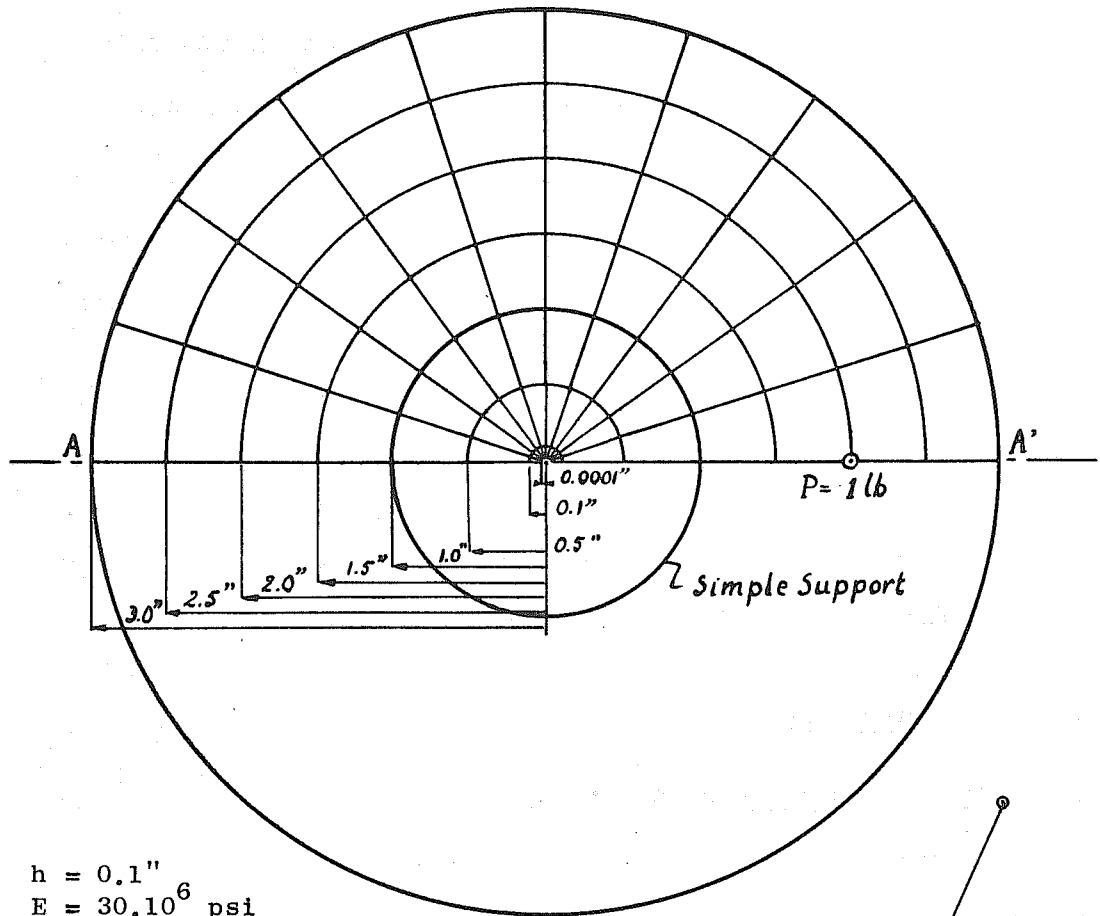
- a) In circular plates undergoing transversal deflections only, the rigid body modes are quite well represented by the cubic interpolation functions used for  $w$ ; they do not need to be added, especially when the elements have only a small parallel opening.
- b) In stress computations, the values at the element center are more reliable than those obtained at corners by averaging results in adjacent elements.

#### 5.4.2 Circular Plate with Concentrated Force

Lee [71] has analytically solved the problem of a circular plate simply supported along a concentric circle and loaded by a concentrated force located inside or outside that circle. One such example is shown in Fig. 5.6a. Again, the symmetry allows to solve only one half of the plate.

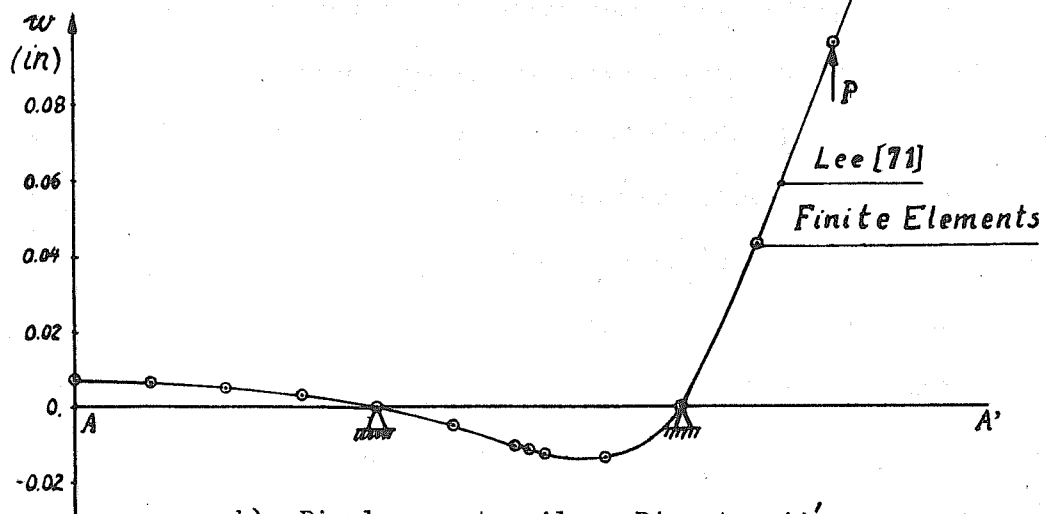
The  $7 \times 10$  mesh used in the analysis of this plate is nearly the most refined mesh acceptable in the program. One small ring of elements is used near the tiny hole replacing the pole to avoid ill-conditioning; surrounding that, 6 segments are evenly spaced along the meridian; the parallel opening of the elements is  $18^\circ$ . This must be considered a rather coarse mesh to represent the concentrated load effect.

Again, the rigid body modes do not play any significant role in this study. The results agree fairly well with those already available in [71], namely the displacement along the loaded diameter (Fig. 5.6b) and the radial moment at the support



$h = 0.1''$   
 $E = 30 \cdot 10^6 \text{ psi}$   
 $\nu = 0.3$   
 $7 \times 10 \text{ Mesh}$

a) Problem Description and Finite Element Idealization.



b) Displacement  $w$  Along Diameter  $AA'$ .

Fig. 5.6. Flexure of Circular Plate by Concentrated Force.

(0.478 P, in the program, versus 0.502 P). Better agreement on the stresses could certainly be obtained with a more refined mesh.

This example does not lead to new conclusions. But it was introduced to show the relative versatility of the program. The preceding curved slab problem was solved with 25 Fourier terms twice faster than with the finite element program. But the present concentrated load and boundary condition cannot be as easily represented in an analytic solution; thus here, the finite elements have the edge.

## 5.5 Cylindrical Shells

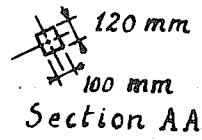
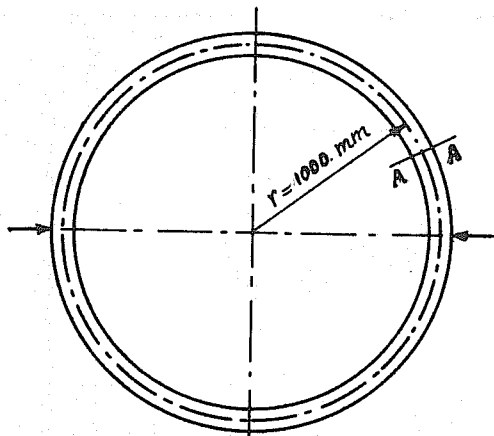
### 5.5.1 Circular Ring Under Diametral Load

A circular ring subjected to diametrically opposed loads was solved several times, either by means of a special program for circular beam elements, or by applying the program NADESOR to an equivalent cylindrical shell having zero Poisson's ratio and subjected to uniform line loads along two diametrically opposed meridians. In either case, symmetry permits one to study one quarter of the ring only. Both coarse and refined meshes were used in the analyses, comprising 4 or 16 elements over  $90^\circ$  respectively. A summary of the results is presented in Table 5.1 and selected results are plotted on Fig. 5.7 and 5.8. A discussion of the results follows.

In case 1, cubic interpolation functions are used for the transversal displacements  $w$  and for the axial displacements  $u$ . With 4 elements, the displacements are "almost" exact, by which

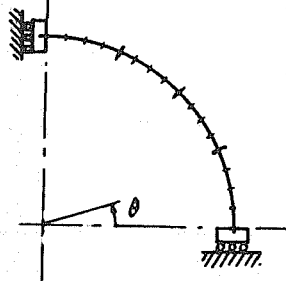
TABLE 5.1. SUMMARY OF RING RESULTS.

Case No.	No. of Elts	Degrees of Freedom	DOF Cond. Out	Displacements	Bending Moments Based on		Normal Forces Based on	
					Strains	Stiff.	Strains	Stiff.
1	4	$v_i, v_i^*, w_i, w_i^*$	-	$\approx$ Exact	Exact $\pm$ 5%	-	70-150% of Ex.	-
2	16	$v_j, v_j^*, w_i, w_i^*, w_j, w_j^*$		Exact	$\approx$ Exact	-	$\approx$ Exact	-
3	4	$v_i, v_i^*, w_i, w_i^*$	$v_i^*, v_j^*$	$\approx$ Exact	Exact $\pm$ 5%	-	Exact $\pm$ 10%	-
4	16	$v_j, v_j^*, w_j, w_j^*$		Exact	$\approx$ Exact	-	$\approx$ Exact	-
5	4	$v_i, v_i^*, w_i, w_i^*$	$v_i^*, v_j^*$	Exact	Exact	-	$\approx$ Exact	-
6	16	$v_j, v_j^*, w_j, w_j^*, v_o, v_o^*, w_o, w_o^*$	$v_o^*, w_o^*$	Exact	Exact	-	Exact	-
7	4	$v_i, w_i, w_i^*$	-	10-15% of Exact	Wrong	Idem	Wrong	Idem
8	16	$v_j, w_j, w_j^*$		65-75% of Exact	60-80% of Ex.	Idem	80-150% of Ex.	Idem
9	4	$v_i, w_i, w_i^*$	$v_o^*, w_o^*$	$\approx$ Exact	Exact $\pm$ 2%	Exact	$\approx$ Exact	Exact
10	16	$v_j, w_j, w_j^*, v_o, v_o^*, w_o, w_o^*$		Exact	Exact	Exact	Exact	Exact

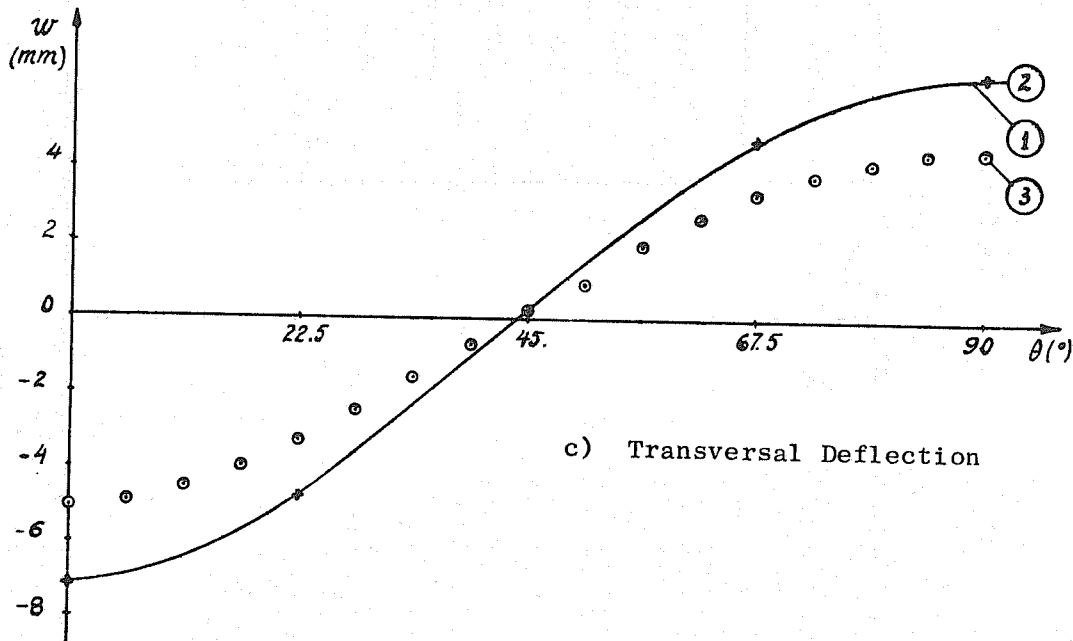


$P = 20000 \text{ kg}$   
 $E = 21000 \text{ kg/mm}^2$   
 $\nu = 0$

a) Problem Description



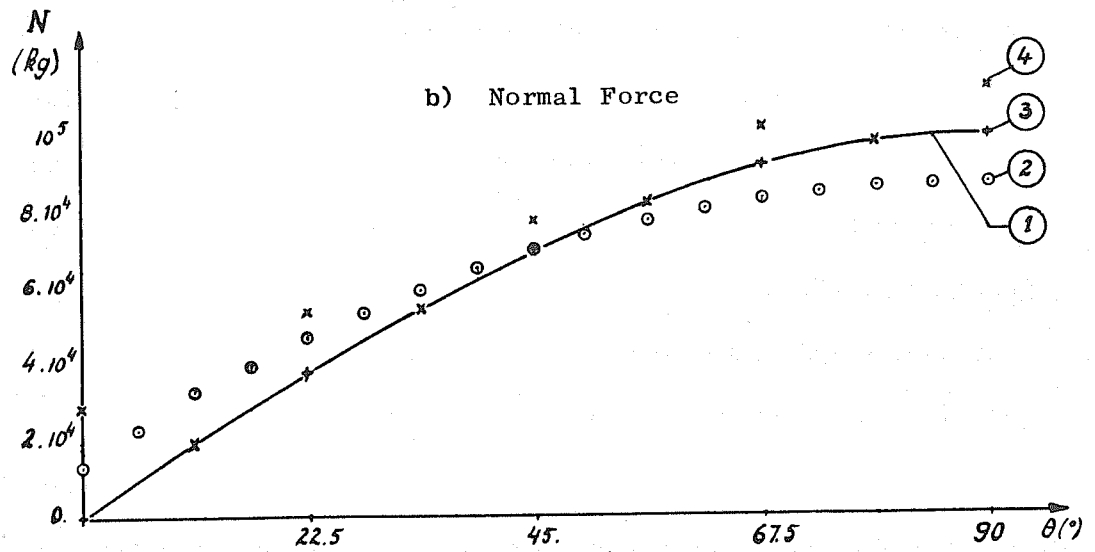
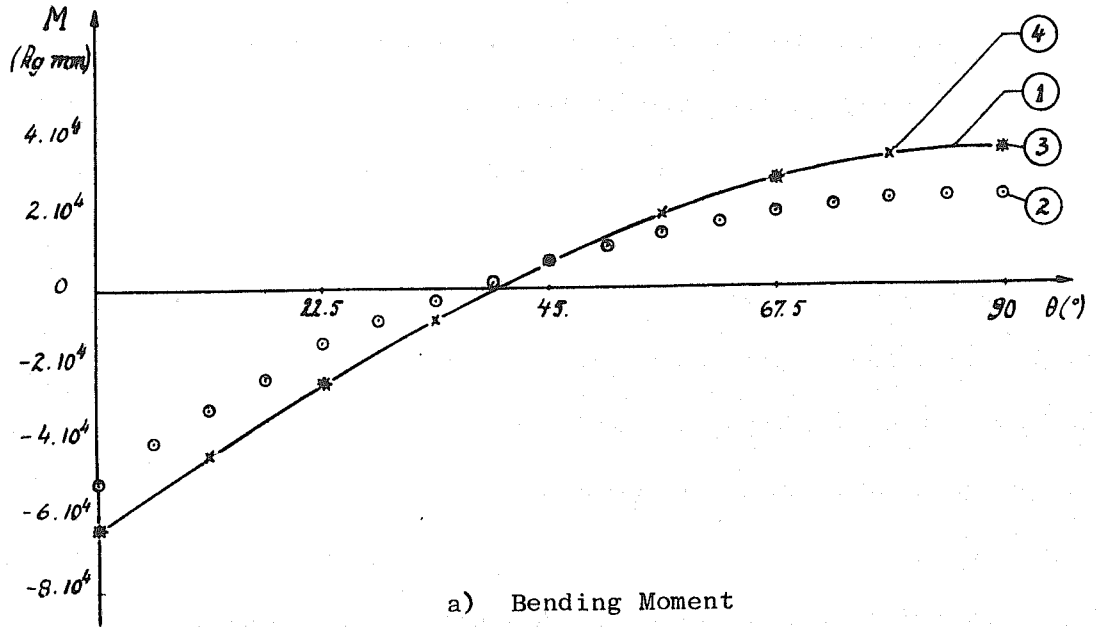
b) Idealization by  
 4 or 16 Elements



c) Transversal Deflection

- Legend:
- ① Exact Curve
  - ② 4 Elts with Rigid Modes (Line 9 in Table 5.1)
  - ③ 16 Elts Without Rigid Modes (Line 8 in Table 5.1)

Fig. 5.7. Ring Under Diametral Load.



- Legend:
- ① Exact Curve
  - ② M & N Based on Strains (Line 8 in Table 5.1)
  - ③ M & N Based on Stiffness (Line 9 in Table 5.1)
  - ④ M & N Based on Strains (Line 9 in Table 5.1)

Fig. 5.8. Ring Under Diametral Load.

it is meant that their divergence from the exact results is well below 1%. However, the bending moments and, above all, the normal forces are not too good; this is due to the fact that unwanted stresses are caused by misrepresented rigid motions. When the mesh is refined, in case 2, the cubic polynomials approximate well enough the trigonometric functions, and the results are much better. This is a typical case in which "the rigid motions are recovered in the limit and can be considered included for all practical purposes."

The DOF  $v_i^* = (\partial v / r \partial \theta)_i$ ,  $v_j^* = (\partial v / r \partial \theta)_j$  are necessary to determine the coefficients in the cubic polynomial for  $v$ . But to keep them among the external DOF amounts to imposing continuity of the axial strain at nodal points. This unnecessary constraint is relaxed if  $v_i^*$  and  $v_j^*$  are condensed out of the stiffness matrix at the element level. This was done in cases 3 and 4 and produced slightly improved results.

A much bigger improvement is obtained when rigid motions are added to augment the stiffness matrix and then condensed out together with  $v_i^*$  and  $v_j^*$ . Because of the special characteristics of the loading, only two out of the four modes which actually are missing in the cylindrical shell element (see Section 4.6) must be added, namely  $v_0$  and  $w_0$  or  $w_0$  and  $\beta_1$ . Both the pairs of rigid motions possess an interesting property: the displacements  $u_R(s, \theta)$ ,  $w_R(s, \theta)$  they produce do not vary as trigonometric functions but are constant along the meridian edges of the cylinder element. In this problem, the deformation displacements  $u_D(s, \theta)$ ,  $w_D(s, \theta)$  are also constant over the height of the cylinder.

Therefore, continuity of total displacements at the extreme nodes of a meridian edge will maintain compatibility of displacements over the whole meridian. It may thus be concluded: In this ring example, the addition and static condensation of rigid modes  $v_0$  and  $w_0$  do not produce incompatibilities. Perfect displacements and almost perfect forces are obtained in case 5 with a coarse mesh; this is remarkable since each element has a parallel opening of  $22.5^\circ$ . With 16 elements, case 6 gives results correct to the sixth digit at least.

Starting with case 7, different levels of interpolation functions are used in the elements: cubic for the transversal displacement  $w$  and linear for the axial displacement  $v$ ; this is the kind of approximation used in the element described in chapter 3 and used in all other examples of the present chapter.

The coarse mesh gives catastrophic results: the displacements are ten times too small and the forces do not even present a recognizable pattern. The results of the refined mesh of case 8 are plotted in Fig. 5.7b, 5.8a and 5.8b. They demonstrate convergence but many more elements would be necessary before the linear interpolation function used for  $v$  provides a satisfactory approximation of the trigonometric functions.

When rigid motions are added and condensed out, cases 9 and 10 show a dramatic improvement. With as few as 4 elements, the displacements and forces are practically correct (see Fig. 5.7b to 5.8b); only the normal forces obtained by averaging at the nodal points diverge from the exact solution. With 16 elements, all results are perfect.



In the ring example, the usual bending moments, normal and shear forces are related to the generalized forces obtained by direct application of the stiffness matrix through

$$\begin{aligned} M_i &= F_{w_i} & , & & M_j &= F_{w_j} \\ N_i &= F_{v_i} + \frac{1}{r} F_{w_i} & , & & N_j &= F_{v_j} + \frac{1}{r} F_{w_j} \\ S_i &= F_{w_i} & , & & S_j &= F_{w_j} \end{aligned} \quad (5.1)$$

In cases 7 and 8, the forces obtained in this way from two adjacent elements do not balance each other at the nodal point; neither do they satisfy overall equilibrium. But they do balance and verify equilibrium in cases 9 and 10 when rigid body modes are introduced. This is a direct consequence of the equilibrium properties of the rows in an element stiffness matrix; these properties were already discussed in Section 3.4.5.

This example confirms several past conclusions and leads to new ones.

- a) When no rigid body modes are added the element with cubic  $w$  and  $v$  is far superior to the element with cubic  $w$  and linear  $v$ , especially with regard to the convergence properties.
- b) The addition of rigid body modes does not always introduce incompatibilities.

In problems where compatibility is maintained, the following conclusions also are valid.

- c) The addition of rigid body modes can make a tremendous difference: 4 elements with rigid modes give much better results in case 9 than 16 elements without rigid modes in case 8.

- d) The addition of rigid modes is preferable to the addition of an equal number of DOF increasing the degree of interpolation functions; the comparison of improvements going from cases 7, 8 to cases 9, 10 or to cases 3, 4 demonstrate this point.

### 5.5.2 Pinched Cylinder

This example, represented on Fig. 5.9, was already solved by Bogner et al. [10] using bicubic interpolation functions for  $u$ ,  $v$ ,  $w$ , and by Cantin [17] who reduced interpolation functions for  $u$  and  $v$  to bilinear polynomials but added rigid modes. It is repeated here because Cantin failed to show how much improvement was provided by the rigid modes themselves.

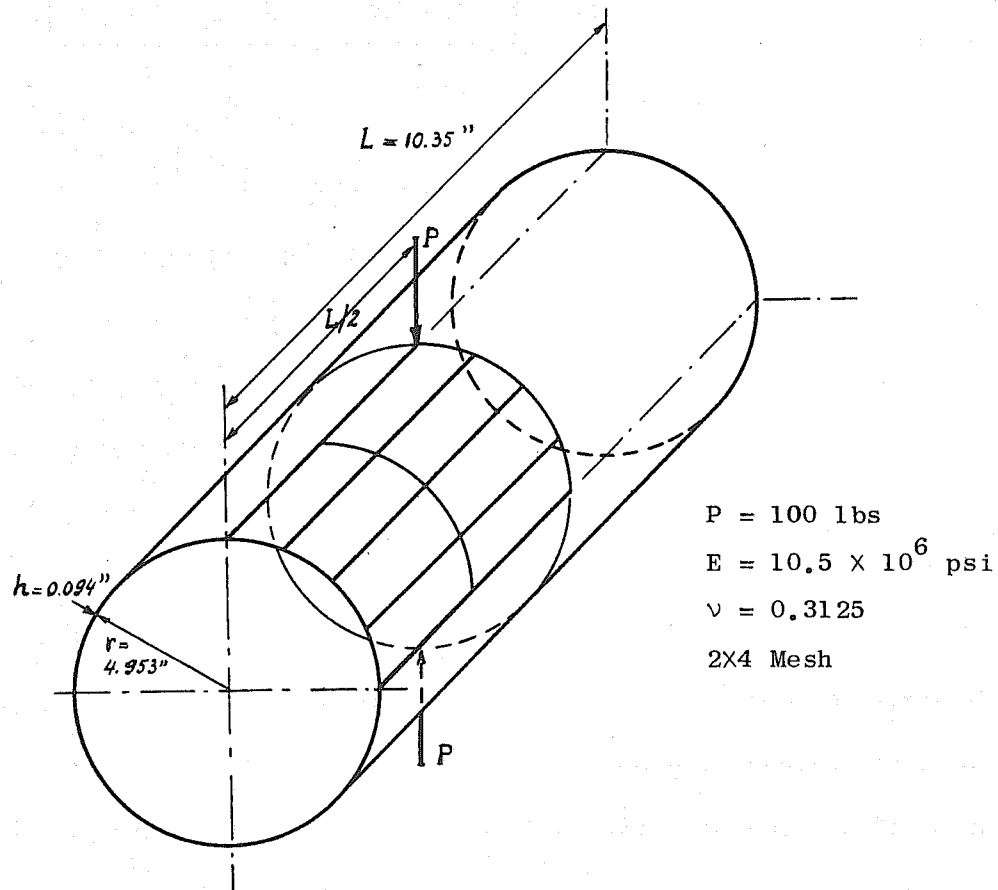


Fig. 5.9. Pinched Cylinder.

The displacements under the load are tabulated here below for different mesh refinements:

Mesh	Bogner et al. Bicubic u, v, w		Cantin Bilinear u, v Bicubic w		Cantin Idem Plus Rigid Motions	
	No. of Eq.	Displmt (in.)	No. of Eq.	Displmt (in.)	No. of Eq.	Displmt (in.)
1x1	-	-	24	- 0.0017	24	- 0.0048
1x4	120	- 0.1087	60	- 0.0152	60	- 0.1099
2x4	180	- 0.1098	-	-	-	-
4x4	-	-	150	- 0.0237	150	- 0.1126
4x8	-	-	270	- 0.0558	270	- 0.1132
8x8	-	-	486	- 0.0582	486	- 0.1139

The deflection obtained by Timoshenko [119] is - 0.1084 in. but he takes only bending deformation into account.

These results confirm for a cylindrical shell example the conclusions reached with the ring.

- a) The complete bicubic interpolation functions converge but slower than the bilinear and bicubic functions with rigid body modes added: 180 versus 60 DOF to attain the same deflection  $w = 0.1098$ .
- b) The bilinear and bicubic functions without rigid body modes produce extremely poor results. The jumps in convergence occur when the number of elements is increased in the parallel direction which attests again that the poor representation of trigonometric functions of  $\theta$  is responsible for the poor behavior of this element.

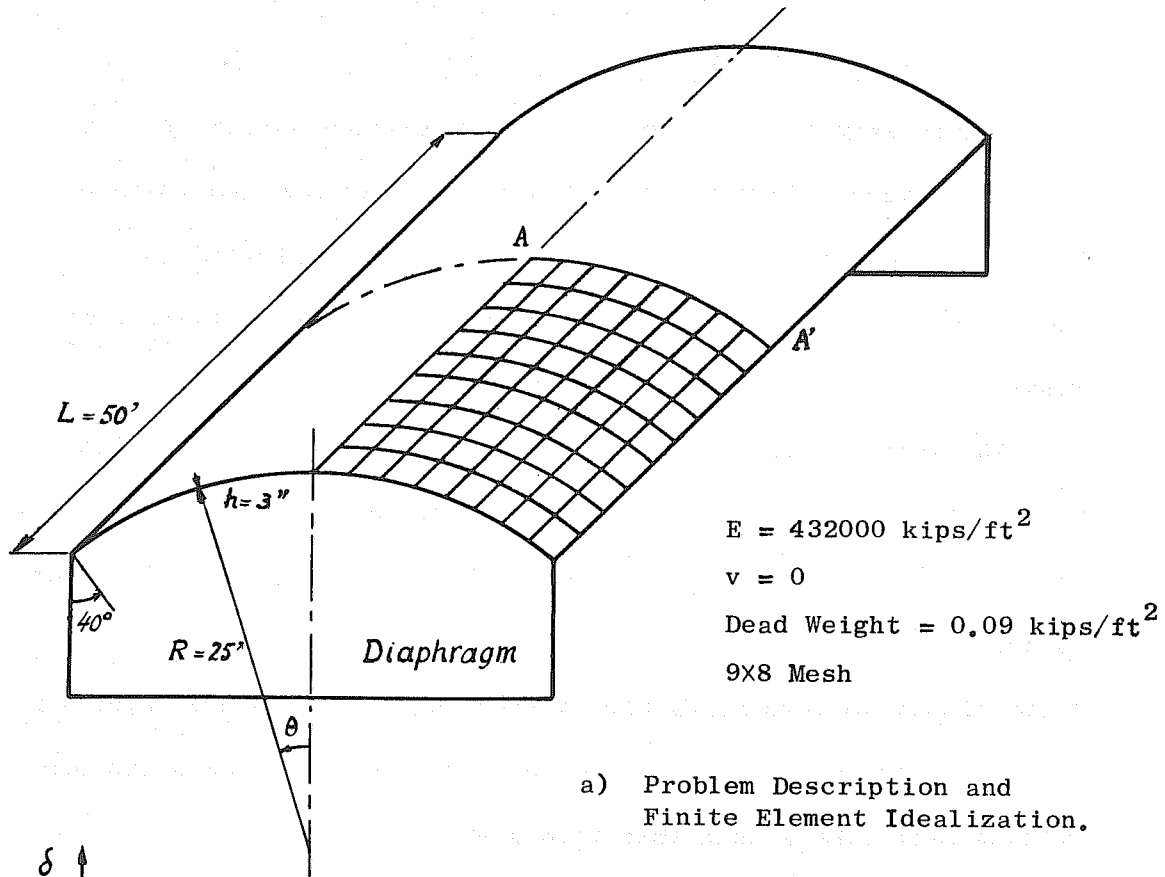
### 5.5.3 Cylindrical Shell Roof

This example, described on Fig. 5.10a was solved by several authors and extensively discussed by Clough and Johnson [21]. The "exact" solution in this reference is plotted on Fig. 5.10b, 5.11a and 5.11b for comparison with some significant results obtained with the program NADESOR.

The vertical deflection along the central section exhibits the usual good or very slow convergence of the element with or without rigid motions, respectively. What is interesting to note is that, without rigid motions, the cross section deflects vertically almost uniformly, without distorting. This is most apparent when only four elements are used and indicates that the structure behaves more like a beam than like a shell. This would be acceptable for a long shell, but for a short one, it really means that an important characteristic of the shell behavior is lost.

The consequences of this lack of distortion appear in the diagrams of  $M_\theta$  and  $N_s$  across the central section. The transverse moments  $M_\theta$ , especially the nodal values are much too small because the section is not transversally distorted. The distribution of longitudinal stress  $N_s$  reproduces almost exactly the profile of the shell:  $N_s$  varies linearly with the vertical distance from a neutral axis; this is typical of beam behavior again and reveals a total absence of warping of the cross section.

By contrast, all results obtained with a 9X8 mesh including rigid body modes look very good. They provide about the same accuracy as a 12X8 mesh of Johnson's quadrilateral elements [55].



a) Problem Description and Finite Element Idealization.

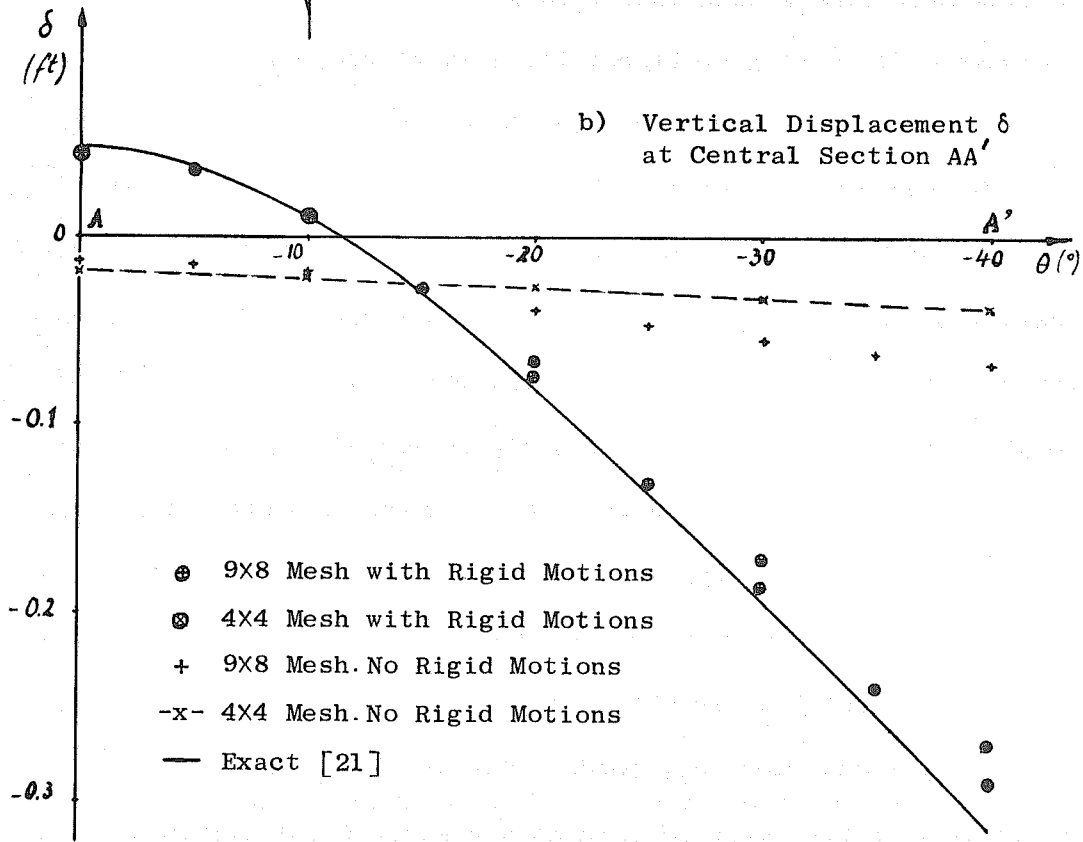


Fig. 5.10. Cylindrical Shell Roof.

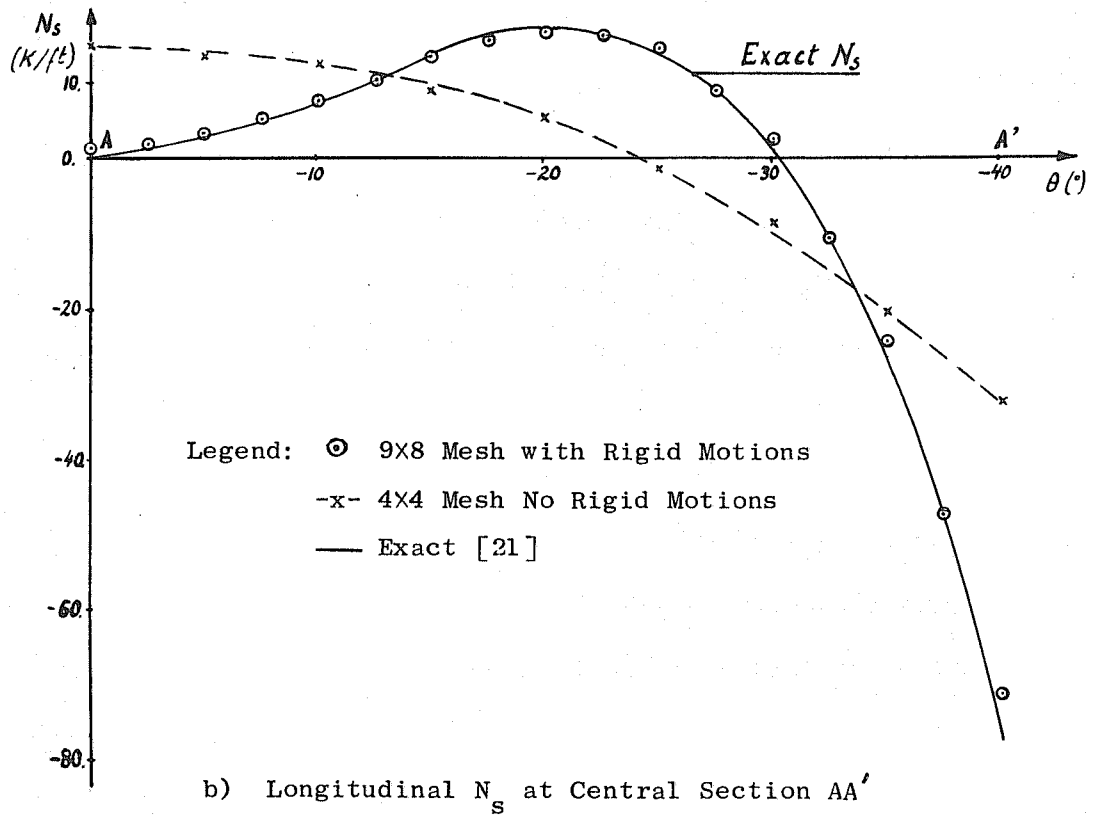
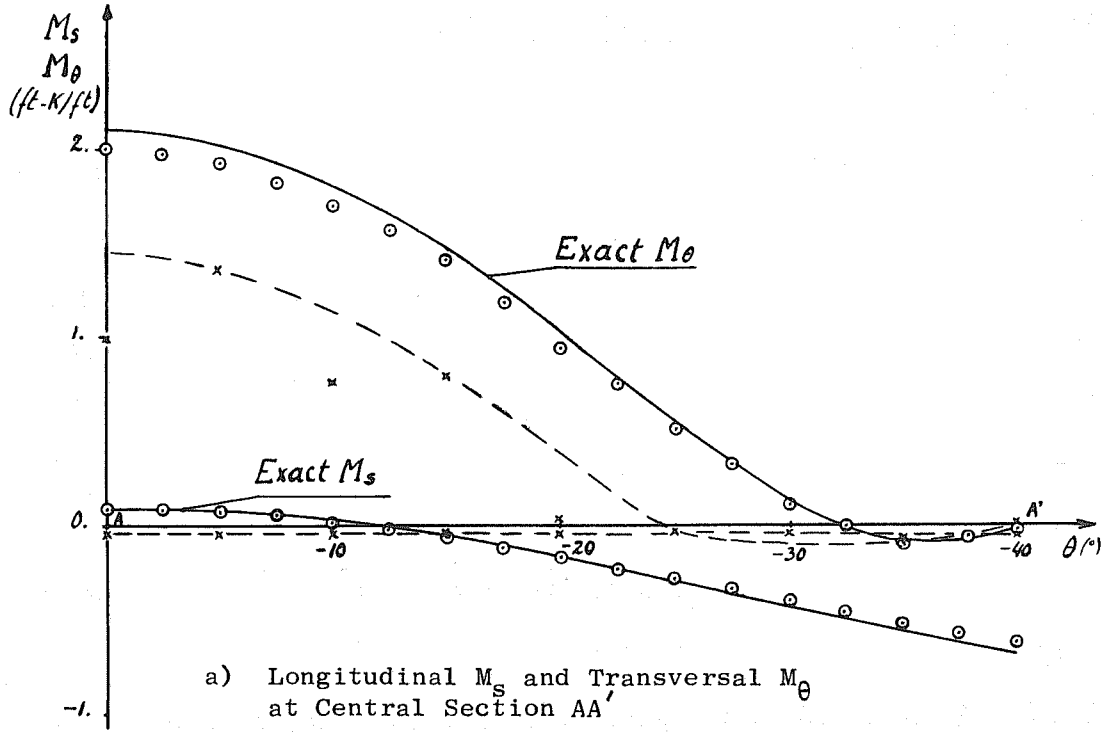


Fig. 5.10. Cylindrical Shell Roof.

On the basis of the examples solved so far, one could conclude that the addition of rigid modes cannot do any harm and in most cases will bring an improvement capable of raising this 24 DOF element to the same level of accuracy as more refined elements. Unfortunately, this optimistic conclusion is soon going to be contradicted.

## 5.6 Spherical Shells

### 5.6.1 Sphere Under Internal Pressure

The data of Fig. 5.12a are borrowed from Key [61]. Under this completely symmetric loading, it suffices to study one typical slice of the half sphere fixed, at one end, on a horizontal roller along the equator, and at the other end, on a vertical roller along the hole replacing the polar point. The expected displacements reduce to a constant  $w = 0.00350''$  over the whole sphere, which should be exactly representable by the polynomial displacement functions. There is no bending, just a uniform state of stress  $N_{\theta} = N_s = 500$  lbs/in. everywhere.

As shown on Fig. 5.12b and c, the displacements and stresses obtained with an uneven mesh of 20 elements with rigid modes added are completely wrong! Attempts to modify the finite element grid, the size of the polar hole, the parallel central angle  $\alpha$  proved equally unsuccessful.

Results obtained without adding the rigid modes, on the other hand, are absolutely correct. Even one single element, with  $\alpha = 5^\circ$  and  $0 \leq \varphi \leq 89^\circ$ , gives

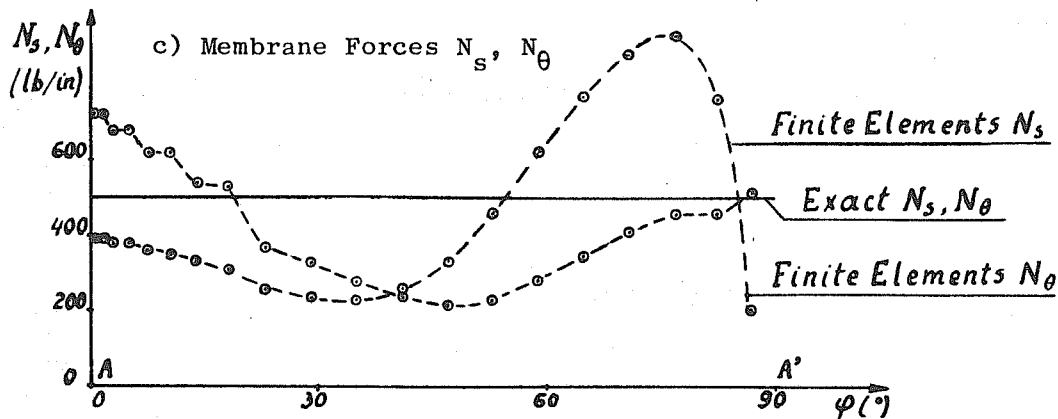
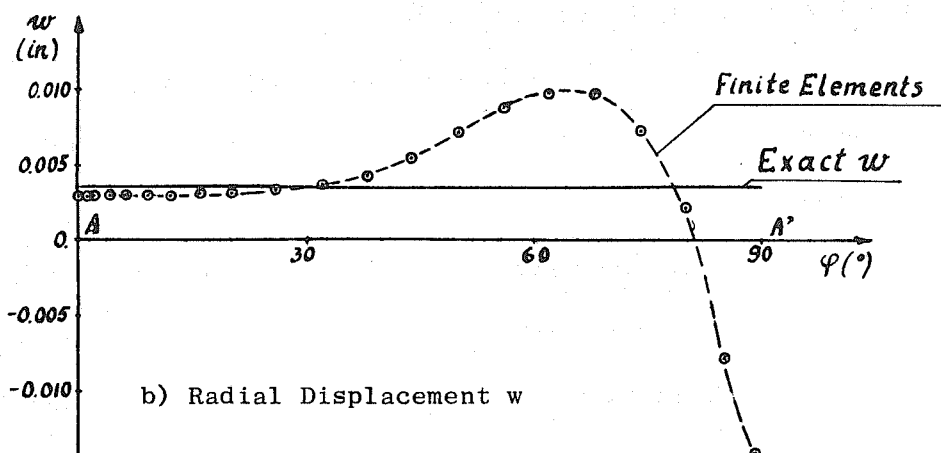
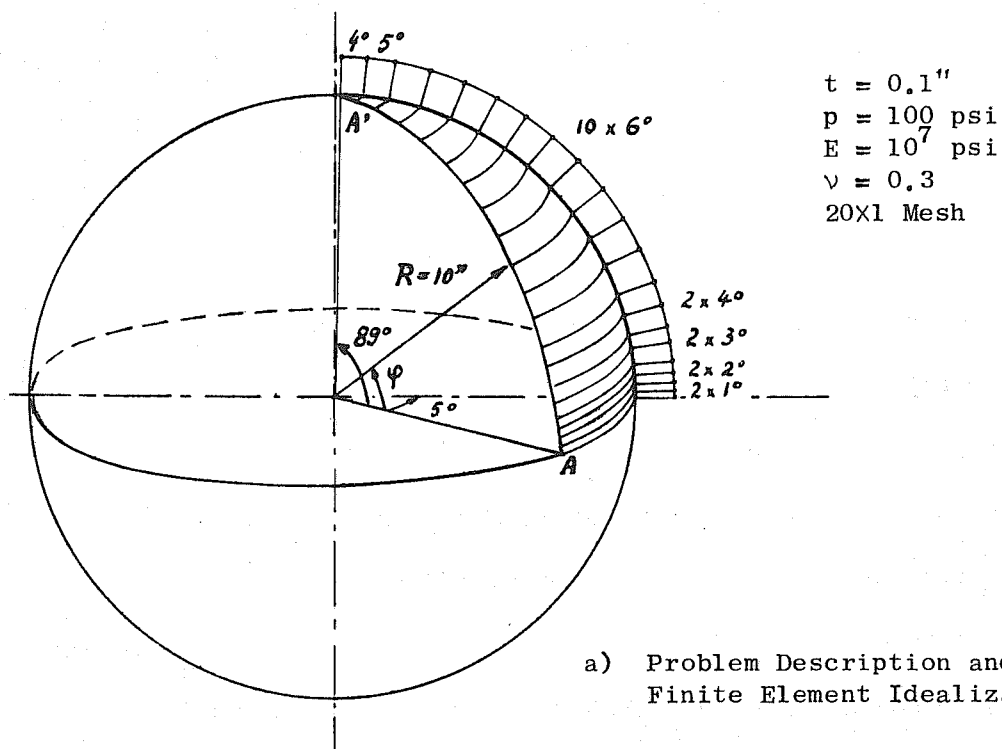


Fig. 5.12. Sphere Under Internal Pressure.



$$0.00350000 \leq w \leq 0.00350001$$

$$499.996 \leq N_s \leq 500.001$$

$$499.982 \leq N_\theta \leq 500.000.$$

In the case with rigid motions, a close scrutiny of intermediate print-outs for the element adjacent to the equator points to the rotation  $\beta_2$  as the principal source of errors in the solution. As sketched on Fig. 5.13, it is possible to find a combination of rigid body motions  $\beta_2$  and  $w_0$  such that the boundary conditions  $u_k = u_l = 0$  will be satisfied while a gap is opening between the two nodes. Of course, the same rigid motions also introduce a rigid contribution to the DOF  $w$ ,  $\partial w / \partial s$ ,  $\partial w / r \partial \theta$ ,  $\partial^2 w / r \partial \theta \partial s$  at  $k$  and  $l$ ; but for this particular boundary element these contributions are small and can easily be compensated by an artificial bending deformation so that the total DOF satisfy again the boundary conditions.

It is likely that the same situation occurs at other parallel interelement boundaries. These incompatibilities introduce unrealistic bending and lead to a complete misrepresentation of the membrane state: it is not surprising that the solution with rigid body modes is bad.

In conclusion, rigid motions and membrane displacements  $u$  and  $v$  are not needed in this problem; therefore, the shell element, as derived in chapter 3, gives very good results. The surprise is that when rigid modes are added, they are found to be different from zero; introduce incompatibilities and throw the solution completely off.

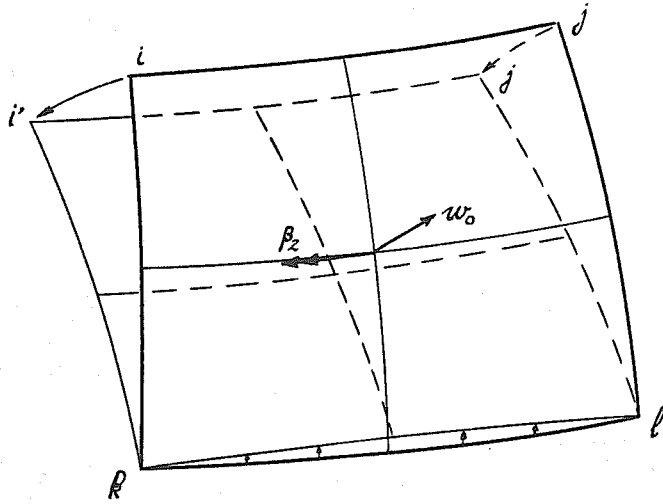


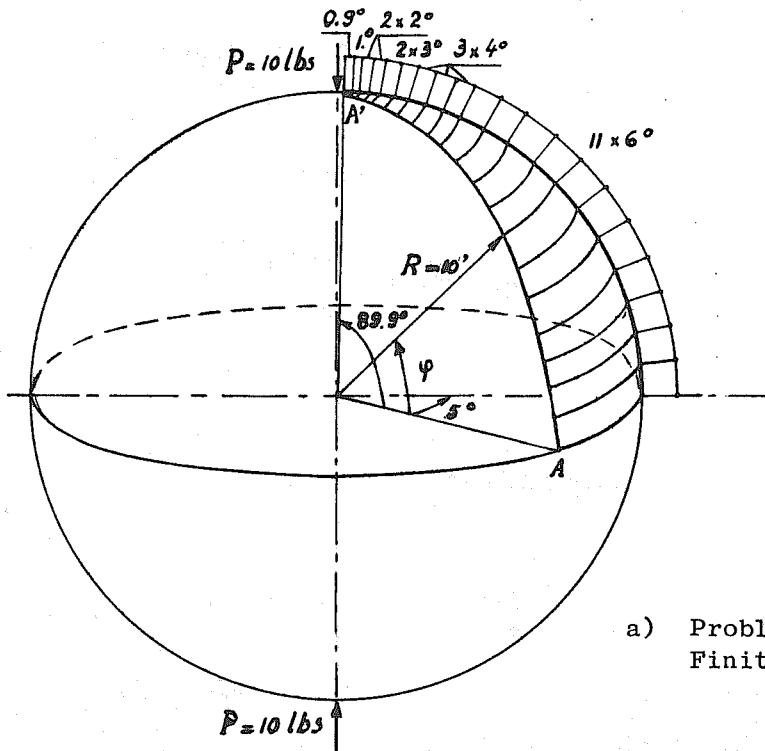
Fig. 5.13. Incompatibility Produced by Rigid Motions.

### 5.6.2 Sphere Under Point Load

If the previous example was designed to test the membrane behavior, this one, also borrowed from Key [61] should test the bending characteristics. The dimensions and elastic properties of the shell are described in Fig. 5.14a. The finite element solution is compared with curves plotted by Key according to formulas found in Flügge [32].

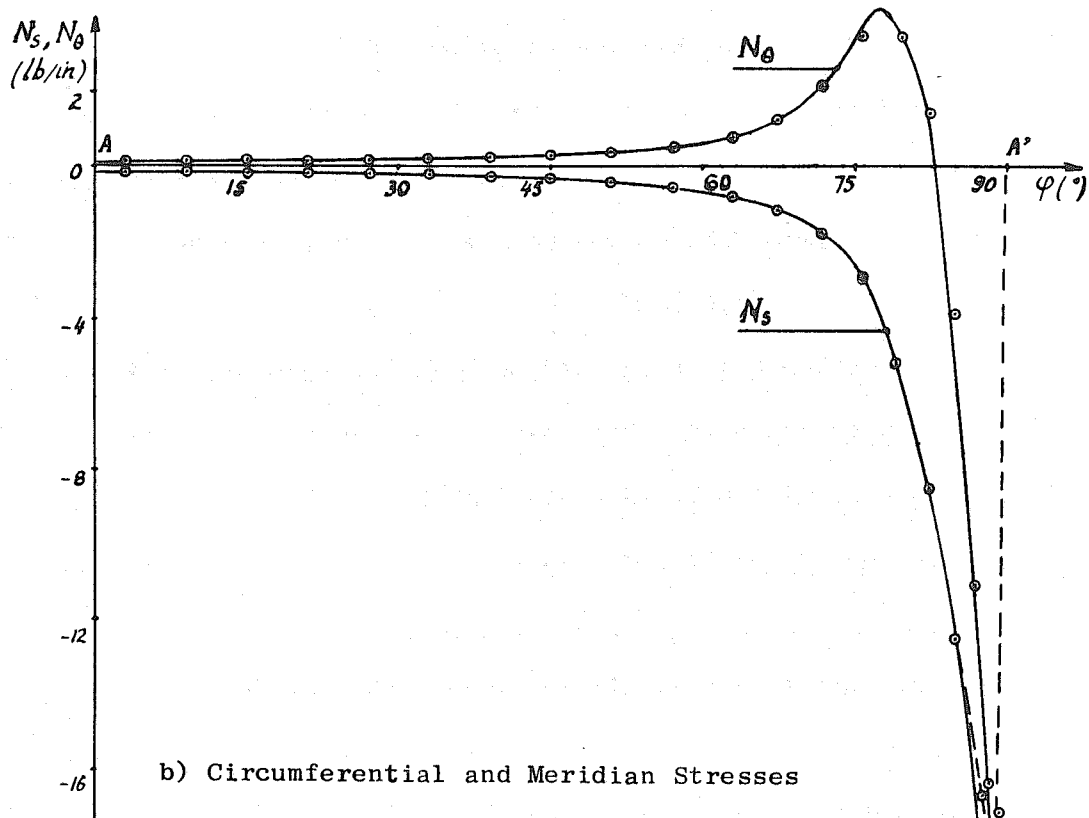
A first solution, taking into account the symmetry of the problem was obtained with a 20x1 mesh of elements with rigid motions added. The displacements are much too large as can be seen from curve ② on Fig. 5.15. The stresses are wide of the mark.

When the rigid motions are not added, the same mesh gives practically correct displacements: curve ① on Fig. 5.15. The shell forces  $N_s$ ,  $N_\theta$  computed at the element centers are represented on Fig. 5.14b. Except very near the polar hole where  $N_s$



$t = 0.1''$   
 $P = 10 \text{ lbs.}$   
 $E = 10^7 \text{ psi}$   
 $\nu = 0.3$   
 20x1 Mesh

a) Problem Description and Finite Element Idealization.



b) Circumferential and Meridian Stresses

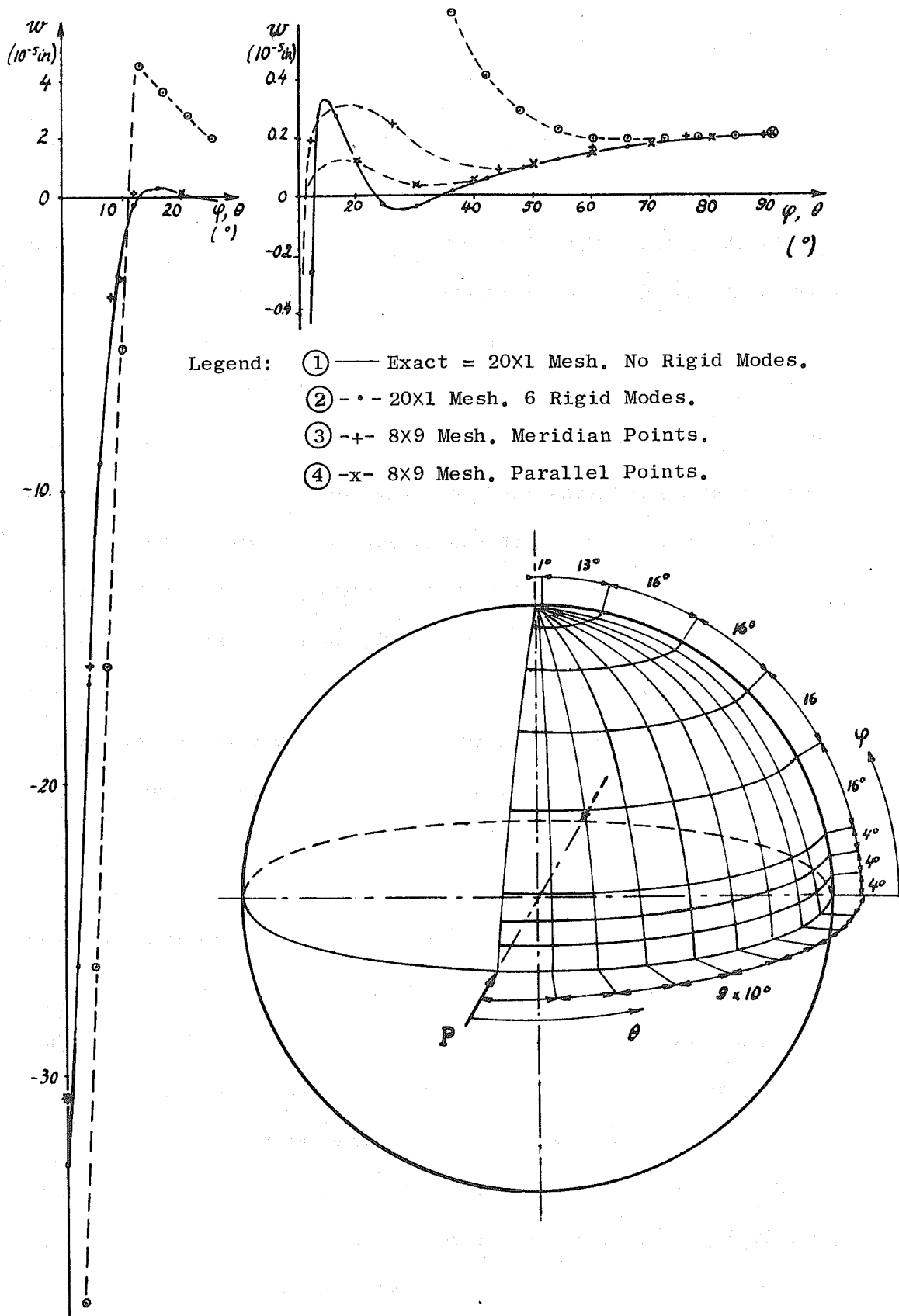
Fig. 5.14. Sphere Under Point Load.

falls to zero instead of going to infinity, they are remarkably good.

The same example was also solved as an unsymmetric problem just by shifting the pair of forces from the polar axis to the equatorial plane. Then, one octant of the sphere must be studied and is divided into  $8 \times 9$  elements (Fig. 5.15). Only a solution without rigid modes was computed. The  $w$  curves along the equator and along the meridian through the load (③ and ④ on Fig. 5.15) should both be equal to the previous result. The agreement is fairly good immediately near the load and more than  $40^\circ$  away from it; between  $10^\circ$  and  $40^\circ$ , there are not enough elements to represent the fast variation of  $w$ . (See Fig. 5.15 and note the change of scale between  $10^\circ$  and  $20^\circ$  to picture accurately large and small displacements.)

The results of this example can be summarized as follows:

- a) The incompatibilities introduced by the rigid motions render the solution with them worse than the solution without them.
- b) The bending and transversal displacements are predominant in this example, therefore, the bilinear  $u$  and  $v$  are not too inconvenient. Good results are obtained without rigid modes when the mesh is refined enough (symmetric case) but results get poor as the mesh gets coarse (unsymmetric case).



Legend: ① — Exact = 20X1 Mesh. No Rigid Modes.  
 ② - · - 20X1 Mesh. 6 Rigid Modes.  
 ③ - + - 8X9 Mesh. Meridian Points.  
 ④ - x - 8X9 Mesh. Parallel Points.

Fig. 5.15. Sphere Under Point Load.

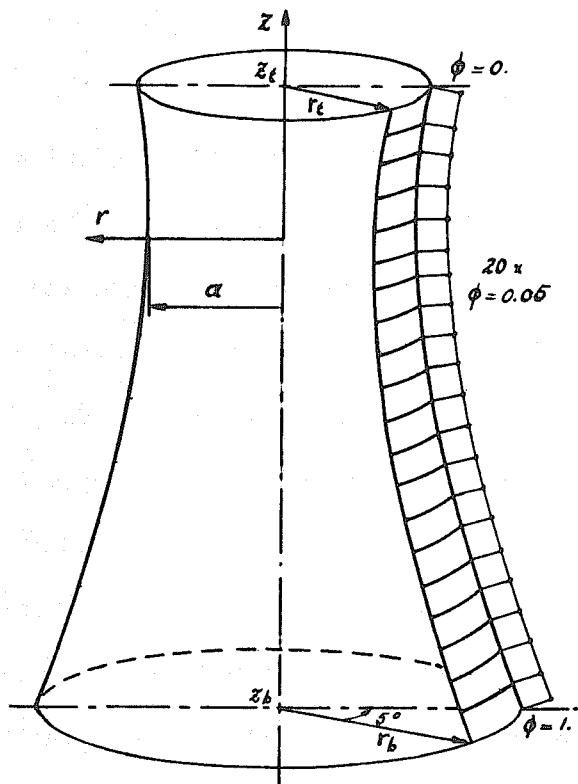
## 5.7 Hyperboloid of Revolution

### 5.7.1 Hyperboloid Under Dead Load

Cooling towers in the form of a hyperboloid of revolution were analyzed by Gould and Lee [42, 43, 109] using a closed form solution, by Albasiny and Martin [2] using the finite differences technique, and by Zienckiewicz [130] and Yeh [18] with finite elements. In the present discussion, the first reference was preferred to the others because its boundary condition, simple support on an infinitely stiff ring, seemed more realistic than the clamped bottom edge used in the others. Later, it turned out that Gould's example was not consistent in its geometric description and required interpolation in tables with large intervals; then, the tower described on Fig. 5.16a was also solved by means of Larsen's program [70] for axisymmetric deformation of shells of revolution; it utilizes a refined isoparametric element of revolution: cubic description of geometry,  $w$  and  $u$ , shear deformation included.

As with the spherical shell, the solutions obtained when rigid body modes are added is far worse than the solution without rigid modes; only the latter will be discussed here.

The displacements found with the program NADESOR will not be plotted because they practically coincide with those given by Gould or Larsen's program. The meridian and hoop stresses, computed at element centers, are plotted on Fig. 5.16b. They are identical to Larsen's results but differ from Gould's curves; the latter cannot be plotted with much accuracy, however.



Geometric Data

- $z_t = 80.24'$
- $r_t = 78.10'$
- $z_b = -253.23'$
- $r_b = 128.39'$

Generation Equation

$$(r/a)^2 - (z/b)^2 = 1$$

with  $a = 70.29'$   
 $b = 165.67'$

Geometric Parameter

$$\phi = (z_t - z)/(z_t + z_b)$$

Other Data

- $E = 432.10^6 \text{ lbs/ft}^2$
- $\nu = 0.2$
- $t = 0.5'$
- $p = 75 \text{ lbs/ft}^2$
- 20X1 Mesh

a) Problem Description and Finite Element Mesh

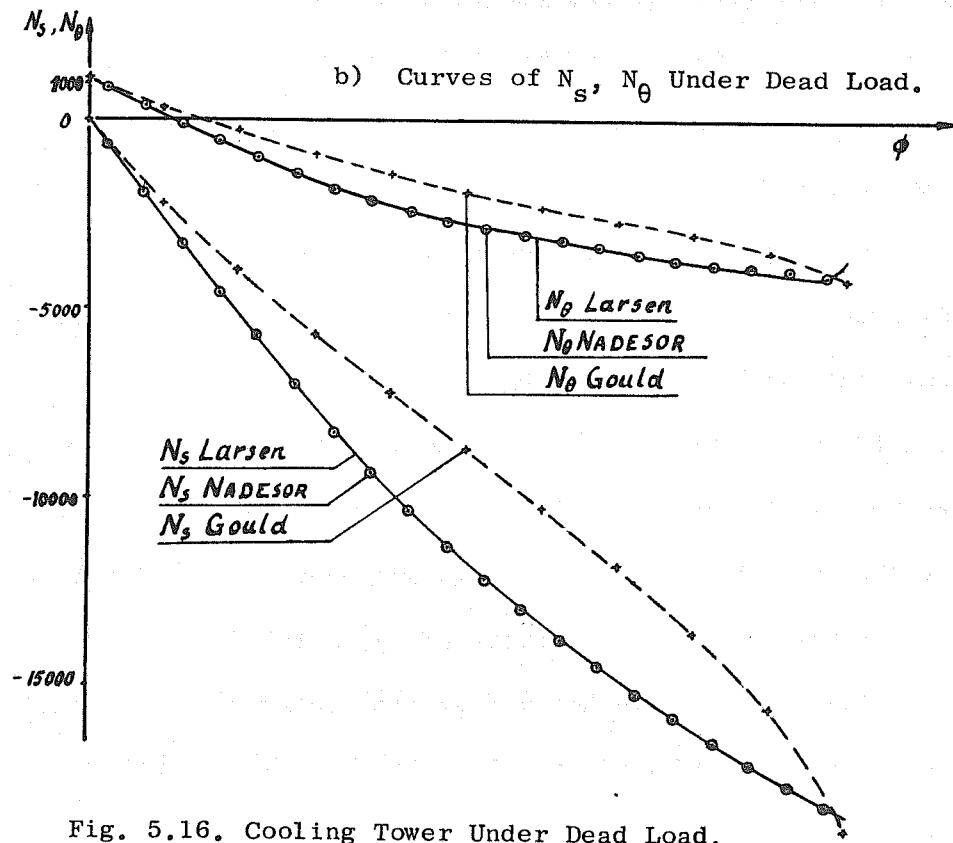


Fig. 5.16. Cooling Tower Under Dead Load.

Unfortunately the bending moments printed by NADESOR differ so much from the exact results that they are not even plotted! The bending, instead of being concentrated near the bottom edge propagates throughout the whole shell. When it was discovered that the consistent loading could produce bending moments along the parallels of the same magnitude as the peaks expected near the boundary, it was replaced by a loading based on the tributary area concept, but to no avail!

All the references mentioned earlier indicate that the dead load induces mostly a membrane state of stress in the hyperboloid of revolution. Fig. 5.16b show that these stresses vary almost linearly with the height. This means that the strain  $\epsilon_{11} = du/ds - w d\phi/ds$  should vary almost linearly with the meridian coordinate  $s$ ; but the most important term  $du/ds$  can only vary by jumps because of the assumed bilinear variation of  $u$ . The membrane strains and stresses are correct at the element centers but intermediate print-outs show that they hardly vary within one element and important out of balance forces exist at the inter-element boundaries. For instance, there is an unbalanced meridional stress of 537 lb/ft along the top parallel and a disequilibrium of 1201 lb/ft along the next one.

It is well known that, in shells with negative Gaussian curvature, perturbations applied at one edge propagate straight to the other edge without dying out as they do in shells with positive Gaussian curvature. It is suspected that such perturbations, induced by the imperfect representation of the membrane



state are responsible for the poor showing of the element in this example.

### 5.7.2 Hyperboloid Under Wind Load

The distribution of wind pressure on a hyperbolic cooling tower, recommended by Rish and Steel [105], based on measurements taken from a wind tunnel experiment, is given on Fig. 5.17, together with the finite element mesh used to solve that problem.

The displacements obtained are plotted on Fig. 5.18. They agree qualitatively with the results published in [109], [2], and [18]. But many more elements would be necessary to get a valid stress analysis. For information, 72 elements are used here versus 432 triangular elements or 15 refined isoparametric elements of revolution with 12 Fourier harmonics in Zienkiewicz [130].

### 5.8 Discussion of Incompatibilities

In concluding this presentation of the results of example calculations, it may be useful to discuss further the problem of the incompatibilities introduced by the rigid body displacements.

If one considers two elements adjacent to the same meridian (Fig. 5.19), the total displacements in elements 1 and 2 and their differences along the common edge are, in terms of the generalized coordinates  $\xi$  and  $\eta$

$$\begin{Bmatrix} u_1(\xi, 1) \\ v_1(\xi, 1) \\ w_1(\xi, 1) \end{Bmatrix}_T, \quad \begin{Bmatrix} u_2(\xi, -1) \\ v_2(\xi, -1) \\ w_2(\xi, -1) \end{Bmatrix}_T, \quad \begin{Bmatrix} u_1(\xi, 1) - u_2(\xi, -1) \\ v_1(\xi, 1) - v_2(\xi, -1) \\ w_1(\xi, 1) - w_2(\xi, -1) \end{Bmatrix}_T.$$

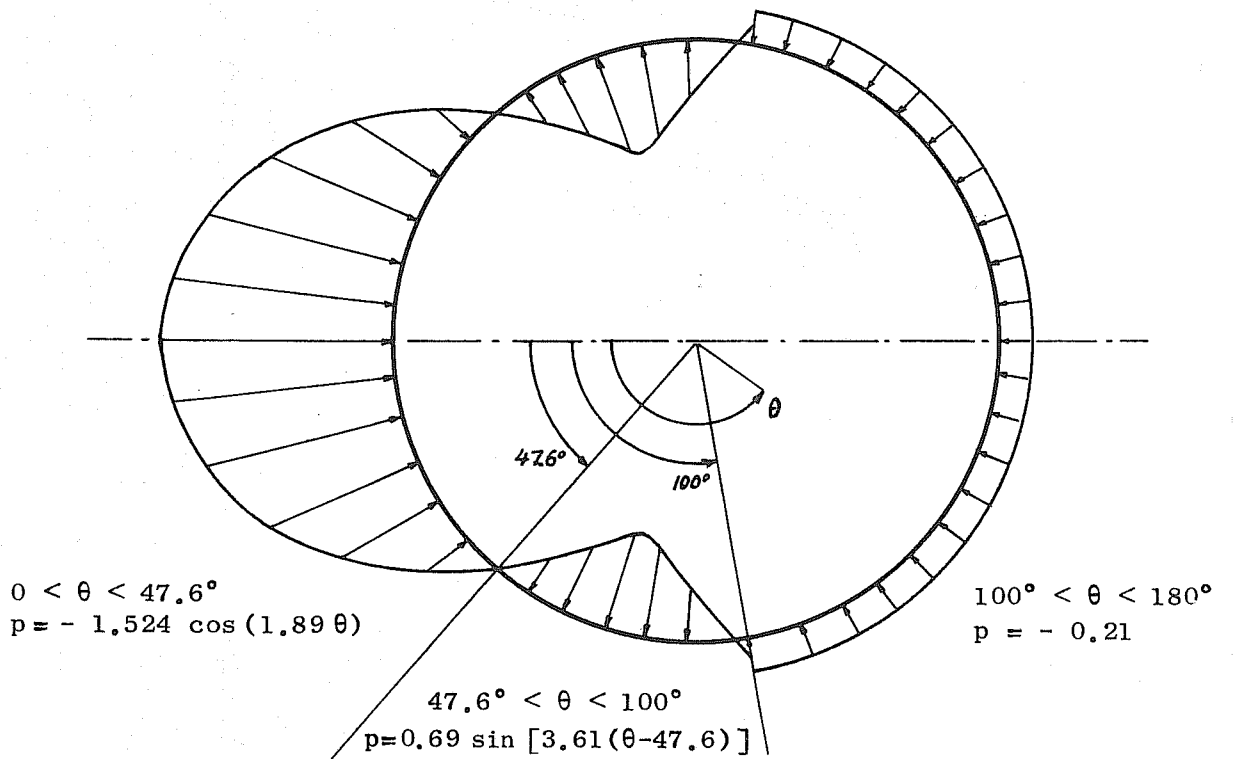
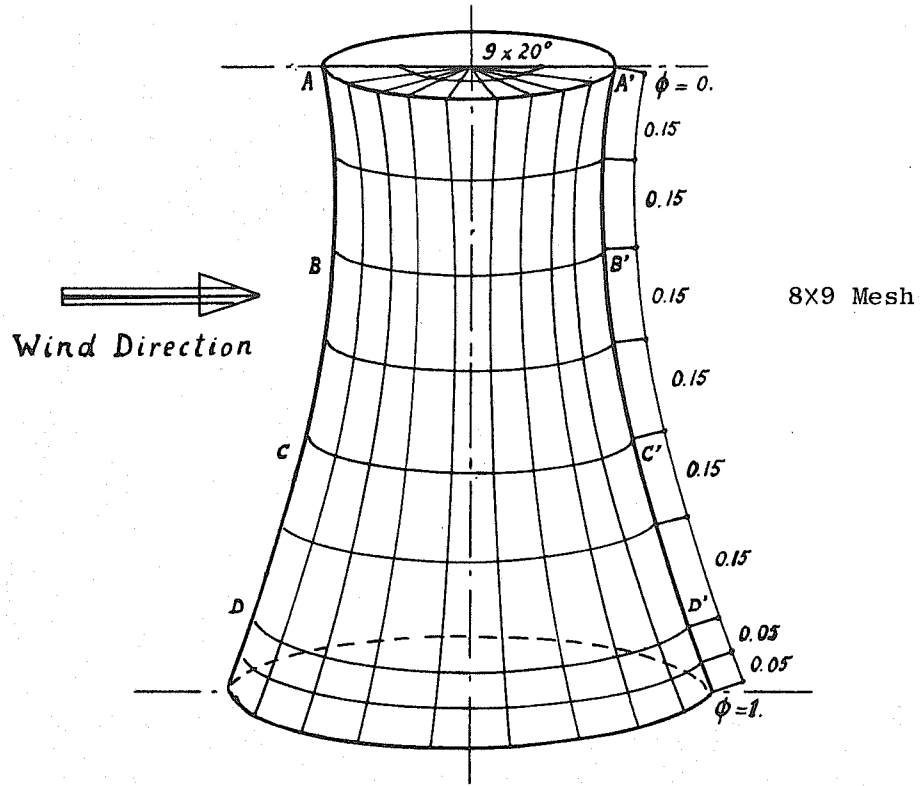


Fig. 5.17. Wind Distribution and Finite Element Mesh.

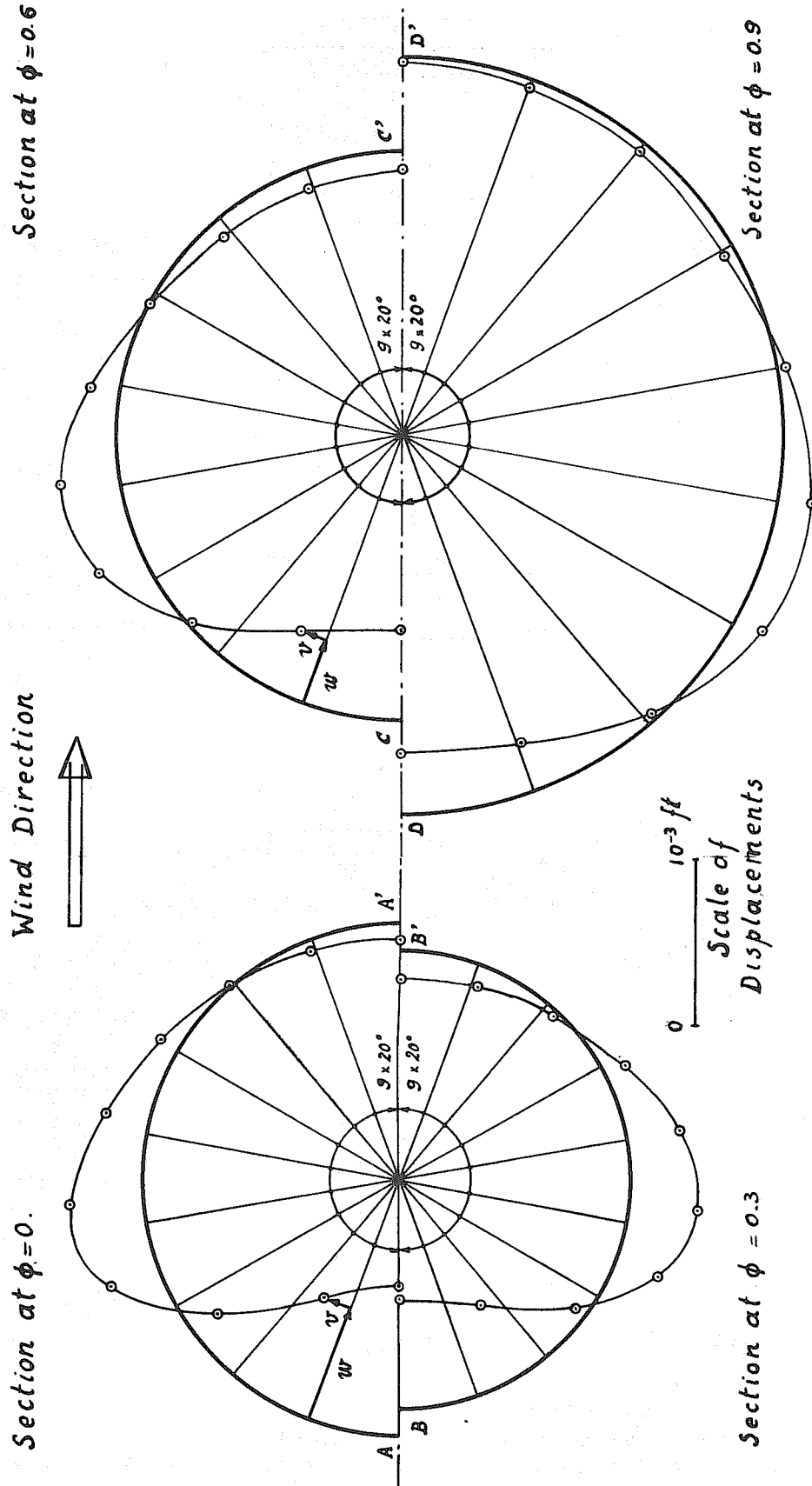


Fig. 5.18. Deformation of the Cooling Tower Under Wind Load.

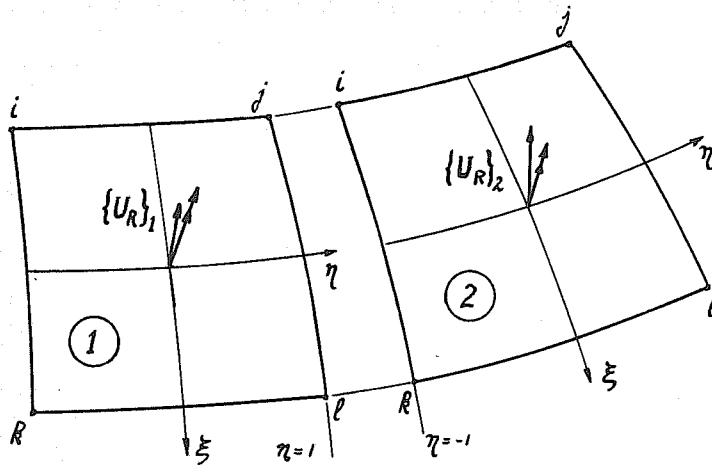


Fig. 5.19. Two Elements Adjacent to the Same Meridian.

The differences and the derivative  $\partial(w_1 - w_2)/\partial s$  vanish at  $\xi = \pm 1$ , as is required by continuity of nodal DOF, but not necessarily in between. This is the incompatibility introduced by the rigid modes announced in section 4.5.2.

It may happen that the structure and its loading are such that only some of the rigid modes need to be added. If these modes do not have any effects on the displacements  $u$  and  $v$ , only a discontinuity on  $w$  will occur. Because this discontinuity results from the difference of smooth functions, the fact that it and its first derivative vanish at the nodes  $A$  and  $A'$  insures that it will remain "small" everywhere along  $AA'$ .

In other circumstances, the common meridian may be a straight line. In such a case, the displacements introduced by the small rigid motions are not expressed by trigonometric functions but by linear polynomials. The deformation part of  $u$  and  $v$  is also a linear polynomial. Hence the sum of rigid and deformation parts is also a linear polynomial and the equality of total  $u$  and  $v$  at

nodes  $A$  and  $A'$  insures full compatibility of these displacements everywhere along  $AA'$ . The same conclusion can be reached for  $w$ .

In the circular plate examples both favorable conditions are met: the active rigid motions affect  $w$  only and full compatibility is maintained along the radial straight edges. Only "small" incompatibilities in  $w$  can occur along the parallel edges. This explains why the rigid motions introduce so little difference in the solution.

In the shells with zero Gaussian curvature, not all modes need to be added and there are always straight edges along which full compatibility is maintained; they probably also have the effect of constraining the rigid modes and prevent them from taking unreasonable values.

In shells with nonzero Gaussian curvature, all six rigid modes need to be added and all four edges are curved. The discontinuities on  $w$  may still be small but discontinuities in  $u$  and  $v$  are surely introduced and the only restriction imposed on them is that they vanish at the corners; gaps can open everywhere else along the four edges. This is enough to ruin the solutions with rigid modes in the sphere and hyperboloid examples.

## 6. SUMMARY AND CONCLUSIONS

A new doubly curved quadrilateral element for shells of revolution has been developed in curvilinear coordinates. With 24 DOF only, it is one of the simplest curved elements developed on the basis of the classical shell theory. An attempt to correct its main defect, the lack of rigid body modes representation, has led to an extensive study of this particular problem.

It has been pointed out that a correct representation of rigid modes must start with a careful choice of the strain-displacement expressions. This may be trivial in general but is not for shells where so many theories have been proposed. A procedure to check that the rigid motions are effectively strain-free has been demonstrated in the linear and nonlinear range using Sanders' strains, finally selected for this research; at this occasion, the effects of linearizing small rotations have also been discussed.

A general process to compute the effects of rigid motions on displacements has been applied to the shell element, which is probably one of the most complicated examples. By going to the limit of an almost flat surface, the degree of approximation involved in some element "containing rigid modes for all practical purposes" has been estimated.

The procedure to find which modes are already included, how well they are represented and how to add the missing ones has also been described in general terms. It can be applied to any element but does in general introduce incompatibilities. This method has

also been used to show why, in some structures or in some loading cases, elements missing particular rigid modes can behave satisfactorily.

The first application examples have demonstrated the element capability to solve rectangular or circular plate problems. The curved beam element, degenerated from a cylindrical shell, has proven that, if they do not introduce incompatibilities, the rigid modes are the most useful DOF to augment a stiffness matrix. The success obtained by Cantin [17] in adding rigid modes to cylindrical elements has been confirmed but, unfortunately has also been found to be limited to shells with zero Gaussian curvature. For shells with positive Gaussian curvature, the elements without rigid modes can give good results if the mesh is refined enough; the degree of refinement depends to a large extent on the circumstances as discovered with the examples of a sphere under pressure or point load. For shells with negative Gaussian curvature, the poor approximation of the membrane state has been held responsible for some disappointing results. Finally, on the basis of these examples, a rationale has been proposed to explain why incompatibilities introduced by rigid body modes have negligible or catastrophic consequences depending on the problem.

In summary, this new element must be considered as a mixed success. It certainly offers an alternative for nonsymmetric problems usually solved by means of elements of revolution with trigonometric functions in the circumferential direction; its advantages are greatest in cases where the Fourier series are not

at their best in dealing with point loads. But two expectations generated by a preliminary study of the circular ring have not been fulfilled.


- a) The addition of rigid modes is not always beneficial. It counteracts the poor quality of  $u$  and  $v$  interpolation functions and greatly improves the element stiffness for a cylindrical shell and its corollary, the circular beam. In these two degenerate cases, the proposed method is probably the most efficient one available since good results have been obtained with elements spanning a parallel angle of up to  $22.5^\circ$ . In circular plates,  $u$  and  $v$  do not appear and the element is efficient enough without rigid modes. But in general shells, the advantages of adding rigid modes are overshadowed by their adverse effect: the introduction of incompatibilities.
- b) When rigid modes are not added, the linear functions chosen for  $u$  and  $v$  require such a refined mesh to obtain adequate membrane strain definition that much of the predicted advantage over a shell idealization by flat elements is lost. It had been hoped that the complexity of using curvilinear coordinates would bring at least one benefit: a drastic reduction in the number of elements necessary to idealize a shell. Now it seems that without rigid modes, a parallel or meridian opening of  $5^\circ$  is the maximum acceptable. With an equal mesh, Johnson's shell element [55], formed by assemblage of four plate membrane triangles, would approximate the curved surface within  $1.25^\circ$ ; the maximum angle between plates,



which is responsible for some degree of approximation in this element, would be  $2.5^\circ$  at most; the results would be good, as demonstrated in [55] [18]; finally, it should be noted that Johnson's elements possess 20 external DOF versus 24 here. Certainly, there are instances in which the curved element is superior to the assemblage of flat plates (the sphere under point load is one) and vice versa (cooling tower) but a priori, for a general shell, there is no compelling reason to choose one element rather than the other.

The author remains convinced, however, of the superiority of curved elements in the nonlinear theory and intends to pursue his research in that direction.

A first step, of course, will be to modify the program to increase the acceptable number of elements. But, if one accepts the idea of more elements to accommodate the membrane behavior, one may wonder: why not keep the same number of elements and improve their membrane characteristics by increasing the number of DOF per element? A logical step in that direction would be to take the same bicubic interpolation functions for u, v and w; this amounts to generalize the 48 DOF cylindrical shell element derived by Bogner, Fox, Schmit [10]. Since it was shown that cubic functions can approximate the rigid modes for elements with central angle up to  $20^\circ$ , this would remove the need for a posteriori addition of rigid modes. Preliminary studies in the large displacement range also indicate that a uniform degree of interpolation may be desirable.



This does not preclude the possibility of a later investigation to replace the element based on classical shell theory by another one derived from a three-dimensional solid.

REFERENCES

1. Ahmad, S., Irons, B. M., and Zienkiewicz, O. C., "Analysis of Thick and Thin Shell Structures by Curved Finite Elements," Int. J. for Numerical Methods in Engineering, 2 (1970) 419-451.
2. Albasiny, E. L., and Martin, D. W., "Bending and Membrane Equilibrium in Cooling Towers," J. of the Engineering Mechanics Div., ASCE, 93, EM3 (1967), 1-17.
3. Almroth, B., "Influence of Edge Conditions on the Stability of Axially Compressed Cylindrical Shells," NASA CR-161, Feb. 1965.
4. Arantes E Oliveira, E. R., "Theoretical Foundations of the Finite Element Method," Int. J. Solids Struct., 4, 10 (1968), 929-952.
5. Archer, R. R., "On the Numerical Solution of the Nonlinear Equations for Shells of Revolution," J. Math. Phys., 41 (1962), 165-178.
6. Argyris, J. H., "Continua and Discontinua," Proc. Conf. on Matrix Methods in Structural Mechanics, AFIT, Wright-Patterson AFB, Ohio, 1965.
7. Argyris, J. H., Buck, K. E., Fried, T., Hilber, H. M., Marezek, G., and Schwarpf, D. W., "Some New Elements for the Matrix Displacement Method," Proc. 2nd Conf. on Matrix Methods in Structural Mechanics, AFIT, Wright-Patterson AFB, Ohio, 1968.
8. Ball, R. E., "A Program for the Nonlinear Static and Dynamic Analysis of Arbitrarily Loaded Shells of Revolution," Proc. Conf. on Computer Oriented Analysis of Shell Structures, Lockheed Palo Alto Research Lab., Palo Alto, Calif., 1970.
9. Bogner, F. K., Fox, R. L., and Schmit, L. A., "The Generation of Inter-Element-Compatible Stiffness and Mass Matrices by the Use of Interpolation Formulas," Proc. of 1st Conf. on Matrix Methods in Structural Mechanics, AFIT, Wright-Patterson AFB, Ohio, 1965.
10. Bogner, F. K., Fox, R. L., and Schmit, L. A., "A Cylindrical Shell Element," AIAA J., 5, 4 (1967), 745-750.

11. Bonnes, G., Dhatt, G., Giroux, Y., and Robichaud, L., "Curved Triangular Elements for the Analysis of Shells," Proc. 2nd Conf. on Matrix Methods in Structural Mechanics, AFIT, Wright-Patterson AFB, Ohio, 1968.
12. Budianski, B., and Radkowski, P. P., "Numerical Analysis of Unsymmetrical Bending of Shells of Revolution," AIAA J. 1, 8 (1963), 1833-1842.
13. Bufler, H., and Stein, E., "Zur Plattenberechnung mittels finiter Elemente," Ingenieur-Archiv, 39 (1970), 248-260.
14. Bushnell, D., "Nonlinear Axisymmetric Behavior of Shells of Revolution," AIAA J., 5, 3 (1967), 432-439.
15. Cantin, G., "Strain Displacement Relationships for Cylindrical Shells," AIAA J., 6, 9 (1968), 1787-1788.
16. Cantin, G., "Rigid Body Motions in Curved Finite Elements," AIAA J., 8, 7 (1970), 1252-1255.
17. Cantin, G., and Clough, R. W., "A Curved, Cylindrical-Shell, Finite Element," AIAA J., 6, 6 (1968), 1057-1062.
18. Chang-Hua Yeh, "Large Deflection Dynamic Analysis of Thin Shells Using the Finite Element Method," Ph.D. dissertation, Department of Civil Engineering, University of California, Berkeley, 1970. (Also published as SESM Report 70-18, 1970).
19. Clough, R. W., "The Finite Element in Plane Stress Analysis," Proc. 2nd ASCE Conf. on Electronic Computation, Pittsburgh, Pa., 1960.
20. Clough, R. W., and Johnson, C. P., "A Finite Element Approximation for the Analysis of Thin Shells," Int. J. of Solids Struct., 4 (1968).
21. Clough, R. W., and Johnson, C. P., "Finite Element Analysis of Arbitrary Thin Shells," Proc. of ACI Symp. on Concrete Thin Shells, ACI Publication SP-28, 1971.
22. Clough, R. W., and Tocher, J. L., "Finite Element Stiffness Matrices for Analysis of Plate Bending," Proc. 1st Conf. on Matrix Methods in Structural Mechanics, AFIT, Wright-Patterson AFB, Ohio, 1965.
23. Connor, J., and Brebbia, C., "Stiffness Matrix for Shallow Rectangular Shell Elements," J. of Engineering Mechanics Div., ASCE, 93, EM5 (1967).

24. Cowper, G. R., and Lindberg, G. M., "Comparison of Two High-Precision Triangular Finite Elements for Arbitrary Deep Shells," Proc. of 3rd Conf. on Matrix Methods in Structural Mechanics, AFIT, Wright-Patterson AFB, Ohio, 1971.
25. Dhatt, G., "Numerical Analysis of Thin Shells Based on Discrete-Kirchhoff Hypothesis," Proc. of Symp. on Application of Finite Element Methods in Civil Engineering, Vanderbilt University, Nashville, Tenn., 1969.
26. Donnell, L. H., NACA Tech. Rept. No. 479, 1933.
27. Dunham, R. S., and Nickell, R. E., "Finite Element Analysis of Axisymmetric Solids with Arbitrary Loading," SESM Report 67-6, University of California, Berkeley, 1967.
28. Dupuis, G. A., Hibbitt, H. D., McNamara, S. F., and Marcal, P. V., "Nonlinear Material and Geometric Behavior of Shell Structures," Proc. Conf. on Computer Oriented Analysis of Shell Structures," Lockheed Palo Alto Research Lab, Palo Alto, Calif., 1970.
29. Family, J., and Archer, R. R., "Finite Asymmetric Deformation of Shallow Spherical Shells," AIAA J., 3, 3 (1965), 506-510.
30. Felippa, C. A., "Plate Bending Finite Elements," Ph.D. dissertation, Department of Civil Engineering, University of California, Berkeley, 1966.
31. Felippa, C. A., and Clough, R. W., "Finite Element Method in Solid Mechanics," AMS Symp. on Numerical Solutions of Field Problems in Continuum Mechanics, Durham, N.C., 1968.
32. Flügge, W., Stresses in Shells, Springer-Verlag, Berlin, 1962.
33. Fraeys de Veubeke, B., "Upper and Lower Bounds in Matrix Structural Analysis," AGARDograph 72, Ed. by B. Fraeys de Veubeke, Pergamon Press, 1964.
34. Fraeys de Veubeke, B., "Bending and Stretching of Plates. Special Models for Upper and Lower Bounds," Proc. Conf. on Matrix Methods in Structural Mechanics, AFIT, Wright-Patterson AFB, Ohio, 1965.
35. Fulton, R. E., Eppink, R. T., and Walz, J. E., "The Accuracy of Finite Element Methods in Continuum Problems," Proc. of 5th U.S. National Congress of Applied Mechanics, ASME, 1966.

36. Fung, Y. C., Foundations of Solid Mechanics, Prentice-Hall, 1965.
37. Gallagher, R. H., "Analysis of Plate and Shell Structures," Proc. of Symp. on Application of Finite Element Methods in Civil Engineering, Vanderbilt University, Nashville, Tenn., 1969.
38. Gallagher, R. H., Lien, S. and Mau, S. T., "A Procedure for Finite Element Plate and Shell Pre- and Post-Buckling Analysis," Proc. of 3rd Conf. on Matrix Methods in Structural Mechanics, AFIT, Wright-Patterson AFB, Ohio, 1971.
39. Gallagher, R. H., and Yang, T. Y., "Elastic Instability Predictions for Doubly Curved Shells," Proc. 2nd Conf. on Matrix Methods in Structural Mechanics, AFIT, Wright-Patterson AFB, Ohio, 1968.
40. Giannini, M., and Miles, G. A., "A Curved Element Approximation in the Analysis of Axisymmetric Thin Shells," Int. J. for Numerical Methods in Engineering, 2 (1970), 459-476.
41. Girkmann, K., Flächentragwerke, 5th Ed., Springer-Verlag, Wien, 1960.
42. Gould, P. L., and Seng-Lip Lee, "Hyperbolic Cooling Towers Under Seismic Design Load," J. of the Structural Div., ASCE, 93, ST3 (1967), 87-107.
43. Gould, P. L., and Seng-Lip Lee, "Bending of Hyperboloid Cooling Towers," J. of the Structural Div., ASCE, 93, ST5 (1967), 125-146.
44. Grafton, P. E., and Strome, D. R., "Analysis of Axisymmetrical Shells by the Direct Stiffness Method," AIAA J., 1, 10 (1963), 2342-2347.
45. Green, A. E., and Zerna, W., Theoretical Elasticity, 2nd Ed., Oxford University Press, 1968.
46. Green, A. E., and Adkins, J. E., Large Elastic Deformations, Oxford University Press, 1960.
47. Greenbaum, G. A., "Comments on Numerical Analysis of Unsymmetrical Bending of Shells of Revolution," AIAA J., 2, 3 (1964), 500-591.
48. Greene, B. E., Jones, R. E., and Strome, D. R., "Dynamic Analysis of Shells Using Doubly-Curved Finite Elements," Proc. 2nd Conf. on Matrix Methods in Structural Mechanics, AFIT, Wright-Patterson AFB, Ohio, 1968.

49. Haisler, W. E., and Stricklin, J. A., "Rigid-Body Displacements of Curved Elements in the Analysis of Shells by the Matrix-Displacement Method," AIAA J., 5, 8 (1967), 1525-1527.
50. Haisler, W. E., and Stricklin, J. A., "Nonlinear Finite Element Analysis Including Higher Order Strain Energy Terms," AIAA J., 8, 6 (1970), 1158-1159.
51. Haug, E., "Finite Element Analysis of Nonlinear Membrane Structures," Ph.D. dissertation, Department of Civil Engineering, University of California, Berkeley, 1972.
52. Hoff, N. J., and Tsai-Chen Soong, "Buckling of Circular Cylindrical Shells in Axial Compression," Int. J. Mech. Sci. 7 (1965), 489-520.
53. Huang, N. C., "Unsymmetrical Buckling of Thin Shallow Spherical Shells," J. Appl. Mech., 31, (1964), 447-457.
54. Jennings, A., "Frame Analysis Including Change of Geometry," J. of the Structural Div., ASCE, 94, ST3 (1968), 627-643.
55. Johnson, C. P., "The Analysis of Thin Shells by a Finite Element Procedure," Ph.D. dissertation, Department of Civil Engineering, University of California, Berkeley, 1967. (Also published as SESM Report 67-22, 1967.)
56. Jones, R. E., and Strome, D. R., "Direct Stiffness Method Analysis of Shells of Revolution Utilizing Curved Elements," AIAA J., 4, 9 (1966), 1519-1525.
57. Junghanss, K., "Berechnung von Rotationsschalen beliebiger Meridianform und veränderlicher Wanddicke," Maschinenbautechnik, 17, 7 (1968), 349-354.
58. Kalnins, A., and Lestingi, J. F., "On Nonlinear Analysis of Elastic Shells of Revolution," J. Appl. Mech., 34, 1 (1967), 59-67.
59. Kao, R., and Perrone, R., "Asymmetric Buckling of Spherical Caps with Asymmetrical Imperfections," Technical Report 16, The Catholic University of America, Washington, D.C., 1969.
60. Kaplan, A., and Fung, Y. C., "A Nonlinear Theory of Bending and Buckling of Thin Elastic Shallow Spherical Shells," NACA TN 3212 (1954).

61. Key, S. W., "The Analysis of Thin Shells with a Doubly Curved Arbitrary Quadrilateral Finite Element," Proc. Conf. on Computer Oriented Analysis of Shells, Lockheed Palo Alto Research Lab, Palo Alto, Calif., 1970.
62. Key, S. W., and Beisinger, Z. E., "The Analysis of Thin Shells with Transverse Shear Strains by the Finite Element Method," Proc. of 2nd Conf. on Matrix Methods in Structural Mechanics, AFIT, Wright-Patterson AFB, Ohio, 1968.
63. Khojasteh-Bakht, M., "Analysis of Elastic-Plastic Shells of Revolution Under Axisymmetric Loading by the Finite Element Method," Ph.D. dissertation, Department of Civil Engineering, University of California, Berkeley, 1967. (Also published as SESM Report 67-8.)
64. Kirchhoff, G. R., J. Reine, Angew. Math., 40, 1850.
65. Koiter, W. T., "On Stability of Elastic Equilibrium," (in Dutch) thesis, Delft, 1945.
66. Koiter, W. T., "A Consistent First Approximation in the General Theory of Thin Elastic Shells," Proc. of IUTAM Symp. on the Theory of Thin Elastic Shells, edited by Koiter, W. T., North Holland Pub. Co., Amsterdam, 1960.
67. Kratzig, W. B., "Beitrag zu einer linearen Approximation der Stabilitätstheorie elastischer Flächentragwerke," Habilitationsschrift, T. U. Hannover, 1968.
68. Kratzig, W. B., Private communication.
69. Kuang-Han Chu and Pinjarkar, S. G., "Analysis of Horizontally Curved Box Girder Bridges," J. of Structural Div. ASCE, 97, ST10 (1971), 2481-2501.
70. Larsen, P., "Large Displacement Analysis of Shells of Revolution Including Creep, Plasticity and Viscoelasticity," Ph.D. dissertation, Department of Civil Engineering, University of California, Berkeley, 1972.
71. Lee, T. M., "Flexure of Circular Plate by Concentrated Force," J. of Engineering Mechanics Div. ASCE, 94, EM3, 841-855.
72. Leigh, D. C., Nonlinear Continuum Mechanics, McGraw-Hill, New York, 1968.
73. Love, A. E. H., Phil. Trans. Roy. Soc. London, A17, 1888.



74. Lu, Z. A., Penzien, J., and Popov, E. P., "Finite Element Solution for Thin Shells of Revolution," J. of the Engineering Mechanics Division, ASCE, 90, EM5 (1964), 119-145.
75. Marguerre, K., "Zur Theorie der Gekrummten Platte grosser Formanderung," Proc. Fifth International Congress of Applied Mechanics, (1938), 93-101.
76. Mebane, P. M., and Stricklin, J. A., "Implicit Rigid-Body Motion in Curved Finite Elements," AIAA J., 9, 2 (1971), 344-345.
77. Melosh, R. J., "Basis for the Derivation of Matrices for the Direct Stiffness Method," AIAA J., 1, 7 (1963), 1631-1637.
78. Meyer, C., "Analysis and Design of Curved Box Girder Bridges," Ph.D. dissertation, Civil Engineering Department, University of California, Berkeley, 1970. (Also published as SESM Report 70-22, 1970.)
79. Meyer, C., and Scordelis, A. C., "Analysis of Curved Folded Plate Structures," J. of Structural Div., ASCE, 97, ST10 (1971), 2481-2501.
80. Meyer, R. R., and Harmon, M. B., "Conical Segment Method for Analyzing Open Crown Shells of Revolution for Edge Loads," AIAA J., 1, 4 (1963), 886-891.
81. Murray, D. W., "Large Deflection Analysis of Plates," Ph.D. dissertation, Department of Civil Engineering, University of California, Berkeley, 1967. (Also published as SESM Report 67-44, 1967.)
82. Murray, D. W., and Wilson, E. L., "Finite Element Large Deflection Analysis of Plates," J. of Engineering Mechanics Div., ASCE, 95, EMI (1969), 143-165.
83. Mushtari, K. M., and Galimov, K. Z., Nonlinear Theory of Thin Elastic Shells, translated from Russian (1957), published by the Israel Program for Scientific Translations, 1961.
84. Nagdhi, P. M., Proc. of Symp. on the Theory of Shells to Honor L. H. Donnell, 34-37.
85. Nagdhi, P. M., "Foundations of Elastic Shell Theory," Progress in Solid Mechanics, vol. 4, Ed. Sneddon, I. N., and Hill, R., John Wiley, New York (1963), 1-90.

86. Nagdhi, P. M., "The Theory of Shells and Plates, Part I: Kinematics and Basic Principles, Part II: Nonlinear and Linear Theories of Elastic Shells," Reports AM 71-1, AM 71-2, Division of Applied Mechanics, University of California, Berkeley, 1971.
87. Nagdhi, P. M., and Nordgren, R. P., "On the Nonlinear Theory of Elastic Shells Under the Kirchhoff Hypothesis," *Quart. Appl. Math.*, 21, 1 (1963), 49-59.
88. N.A.S.A., TND-1510. "Collected Papers on Instability of Shell Structures," Langley Research Center (1962).
89. Nash, W. A., "Bibliography on Shells and Shell-Like Structures," Part I, David Taylor Model Basin Report 863 (1954). Part II, Dept. of Eng. Mech., Univ. of Florida (1957).
90. Navaratna, D. R., "Computation of Stress Resultants in Finite Element Analysis," *AIAA J.*, 4, 11 (1966), 2058-2060.
91. Navaratna, D. R., "Elastic Stability of Shells of Revolution by the Variational Approach Using Discrete Elements," Sc.D. thesis, Massachusetts Institute of Technology, Department of Aeronautics and Astronautics, Cambridge, Mass., 1966.
92. Navaratna, D. R., Pian, T. H. H., and Witmer, E. A., "Stability Analysis of Shells of Revolution by the Finite Element Method," *AIAA J.*, 6, 2 (1968), 355-361.
93. Novozhilov, V. V., Foundations of the Nonlinear Theory of Elasticity, Graylock Press, Rochester, N.Y., 1953.
94. Novozhilov, V., The Theory of Thin Shells, P. Noordhoff, Groningen, Netherlands, 1964.
95. Olson, M. D., and Lindberg, G. M., "Vibration Analysis of Cantilevered Curved Plates Using a New Cylindrical Shell Finite Element," *Proc. 2nd Conf. on Matrix Methods in Structural Analysis*, AFIT, Wright-Patterson AFB, Ohio, 1968.
96. Pawsey, S. F., "The Analysis of Moderately Thick to Thin Shells by the Finite Element Method," Ph.D. dissertation, Department of Civil Engineering, University of California, Berkeley, 1970. (Also published as SESM Report 70-12, 1970.)
97. Pecknold, D. A. and Schnobrich, W. C., "Finite Element Analysis of Skewed Shallow Shells," *J. of Struct. Div.*, ASCE, 95, ST4 (1969).

98. Percy, J. H., Pian, T. H. H., Klein, S. and Navaratna, D. R., "Application of Matrix Displacement Method to Linear Elastic Analysis of Shells of Revolution," AIAA J., 3, 11 (1965), 2138-2145.
99. Radhamohan, S. K., Setlur, A. V., and Goldberg, J. E., "Stability of Shells by Parametric Differentiation," J. of Struct. Div., ASCE, 97, ST6 (1971), 1775-1790.
100. Radkowski, P. P., Davis, R. M., and Bolduc, M. R., "Numerical Analysis of Equations of Thin Shells of Revolution," ARS J. 32 (1962), 36-41.
101. Reissner, E., "A New Derivation for the Equations for the Deformations of Elastic Shells," Amer. Journal of Math., 63, 1 (1941), 177-184.
102. Reissner, E., "On Axisymmetric Deformations of Thin Shells of Revolution," Proc. 3rd Symp. in Applied Mathematics, McGraw-Hill Book Co., New-York, 1950, 27-52.
103. Reissner, E., "Stress Strain Relations in the Theory of Thin Elastic Shells," J. Math. Phys., 31 (1952), 109-119.
104. Reissner, E., "On Some Problems in Shell Theory," Proc. 1st Symp. on Naval Structural Mechanics, Pergamon Press, New York, 1960.
105. Rish, R. F., and Steel, T. F., "Design and Selection of Hyperbolic Cooling Towers," J. of the Power Division, ASCE, 85, PO5 (1959), 89-117.
106. Sanders, J. L., "An Improved First Approximation Theory for Thin Shells," N.A.S.A. Report 24, June 1959.
107. Sanders, J. L., "Nonlinear Theories for Thin Shells," Quart. Appl. Math., 21, 1 (1963), 21-36.
108. Schmit, L. A., Bogner, F. K., and Fox, R. L., "Finite Deflection Structural Analysis Using Plate and Shell Discrete Elements," AIAA J. 6, 5 (1968), 781-791.
109. Seng-Lip Lee and Gould, P. L., "Hyperbolic Cooling Towers Under Wind Load," J. of the Structural Division, ASCE, 93, ST5 (1967), 487-514.
110. Sharifi, P., "Nonlinear Analysis of Sandwich Structures," Ph.D. dissertation, Department of Civil Engineering, University of California, Berkeley, 1970.

111. Sobel, L. H., and Flügge, W., "Stability of Toroidal Shells Under Uniform External Pressure," AIAA J. 5, 3 (1967), 425-431.
112. Strickland, G., and Loden, W., "A Doubly-Curved Triangular Shell Element," Proc. 2nd Conf. on Matrix Methods in Structural Mechanics, AFIT, Wright-Patterson AFB, Ohio, 1968.
113. Stricklin, J. A., De Andrade, J. C., Stebbins, F. J., and Cwiertny, A. J., "Linear and Nonlinear Analysis of Shells of Revolution with Asymmetrical Stiffness Properties," Proc. 2nd Conf. on Matrix Methods in Structural Mechanics, AFIT, Wright-Patterson AFB, Ohio, 1968.
114. Stricklin, J. A., Haisler, W. E., McDougall, H. R., and Stebbins, F. J., "Nonlinear Analysis of Shells of Revolution by the Matrix Displacement Method," AIAA J., 6, 12 (1968), 2306-2312.
115. Stricklin, J. A., and Martinez, J. E., "Dynamic Buckling of Clamped Spherical Caps Under Step Pressure Loading," AIAA J., 7, 6 (1969), 1212-1213.
116. Stricklin, J. A., Martinez, J. E., Tillerson, J. R., Hong, J. H., and Haisler, W. E., "Nonlinear Dynamic Analysis of Shells of Revolution by Matrix Displacement Method," Report 69-77, Texas A & M University College Station, Texas, 1970.
117. Stricklin, J. A., Navaratna, D. R., and Pian, T. H. H., "Improvements on the Analysis of Shells of Revolution by the Matrix Displacement Method," AIAA J., 4, 11 (1966), 2069-2072.
118. Timoshenko, S., and Gere, J., Theory of Elastic Stability, McGraw-Hill Book Co., 1965.
119. Timoshenko, S., and Woinowsky-Krieger, S., Theory of Plates and Shells, McGraw-Hill, New York, 1959.
120. Truesdell, C., and Toupin, R. A., The Classical Field Theories, Handbook der Physik, Vol. III/1, ed. by Flügge, S., Springer-Verlag, Berlin, 1960.
121. Turner, M. J., Clough, R. W., Martin, H. C., and Topp, L. J., "Stiffness and Deflection Analysis of Complex Structures," J. Aero. Sci., 23, 9 (1956), 805-823.
122. Utku, S., "Stiffness Matrices for Thin Triangular Elements of Nonzero Gaussian Curvature," AIAA J., 5, 9 (1967).

123. Vlasov, V. Z., Allgemeine Schalentheorie und ihre Anwendung in der Technik, (translated from the 1949 Russian ed.), Akademie Verlag, Berlin, 1958.
124. Weinitschke, H. J., "On Asymmetric Buckling of Shallow Spherical Shells," *J. Math. Physics*, 44, (1965).
125. Wempner, G., "Finite Elements, Finite Rotations and Small Strains of Flexible Shells," *Int. J. Solids Structures*, 5 (1969), 117-153.
126. Wempner, G. A., Oden, G. T., and Kross, D. A., "Finite Element Analysis of Thin Shells," *J. of Eng. Mech. Div.*, ASCE, 94, EM6 (1968), 1273-1294.
127. Wilson, E. L., Taylor, R. L., Doherty, W. P., and Ghaboussi, J., "Incompatible Displacement Models," (to be published in the Proc. of ONR Symposium, Urbana, Illinois, 1971).
128. Yaghmai, S., "Incremental Analysis of Large Deformations in Mechanics of Solids with Application to Axisymmetric Shells of Revolution," Ph.D. dissertation, Department of Civil Engineering, University of California, Berkeley, 1968. (Also published as SESM Report 68-17, 1968).
129. Zienkiewicz, O. C., The Finite Element Method in Structural and Continuum Mechanics, McGraw-Hill, London, 1967.
130. Zienkiewicz, O. C., The Finite Element Method in Engineering Science, McGraw-Hill, London, 1971.
131. Zienkiewicz, O. C., and Nayak, G. C., "A General Approach to Problems of Large Deformations and Plasticity Using Iso-Parametric Elements," Proc. 3rd Conf. on Matrix Methods in Structural Mechanics, AFIT, Wright-Patterson AFB, Ohio, 1971.